Cenozoic Variations in the Deep Western Boundary Current as Recorded in the Seismic Stratigraphy of Contourite Drifts, Newfoundland Ridge, Offshore Canada

Patrick R. Boyle

Thesis submitted to the faculty of the Virginia Polytechnic Institute and State University
in partial fulfillment of the requirements for the degree of

Master of Science
In
Geosciences

Brian W. Romans, Chair
Benjamin C. Gill
Kenneth A. Eriksson

April 29, 2014
Blacksburg, VA

Keywords: Seismic stratigraphy, paleoceanography, contourite drifts, Deep Western Boundary Current, Southeast Newfoundland Ridge.

Cenozoic Variations in the Deep Western Boundary Current as Recorded in the Seismic Stratigraphy of Contourite Drifts, Newfoundland Ridge, Offshore Canada

Patrick R. Boyle

ABSTRACT

A contourite drift complex on the J-Anomaly Ridge (JAR) and Southeast Newfoundland Ridge (SENR), offshore eastern Canada, records an extensive archive of North Atlantic circulatory and sedimentary dynamics formed under the influence of the Deep Western Boundary Current (DWBC). Seismic-reflection profiles constrained by drill sites from IODP Expedition 342 are used to map the spatial and temporal distribution of contourite sedimentation and to evaluate the Cenozoic history of the DWBC within a preexisting climatic framework. This study indicates three phases of sedimentation termed here Pre-Contourite-Drift Phase (~115-50 Ma), Active-Contourite-Drift Phase (~50-2.6 Ma), and Post-Contourite-Drift Phase (~2.6-0 Ma). Bottom current controlled sedimentation began at the boundary between Pre-Contourite-Drift Phase and Active-Contourite-Drift Phase (~50 Ma), and correlates to a long-term global cooling trend that initiated at the end of the Early Eocene Climatic Optimum. Within the Active-Contourite-Drift Phase at ~30 Ma depocenters shifted deeper and current energy and focus is interpreted to have increased in association with global oceanographic change at the Eocene-Oligocene transition. The beginning of Post-Contourite-Drift Phase sedimentation (~2.6 Ma) marks a shift in bottom current path towards shallower water depths, and corresponds with the onset of Northern Hemisphere ice sheets. These events of circulatory reorganization correlate with other North Atlantic seismic stratigraphic studies, suggesting that these events occurred throughout the North Atlantic. An improved understanding of long-term ($\geq 10^6$ yr) dynamics of North Atlantic circulation in response to significant reorganization of Cenozoic climate provides important context towards refining models and prediction of oceanic response to contemporary climate change.

ACKNOWLEDGEMENTS

I am only partially responsible for the success of this thesis, and would like to acknowledge those whose efforts contributed. First I would like to thank my advisor, Dr. Brian W. Romans, for the opportunity to work with and learn from him. Without his patience, support, and guidance I would not have survived. I am appreciative for the continued feedback on my progress provided by Kenneth A. Eriksson and Benjamin C. Gill, and am grateful to have had the opportunity to learn from them during my graduate studies. The foundation for all my accomplishments thus far, and into the future, was developed through the experiences I had at Indiana University of Pennsylvania and Virginia Tech. I am thankful to the faculty and staff in the Department of Geosciences at both of these institutions for cultivating an environment in which it was possible to develop such a strong foundation. In addition I would like to thank my graduate colleagues in the Sedimentary Systems Research and Sedimentary Geochemistry Research Group at Virginia Tech. Without daily conversations with Neal Auchter, Cody Mason, Ty Buller, Angela Gerhardt, and Teddy Them, my time at Virginia Tech would have been less academically rewarding, and my graduate experience less weird.

I would also like to acknowledge the Virginia Tech Department of Geosciences, the Integrated Ocean Drilling Program, and ConocoPhillips for financial support throughout my graduate studies. Without the support provided by these organizations none of this would have been possible.

Most importantly, I would like to thank my family for their love, support, and encouragement. The path I have wandered has been paved with support, free of unwanted influence, and guided through experiences. My parents, George and Anita, allowed me the freedom to set my own path and to measure my own success. My best friends and siblings, Kevin and Kathryn, have constantly reminded me not to take life too seriously and to keep moving when things get tough. My Aunt Patti has shared many experiences with me that have changed my perspective on life, and have guided my voyage. My brother-in-law, Jeff Dereume has been a mentor and friend throughout my journey, and without him my path would not have been as smooth. I am thankful to have such a fantastic family.

CONTENTS

FIGURES

TABLES

1. INTRODUCTION

Thermohaline circulation is intimately linked to the global climate system (Dickson and Brown, 1994; Broecker, 1997; Rahmstorf, 2000; Clark et al., 2002; Kuhlbrodt et al., 2009). Deep oceanic currents that parallel bathymetric contours are driven, in part, by thermohaline circulation (Rahmstorf, 2003) and play a significant role in deep-sea sedimentation (Faugères et al., 1999; Rebesco et al., in press). Large sedimentary drifts deposits and regional unconformities have been documented throughout the world oceans, and are associated with bathymetric contour parallel currents (Miller and Tucholke, 1983; Faugères et al., 1999; Stow et al., 2002; Rebesco et al., in press). Sedimentary drifts deposited under the influence of bathymetric contour parallel currents are termed contourites and are known to display unique morphologies related to their formation (Faugères et al., 1999; Rebesco and Stow, 2001; Stow et al., 2002; Rebesco et al., in press). Therefore, understanding the evolution of contourite drifts within the context of past environmental change provides the opportunity to better understand the link between thermohaline circulation and global climate (Stow et al., 2002; Norris et al., 2014). Additionally, an increased familiarity with contourite drift evolution allows for an elevated understanding of the dynamics involved in sedimentary systems deposited under the influence of bottom current activity, and their control on the shaping of continental margins.

In the North Atlantic Ocean, bathymetric contour parallel currents have been associated with regional unconformities and contourite drifts that exceed 2 km in thickness and extend for 100s of km (Faugères et al., 1999; Stow et al., 2002; Rebesco et al., in press). The modern, southward-flowing Deep Western Boundary Current (DWBC) is the primary deep-water current acting in the North Atlantic Ocean and is largely sourced by sinking surface waters in the Norwegian-Greenland and Labrador Seas (Bower and Hunt, 2000; Stow et al., 2002; Rahmstorf, 2006). Contourite drifts in the North Atlantic Ocean have been used to infer variations in deep-water circulation through the Cenozoic (Davies et al., 2001; Hohbein et al., 2012), a period that experienced several intervals of abrupt global-scale climate change (Zachos et al., 2001; 2008). However, these studies produce conflicting interpretations of the evolution of North Atlantic deep-water formation driven by thermohaline circulation. For example, dates for the onset of

deep-water formation in the North Atlantic vary from as young as early Miocene to as old as early Eocene (Miller and Tucholke, 1983; Davies et al., 2001; Stocker et al., 2005; Hohbein et al., 2012). Additionally, the studies that document the evolution of bottom current-controlled sedimentation in the North Atlantic Ocean are from discrete locations that are separated by vast areas of unstudied marine sediment.

The Newfoundland Ridge Drift Complex overlies the J-Anomaly (JAR) and Southeast Newfoundland Ridge (SENR) offshore Newfoundland Canada (Figure 1). This complex yields an extensive archive of Cenozoic sedimentary deposits that provides the opportunity to evaluate the evolution of North Atlantic deep-water circulation. Contemporary understanding of the sedimentological and deep-water circulation evolution of the Cenozoic North Atlantic Ocean Basin is inferred from studies north and south of the Newfoundland Ridge Drift Complex. Thus, study of the Newfoundland Ridge Drift Complex will shorten the spatial gap between those previous studies and allow for a more comprehensive and continuous understanding of the evolution of North Atlantic deep-water circulation.

The Integrated Ocean Drilling Program (IODP) has collected an extensive dataset including seismic-reflection profiles and sediment core data over the JAR and SENR. Here, we document the Cenozoic evolution of North Atlantic deep-water circulation as delineated by seismic stratigraphic analysis of the Newfoundland Ridge contourite drift complex. Seismic stratigraphic interpretations are tied to age control provided by data from sediment cores, which allows seismic stratigraphic interpretations to be placed within a temporal framework and climatic history. We then discuss how seismic stratigraphic interpretations observed over the JAR and SENR tie into a preexisting understanding of the evolution of the North Atlantic Ocean Basin. Finally, these new results provide insight towards the dynamics of sedimentary systems deposited under the influence of bathymetric contour parallel currents.

2. GEOLOGIC BACKGROUND

2.1 Contourite Drifts

In the 1960s it was first observed through photographing bedforms such as scours and ripples on the sea floor that bottom currents are capable of reworking and depositing

sediment at depths exceeding 5000 m (Heezen and Hollister, 1964). It is now understood that thermohaline-driven bottom currents play a significant role in deep-sea sedimentation, and are capable of creating sediment drifts greater then 10^5 km^2 in area with thicknesses of 10^2-10^3 m (Faugères et al., 1999; Rebesco et al., in press). Contourite drifts can be composed of mud, silt, or sand and, rarely, gravel that is sourced up-current of accumulation, and transported within the nepheloid layer (Stow et al., 2002). Accumulation rates in these systems can be much higher compared to typical deep-sea pelagic sedimentation achieving rates of 5-100 cm/kyr, and these rates are fairly continuous over long timescales (Stow and Faugères, 2008; Rebesco et al., inpress). These relatively high accumulation rates make contourite drifts high-resolution archives for studies seeking to reconstruct paleoceanographic conditions and the interplay between oceanic circulation and climate (Keigwin and Jones, 1989; Norris et al., 2014).

2.2 Geologic Evolution of the J-Anomaly and SE Newfoundland Ridge

The opening of the central North Atlantic Ocean initiated during the Middle Jurassic, creating a transform boundary along the southwestern margin of the Grand Banks offshore Newfoundland, Canada (Figure 1) (Tucholke and Ludwig, 1982; Pe-Piper et al., 2007). Continued Early Cretaceous (~128 Ma) seafloor spreading led to the separation of Newfoundland from Iberia, and spreading propagated northward where it eventually created the Labrador Sea and then the northeastern extent of the Atlantic Ocean (Pe-Piper et al., 2007). The SENR, a positive bathymetric feature trending northwest-southeast off the Grand Banks, has been interpreted as a fracture zone associated with Middle Jurassic transform faulting (Tucholke and Ludwig, 1982). To the southwest of the SENR, and perpendicular to its orientation, is another positive bathymetric feature known as the JAR. The JAR is associated with a prominent magnetic anomaly known as the "J" magnetic anomaly, which is the oldest known magnetic anomaly related to seafloor spreading in the region (Sullivan and Keen, 1978; Tucholke et al., 1989). The crust supporting both of these bathymetric features is oceanic in composition and volcanic in origin, with magma being sourced from a mantle plume (Sullivan and Keen, 1978; Tucholke et al., 1979; Tucholke et al., 2007; Norris et al., 2014).

Several lines of evidence suggest that the volcanic basement making up the SENR and JAR was emergent or exposed in a shallow-water environment during its early history. Drill core from DSDP Site 384 penetrated the top of the JAR and recovered basalt with vesicularity typical of water depths less than 500 m along with shallow-marine fossil assemblages overlying the volcanic basement (Tucholke et al., 1979). Seismic-reflection profiles in the region suggest the presence of shallow water carbonates reefs (Tucholke et al., 1979), and sediment cores from IODP Expedition 342 recovered Albian coral fragments at Site U1407 on the SENR (Norris et al., 2014). At present day, the SENR ranges from ~2500 to 5000 meters below sea level (mbsl), whereas the JAR ranges from ~3500 to 5000 mbsl. Thermal and tectonic subsidence of volcanic basement combined with isostatic compensation of sediment overburden have contributed to the subsidence of this region to its present depth (Tucholke et al., 1979).

2.3 Oceanographic Setting

The Deep Western Boundary Current (DWBC) is a deep-water thermohaline-driven contour current that intersects the JAR and SENR as it flows south along the western margin of the North Atlantic Ocean (Richardson et al., 1981). Coriolis forcings cause the equator-ward flowing DWBC to focus along the western margin of the North Atlantic Ocean. South of the JAR and SENR, along the continental rise of Nova Scotia, DWBC velocities were measured over a two week period at 5000 mbsl; results showed mean current velocities exceeded 30 cm/sec and maximum velocities exceeded 70 cm/sec (Richardson et al., 1981). Cold, high-salinity deep waters transported by the DWBC are collectively referred to as North Atlantic Deep Water (NADW) (Fine and Molinari, 1988), which at present day accounts for roughly half of the world's deep-water formation, making it a significant contributor to thermohaline circulation and global heat transfer (Broecker et al., 1998).

Three main components make up the modern NADW; the shallow DWBC water, Labrador Sea water (LSW), and the Norwegian-Greenland overflow water (NGOW) (Pickart, 1992). The shallow DWBC and the LSW form from overturning in the Labrador Sea while the NGOW forms through overturning in the Norwegian-Greenland Sea, north of the Greenland-Scotland Ridge (GSR) (Pickart, 1992, Hansen and Østerhus, 2000). The

GSR is a bathymetric sill that restricts, but does not inhibit, the flow of cold deep water formed in the Norwegian-Greenland Sea south into the North Atlantic Ocean (Miller and Tucholke, 1983). Water exchange across the GSR accounts for a large portion of NADW, and contributes significantly to North Atlantic thermohaline circulation (Hansen and Østerhus, 2000). Warm surface waters flow north from the Atlantic Ocean into the Labrador and Norwegian-Greenland Sea where decreasing temperatures and increasing salinities due to evaporation and sea ice formation cause surface waters to sink (Hansen and Østerhus, 2000). All three components of NADW coalesce into the DWBC, with the LSW representing the last component to contribute to the DWBC ~1500 km north and up-current of the JAR and SENR (Palter et al., 2008).

3. DATA

3.1 Seismic-reflection Profiles

IODP acquired 56 high-resolution 2-D seismic-reflection profiles over the JAR and SENR aboard the RV Knorr, from July 16 to August 15 2004, during Knorr cruise 179-1. These data were acquired using the Lamont-Doherty Earth Observatory (LDEO) HiRes multi-channel seismic (MCS) system, which comprised a 75/75 cubic inch generator-injector (GI) airgun fired at 10 sec interval and a 600 m long, solid-state ITI 48-channel streamer with a total length of 600 m towed at 2 m depth. The data were digitized at 1 msec. The airgun was configured in true GI mode and floated at a depth of 4 m, which produced a pulse with a spectral peak extending between 30 Hz and 250 Hz and cresting at 90-100 Hz. Despite strong and variable surface currents, the ship maintained a speed over ground of 4.5 - 4.9 knots. This survey covers approximately 70,000 km^2 with the tightest grid spacing over the JAR between 52°W to 53°W and 40°N to 41°N, and also over the SENR in close proximity to the seamounts between 50°W to 48°W and 41°N to 42°N (Figure 2). Grid spacing over the JAR is 7-14 km and 10-18 km over the SENR seamounts (Figure 2). Profiles have a vertical resolution on the order of 20 m, and data quality is generally excellent; however, the southern extent of line 46 displays substandard data quality and has been used with discretion (Figure 2).

Seismic reflection data were processed with SIOSEIS software package. Processing included nulling of six bad traces, application of a frequency domain zero

phase bandpass filter with corner frequencies of 35 Hz and 300 Hz and a rolloff of 48 db/octave, an outside mute, and stacking after normal moveout correction using a single sediment layer velocity profile based on rms velocity analyses from an earlier Newfoundland Basin MCS cruise that used a 3.1 km long streamer (Tuckolke et al., 1989). The stacked traces were processed with Stolt migration using the velocity of water (1500 m/s) and assuming that the traces were uniformly spaced. Trace amplitude was adjusted using time-varying gain. These data are publically available and were downloaded from the IODP Site Survey Data Base (SSDB) for use in this study.

3.2 Sediment Cores

In the summer of 2012 IODP Expedition 342 sailed on the JOIDES Resolution and recovered sediment cores across the study area. Nine drill sites (Sites U1403 – U1411) yielded 25 cored holes with a combined sediment recovery length of nearly 5400 m (Figure 2). Drill sites were selected using the seismic-reflection data described above to target Paleogene sediments and were drilled along depth transects in order to account for stratification of seawater and changes in ocean chemistry through the Paleogene. Four drill sites targeted drifts on the JAR (Figure 2; Figure 3) and the remaining five targeted SENR drift accumulations (Figure 2; Figure 4) (Norris et al., 2014). Relatively high accumulation rates in drift systems can result in a relatively high-resolution deep-sea archive of climatic and oceanographic change (Keigwin and Jones, 1989; Norris et al., 2014), which was the primary motivation to drill these sediments during IODP Expedition 342 (Norris et al., 2014).

Sediment cores were acquired using a combination of two tools, the Advanced Piston Corer (APC), and the Extended Core Barrel system (XCB) (Norris et al., 2014). The APC is used to sample soft- to-firm marine sediment and generally yields complete and relatively undisturbed cores. The XCB is used in soft to moderately hard formations, and is typically deployed after sediment recovery using the APC is prevented due to increased formation hardness (Graber et al., 2002). Sediment cores used in this study were recovered from the first hole at each drill site (Hole A); however, at site U1411 core from the second hole (Hole B) was used due to drilling complications with Hole A.

Information on sediment character was documented in descriptive reports by the shipboard scientific party and can be linked to seismic interpretations. Sediment cores have been assigned age values via biostratigraphic data (i.e., calcareous nannofossils, radiolarians, and foraminifera) combined with magnetostratigraphic chron boundaries. Downhole logs are not available for any of the sites as a result of logging operations issues that could not be fixed for the remainder of the expedition (Norris et al., 2014). However, shipboard measurements of physical property data were used to aid the linkage of seismic-reflection data and cores. P-wave values were obtained using a P-wave Caliper (PWC) also known as a split core system, and P-wave Logger (PWL) tool. Generally PWL data do not yield reliable signals (Blum, 1997), and as such have been excluded from this study. PWC data were acquired by transmitting a 500 kHz P-wave pulse across a core split in half along its long axis, and travel time was recorded as the first P-wave signal. Density data were derived using a standard balance to obtain values for mass, and helium pycnometry to obtain values of volume (Blum, 1997). PWC and density data were sampled in 0.5 m increments through the entire length of each core.

4. METHODS

An integrated dataset comprising 56 2-D seismic-reflection profiles along with nine drill sites with a combined length of >5 km of sediment cores were utilized to develop a seismic stratigraphic framework over the JAR and SENR. This framework was then used to facilitate a better understanding of bottom current-controlled deposition and deep-water circulation in the North Atlantic Ocean during the Cenozoic.

4.1 Seismic Stratigraphic Mapping

Vertical and horizontal variations in seismic-reflection facies are interpreted to represent variations in the sediment character and, thus, bottom current energy and sediment availability through time. Differences in amplitude, concordance, and continuity in reflections enable the identification and classification of distinct seismic facies (Sangree and Widmier, 1978; Müller-Michaelis et al., 2013).

Recognition of regionally significant horizons that delineate stratigraphic packages is based on four main criteria: (1) onlap, (2) downlap, (3) apparent truncation,

and (4) seismic facies changes (Figure 5). This method has two main limitations when using this dataset. One limitation is that drill cores do not penetrate all seismic horizons identified, and the other is that all horizons are not mappable on each of the 56 profiles within the spatial resolution of the seismic grid (Table 1; Figure 3; Figure 4). In order to overcome these limitations, seismic stratigraphic units, which are constrained at their tops and bottoms by regionally mappable and datable boundaries, were defined (Figure 5). Seismic stratigraphic interpretations cannot be confidently correlated to the tops of the SENR seamounts and, thus, these regions have been excluded from our interpretation. Schlumberger's seismic interpretation software Petrel® was used to map horizons throughout the study area.

4.2 Tying Borehole to Seismic Data

When integrating a dataset containing both seismic-reflection and sediment core data, one of the most important steps is to bridge the gap between two-way-time (TWT) and depth. Data collected during IODP Expedition 342 does not include any down-hole logs useful for calibration; however, shipboard physical property measurements of P-wave velocity and bulk density were used in place of down-hole measurements to circumvent this problem. These data were used to generate acoustic impedance (i.e., product of density and velocity) logs, which were compared to mapped seismic horizons and provided a connection between time and depth domains (Figure 6). Some horizons are associated with chert-rich intervals; however, individual chert beds typically have thicknesses <10 cm. Because PWC data are sampled at a much coarser resolution (~0.5 m) these beds may not be represented in acoustic impedance logs. Horizons associated with chert have been tied to depth with IODP Expedition 342 descriptive reports that record the observation of chert in core, or drilling disturbances associated with chert beds. Pressure, temperature, and fluid content are altered when core is brought to the surface, and although shipboard conditions vary from down-hole conditions, sediment core data enable a meaningful correlation of depth and time.

4.3 Dating Horizons

Interpreted seismic horizons were assigned ages using temporal control provided by biostratigraphic data (i.e., planktonic nannofossils, radiolarians, foraminifera) and magnetostratigraphic chron boundaries at each drill site (Table 2). Seismic horizons were not penetrated at every drill site because IODP Expedition 342 specifically targeted Paleogene drift accumulations and because sediment thickness is greater than the maximum borehole-penetration depth in many areas (Table 1; Figure 3; Figure 4). Horizons yield different ages at different drill sites due to resolution of age data and presence of hiatuses. Therefore, average ages were calculated for each horizon (Table 2).

4.4 Generating Isochron Maps

Understanding the spatial distribution of sediments with respect to time is a crucial step towards interpreting the dynamics and history of oceanic circulation. Thicknesses between horizons were calculated in Petrel® using the surface attributes process, and were subsequently used to create isochron maps. This process calculates the value in TWT thickness between specified seismic horizons at Common Depth Points (CDP) in each seismic transect, and assigns the calculated thickness attribute to the stratigraphically younger horizon. Computer generated isochron maps were produced with a user-selected convergent interpolation algorithm, which applied 10 smoothing iterations and a filter width of 10. Computer-generated maps are biased to available data because algorithms focus interpretations around seismic transects. In an effort to overcome this limitation, thickness between horizons were converted to points, filtered to every 500th CDP, labeled and displayed, which generated a grid of points with thickness values. Computer-generated isochron maps were overlain with the computer-generated thickness point data grid, and finalized isochron maps were generated by hand contouring. This integrated procedure generated the most accurate representation of sediment thickness distribution.

4.5 Average Unit Velocities

P-wave velocities for each seismic stratigraphic unit were calculated from PWC data measured from a single core with the most extensive and complete record at each

drill site (Table 3). Additionally, an average P-wave velocity was calculated for each seismic stratigraphic unit (Table 3). Calculated average P-wave velocity values were used to determine seismic stratigraphic unit thickness and provided a more accurate representation of sediment cover across the study area.

4.6 Volumetric Sedimentation Rates

Hand-contoured isochron maps were imported into a mapping software package and geo-referenced such that calculation of the area for each contour interval in each seismic unit could be calculated. Areas were summated and multiplied by thickness in order to obtain bulk volume of each seismic stratigraphic unit. Average age spans were used to obtain bulk volumetric accumulation rates by dividing volume by time (Table 4). The shipboard measured dry density data were averaged through each seismic unit and multiplying by volumetric accumulation rates, which resulted in values for sediment mass. This value for sediment mass was then divided by average unit duration to obtain a value for mass accumulation rate (Table 4).

5. RESULTS

5.1 Seismic Stratigraphic Units

Seven distinct seismic facies (Facies A-G) were identified based on variations in seismic-reflection character. The top of each facies was mapped as a horizon (H1-H7), where Horizon H1 corresponds to the top of Seismic Facies A (Figure 5). Each seismic facies and corresponding horizon are not continuously distributed across the study area, with the exception of Seismic Facies A. Seismic Facies A is the acoustic basement, and consequently no underlying seismic facies were identified, making Horizon H1 the oldest regionally mappable horizon. Horizon H6, which marks the upper boundary of Seismic Facies F, does not have a significant spatial distribution, making regional mapping of this horizon impossible within the resolution of our seismic grid. Additionally, drill cores from IODP Expedition 342 specifically targeted Paleogene drift accumulations, and as a consequence, younger seismic horizons (H5 and H6) were not penetrated by drill core and are not directly datable with our dataset (Table 2; Figure 4; Figure 5). It is for these reasons that seismic stratigraphic units used here were defined as stratigraphic packages

that display distinct seismic-reflection character and are constrained at their top and bottom by regionally mappable and datable boundaries. Since seismic horizons are assigned at the top of each seismic facies, and seismic facies are not continuously distributed across the study area, it is common for seismic stratigraphic units to be bound by more than one seismic horizon, depending on the presence of overlying and underlying facies. Five seismic stratigraphic units (Unit 1- Unit 5) identified in this study are described in detail below (Figure 5).

5.1.1 *Seismic Stratigraphic Unit 1*

Seismic Stratigraphic Unit 1 is composed of moderate to high-amplitude continuous to semi-continuous reflectors of Seismic Facies B, which directly overlie the moderate to high-amplitude, chaotic to semi-continuous reflectors of Seismic Facies A (Figure 5). The base of Seismic Stratigraphic Unit 1 is a conformable, but rough, boundary defined as Horizon H1. Because Horizon H1 marks the top of the acoustic basement, and is the only horizon mappable across the entire study area, it should be noted that the spatial distribution of Horizon H1 is much greater than the distribution of Horizon H2, which marks the upper boundary of Seismic Facies B (Figure 7). Internal reflectors of Seismic Facies B are commonly observed downlapping and onlapping Horizon H1 in multiple directions across the JAR and SENR (Figure 7; Figure 8; Figure 9). The boundary between Seismic Facies A and B has been assigned an age of 115 ± 3 Ma based on data from the core obtained at DSDP Drill Site 384 (Tucholke et al, 1979) (Table 2). Horizon H1 is observed at a minimum depth of 3.26 sec two-way-time (TWT) over the SENR seamounts, and at a maximum depth of 7.90 sec TWT. Overall Horizon H1 has been observed extending into deeper water away from the crest of the JAR and SENR in multiple directions.

The upper boundary of Seismic Stratigraphic Unit 1 is marked with a sharp contact identified by a moderate to high-amplitude, continuous to semi-continuous reflector that is defined as Horizon H2. Depending on the spatial distribution of overlying facies, either Seismic Facies C or Seismic Facies D is observed directly overlying Horizon H2 (Figure 7). Horizon H2 gently dips toward the southern portion of the study area where it commonly downlaps (Figure 7), and in other cases onlaps onto Horizon H1

(Figure 8; Figure 9). Horizon H2 is observed at a minimum depth of 3.90 sec TWT, and at a maximum depth of 7.73 sec TWT. In some areas the internal reflectors of Seismic Facies B are truncated by Horizon H2, which is a prominent characteristic used to identify and map this horizon (Figure 7). Horizon H2 was penetrated only at IODP Expedition 342 Site U1407, at a depth of 228.72 m. The presence of calcareous nannofossils and planktonic foraminifera allows an age of 93.53 Ma to be assigned to this horizon, which indicates that Seismic Stratigraphic Unit 1 spans 21.47 ± 3 myr (Figure 10). Seismic Stratigraphic Unit 1 thickens to >0.4 sec TWT and thins below the resolution of our seismic-reflection data.

Seismic Facies A is interpreted as volcanic basement, and the irregular boundary between Seismic Facies A and Seismic Facies B, defined as Horizon H1, is interpreted to be topography inherited from the volcanic origin of the SENR and JAR. Drill core from DSDP Site 384 on the JAR confirms that Seismic Facies A is composed of basalt (Tucholke et al, 1979). Shallow-water carbonate reefs recovered in this core directly above the basalt provide evidence that the SENR and JAR were exposed to shallower-water environments early after their formation (Tucholke et al, 1979). Additionally, IODP Expedition 342 Site U1407A recovered shallow-water carbonates of Albian age above the volcanic basement that are interpreted to represent carbonate reefs and other localized carbonate build-ups (Norris et al., 2014). Localized carbonate build-ups and reefs display similar seismic-reflection character to volcanic basement and may be included below Horizon H1. Seismic Facies B displays an interbedded appearance of high- to moderate-amplitude, continuous to semi-continuous reflectors, which are interpreted as interbedded pre-contourite-drift accumulations of hemipelagic to pelagic sediment. Lithologic descriptions from descriptive core reports confirm that Seismic Facies B, and thus, Seismic Stratigraphic Unit 1, is composed primarily of chalk with rare intervals of organic-rich claystone and displays alternating beds of lighter and darker sediment (Norris et al., 2014). The moderate to high-amplitude reflector associated with Horizon H2 is interpreted to be a thin, regionally continuous chert-rich interval. Descriptive reports from IODP Expedition 342 drill site U1407 document a thin chert bed at 228.72 m with a thickness <3 cm that has been linked to Horizon H2.

5.1.2 *Seismic Stratigraphic Unit 2*

Seismic Stratigraphic Unit 2 is composed entirely of moderate- to high-amplitude semi-continuous to chaotic reflectors of Seismic Facies C (Figure 5). Depending on the spatial distribution of Horizon H2, the lower boundary of Seismic Stratigraphic Unit 2 is defined by either Horizon H1 or Horizon H2 (Figure 8). Internal reflectors of Seismic Facies C are frequently observed onlapping Horizon H1 and Horizon H2, and are observed downlapping Horizon H2 (Figure 8). As a result of Horizon H2 onlapping and downlapping Horizon H1, the lower boundary of Seismic Stratigraphic Unit 2 is assigned an age of 93.53 Ma. This infers that in locations where Seismic Stratigraphic Unit 2 directly overlays Horizon H1, sedimentation of Seismic Faces B was minimal or nonexistent before the Turonian.

The upper boundary of Seismic Stratigraphic Unit 2 is marked with a moderate- to high-amplitude semi-continuous reflector, which has been defined as Horizon H3. This boundary commonly marks a sharp transition into overlying seismic facies; however, in some areas, this boundary contains notable erosional features that truncate internal reflectors of Seismic Stratigraphic Unit 2. In most locations, internal reflectors of Seismic Stratigraphic Unit 2 run roughly parallel to Horizon H3 (Figure 7; Figure 8; Figure 9). Horizon H3 gently dips toward the south where it downlaps onto Horizon H2, causing a tapering of Seismic Stratigraphic Unit 2 with increasing depth (Figure 7). IODP Expedition 342 drill core penetrate Horizon H3 at Drill Site U1403, U1406, U1407, U1408, U1409, and U1410 (Figure 3; Figure 4). Calcareous nannofossils biostratigraphy at these drill sites suggests that Horizon H3 spans an age range from 46.92 to 53.70 Ma. Age-depth models show that Horizon H3 is commonly associated with a hiatal surface that spans up to 7.5 myr (Figure 10). Horizon H3 has been assigned an average age of 50.31 ± 3.39 Ma, yielding an average age span of 43.22 ± 3.39 myr for Seismic Stratigraphic Unit 2. At the deepest point, Horizon H3 reaches 7.66 sec TWT and is documented as shallow as 3.93 sec TWT. Seismic Stratigraphic Unit 2 reaches a maximum thickness exceeding 0.4 sec TWT and thins to a thickness below the resolution of seismic data. Seismic Stratigraphic Unit 2 commonly displays a variable response on acoustic impedance logs generated from shipboard measurements of physical property data (Figure 6).

Seismic Facies C is interpreted to be associated with pre-contourite-drift accumulations of interbedded pelagic sediment. Descriptive reports from IODP Expedition 342 drill cores that penetrate Seismic Facies C confirm that Seismic Stratigraphic Unit 2 is composed of nannofossil ooze and biosiliceous ooze, which is commonly interbedded with chert (Norris et al., 2014). The moderate- to high-amplitude continuous reflector defined as Horizon H3 is associated with a regionally mappable chert bed. IODP drilling reports, and descriptive reports from core show that a regionally mappable chert bed <10 cm in thickness is responsible for the impedance contrast associated with Horizon H3. This boundary is commonly associated with a hiatus that spans up to 7.5 myr (Norris et al., 2014) and has been interpreted to represent a diagenetic boundary (Tucholke, 1981) between chert and underlying biosiliceous oozes (Norris et al., 2014). Rare erosional scours are observed cutting into Horizon H3 and truncating the internal reflectors of Seismic Stratigraphic Unit 2, and are interpreted to be the result of increased bottom current energy.

5.1.3 *Seismic Stratigraphic Unit 3*

Seismic Stratigraphic Unit 3 is composed entirely of low-amplitude transparent internal reflectors of Seismic Facies D. Seismic Facies D commonly overlies Seismic Facies C and Seismic Facies A but rarely overlies Seismic Facies B (Figure 3; Figure 7; Figure 8; Figure 9). Depending on the distribution of underlying horizons, the bottom boundary of Seismic Stratigraphic Unit 3 is commonly marked by Horizon H1 or Horizon H3, and rarely by Horizon H2 (Figure 7). In several areas Horizon H3 downlaps and onlaps Horizon H2 while Horizon H2 onlaps and downlaps Horizon H1. Consequently the bottom boundary of Seismic Stratigraphic Unit 3 has been dated to 50.31 ± 3.39 Ma, the age assigned to Horizon H3. Where Seismic Facies D directly overlies Seismic Facies A, sediment accumulation between 115 ± 3 Ma and 50.31 ± 3.39 is negligible and does not make up a significant component of Seismic Stratigraphic Unit 3. Internal reflectors of Seismic Facies D rarely display more apparent seismic-reflection character and are observed onlapping Horizon H3 (Figure 9).

The upper boundary of Seismic Stratigraphic Unit 3 is defined as Horizon H4, which marks the upper limit of Seismic Facies D (Figure 5). Delineation of the boundary

between Seismic Facies D and overlying Seismic Facies E can prove difficult, as the boundary is gradational. Horizon H4 is commonly picked at a boundary identified by subtle variations in seismic-reflection character. Seismic Facies F and Seismic Facies G overlie Seismic Facies D in locations where Seismic Facies E is not present. In many areas Seismic Stratigraphic Unit 3 displays a mounded morphology parallel to bathymetric contours (Figure 7). Depth to Horizon H4 varies from 3.877 sec TWT to 7.577 sec TWT across the SENR and JAR.

Horizon H4 was penetrated at IODP Expedition 342 Sites U1403A, U1404A, U1406A, U1407A, U1408A, U1409A, U1410A, and U1411A (Figure 3; Figure 4). Calcareous nannofossil biostratigraphy and chron boundaries in sediment cores suggest that Horizon H4 spans from 25.91 to 34.44 Ma, and has been assigned an average age of 30.22 ± 4.23 Ma, which assigns Seismic Stratigraphic Unit 3 an average age span of 20.09 ± 7.62 myr (Figure 10). Seismic Stratigraphic Unit 3 thickens across the JAR and SENR to >1.0 Sec TWT and thins below the vertical resolution of the seismic data. Acoustic impedance logs, generated from shipboard measured density and velocity data from cores, show that acoustic impedance logs between Horizon H4 and Horizon H3 have less variability than acoustic impedance logs below Horizon H3 (Figure 6). There is a gradual increase in acoustic impedance at drill sites U1404A and U1406A on the JAR, which is associated with Horizon H4 (Figure 6).

The low-amplitude transparent reflectors of Seismic Facies D are interpreted to represent highly bioturbated muddy drift deposits. Drill cores from IODP Expedition 342 show that Seismic Unit 3 is composed of nannofossil clay, nannofossil ooze, and biosiliceous ooze (Norris et al., 2014). The homogeneous and therefore transparent seismic-reflection character associated with Seismic Facies D is interpreted to be a result of significant Bioturbation that destroyed the primary sedimentary fabric. Horizon H3 is associated with a period of non-deposition, and in some areas is marked with erosional features, that are interpreted to be a result of bottom current activity. Sediment bodies of Seismic Stratigraphic Unit 3 are commonly mounded and parallel to bathymetric contours, which is a diagnostic criterion for the identification of contourite drifts (Faugères at al., 1999; Rebesco and Stow, 2001). Mounded drift features of seismic

facies D overlying the hiatal surface of Horizon H3 are interpreted to represent the onset of bottom current-controlled sedimentation on the JAR and SENR.

5.1.4 *Seismic Stratigraphic Unit 4*

Seismic Stratigraphic Unit 4 is composed of moderate- to low-amplitude concordant wavy reflectors of Seismic Facies E, along with moderate- to high-amplitude parallel- to semi-continuous reflectors of Seismic Facies F. Because IODP Expedition 342 targeted Paleogene drift accumulations, Horizon H6, which marks the upper limit of Seismic Facies F, was not penetrated, and as such is not datable (Figure 3; Figure 4). Therefore Seismic Stratigraphic Unit 4 is composed of Seismic Facies E and Seismic Facies F, which are constrained at their top and bottom by regionally mappable and datable boundaries.

Horizon H4 marks the bottom boundary of Seismic Stratigraphic Unit 4 in locations where Seismic Facies D is overlain by Seismic Facies E or Seismic Facies F (Figure 5; Figure 7; Figure 8; Figure 9). Internal wavy reflectors of Seismic Facies E are commonly observed onlapping Horizon H4 toward the north (Figure 7). The wavy reflectors of Seismic Facies E are not present on the SENR in close proximity to the seamounts in water depths above ~3500 m. Seismic Facies F commonly occurs in mounded sediment bodies in close proximity to the SENR seamounts, and internal reflectors of this unit are observed onlapping Horizon H4 (Figure 7; Figure 9). As a result, Seismic Stratigraphic Unit 4 is entirely composed of Seismic Facies F in close proximity to the SENR seamounts.

The upper limit of Seismic Facies E is defined as Horizon H5, which is marked by erosional scours filled with Seismic Facies G, sharp contacts between Facies E and G, or the ocean-sediment interface. Internal wavy reflectors of Seismic Facies E are commonly observed onlapping Horizon H4 toward the north in the up-slope direction (Figure 7). Sediment bodies composed of Seismic Facies E are frequently observed as mounded bodies that taper up-slope and down-slope (Figure 7). Horizon H5 spans from 3.63 sec TWT to 7.22 sec TWT. Horizon H5 and is not datable with IODP Expedition 342 cores; however, an age of 2.6 Ma has been inferred. This age is justified based on similarities in seismic-reflection (Arthur et al., 1989; Müller-Michaelis et al., 2013) and sediment

character (Driscoll and Haug, 1998), between Seismic Facies G and units discussed in other North Atlantic studies (Arthur et al., 1989; Driscoll and Haug, 1998; Müller-Michaelis et al., 2013). Horizon H6 marks the upper boundary of Seismic Facies F and is commonly observed downlapping Horizon H4 (Figure 9). Internal reflectors of Seismic Facies F are observed to be truncated by Horizon H6, which is a key criterion used for the identification of Horizon H6 (Figure 9). Horizon H6 spans a depth between 4.02 sec TWT and 5.34 sec TWT across the SENR and was not assigned an age because IODP Expedition 342 cores did not penetrate this horizon. Depending on the spatial distribution of Seismic Facies E and Seismic Facies F, the upper boundary of Seismic Stratigraphic Unit 4 is marked by either Horizon H5 or Horizon H6. Seismic Stratigraphic Unit 4 thickens to >1.10 sec TWT and thins to a thickness below the vertical resolution of seismic data.

Seismic Facies E is interpreted to be composed of drift deposits containing mud waves, that were deposited under higher energy conditions than Seismic Facies D. IODP Expedition 342 drill core confirm that Seismic Facies E is composed primarily of clay and nannofossil ooze (Norris et al., 2014). Moderate- to high-amplitude parallel semi-continuous internal reflectors of Seismic Facies F are interpreted to be associated with levee drift deposits likely composed of mud- to silt-sized sediment. However, IODP Expedition 342 drill cores did not penetrate Seismic Facies F therefore this interpretation cannot be confirmed. Sediment waves observed in Seismic Facies E suggests that a force capable of reworking and depositing sediment was active during their formation. Additionally, the mounded nature of Seismic Facies E is diagnostic of contourite drifts (Faugères at al., 1999; Rebesco and Stow, 2001). Internal wavy reflectors of Seismic Facies E onlap Horizon H4 toward the north, and are absent on the SENR in close proximity to the seamounts, suggesting a shift in intensity and focus of bottom current activity from shallower to deeper depths. The gradual nature of the transition from Seismic Faces D to Seismic Facies E suggests a constant and steady increase in current strength, as opposed to a rapid transition. In locations where internal reflectors of Seismic Facies E onlap Horizon H4, the transition from Seismic Facies D to Seismic Facies E appears to be more abrupt. Mounded and tapered morphologies of Seismic Facies F occur in close proximity to the SENR seamounts, suggesting that these features were formed by

the interaction of bottom currents with the SENR seamounts. The bottom boundary of Seismic Stratigraphic Unit 4 has been assigned an age of 30.22 ± 4.23 and the upper boundary has an inferred age of 2.6 Ma, which gives Seismic Stratigraphic Unit 4 an age span of 27.62 ± 4.23 myr. Seismic Stratigraphic Unit 4 thickens across the JAR and SENR to <1.1 Sec TWT and thins below the vertical resolution of our seismic data.

5.1.5 Seismic Stratigraphic Unit 5

Seismic Stratigraphic Unit 5 is composed entirely of high-amplitude parallel reflectors of Seismic Facies G (Figure 5). Seismic Facies G is commonly observed overlying Seismic Facies D, Seismic Facies E, or Seismic Facies F across the JAR and SENR (Figure 7; Figure 8; Figure 9). The lower boundary of Seismic Stratigraphic Unit 5 is defined by Horizon H4, Horizon H5, or Horizon H6 depending on their spatial distribution. The bottom boundary of Seismic Stratigraphic Unit 5 is marked with erosional depressions, and internal reflectors of Seismic Facies G are commonly observed onlapping this boundary and infilling the erosional features (Figure 7; Figure 8; Figure 9). Where erosional features are absent, Seismic Facies G appears to be draping over underlying units. This characteristic is particularly pronounced where Seismic Facies G directly overlies the mounded levee drifts of Seismic Facies F (Figure 9). In close proximity to the SENR seamounts, Seismic Facies G accumulates into mounded drift bodies that are notable but not defining features of Seismic Stratigraphic Unit 5.

The upper boundary of Seismic Stratigraphic Unit 5 is marked by a high-amplitude continuous reflector, which has been defined here as Horizon H7. This upper boundary appears to be a smooth and continuous high-amplitude horizon, which occurs at the ocean-sediment interface. Seismic Facies G thickens to >400 ms TWT and thins below the vertical resolution of the seismic data. In areas where Seismic Facies G thins below the vertical resolution of the seismic data, it has been excluded from seismic stratigraphic mapping. Consequently, both Horizon H5 and Horizon H7 are commonly observed at the ocean-sediment interface (Figure 8; Figure 7). Internal reflectors of Seismic Facies G onlap Horizon H5, which has been assigned an age of 2.6 Ma, as discussed in above section. In locations where Horizon H5 is at the ocean-sediment interface it is assumed that the deposition of Seismic Facies G has been negligible since

the Pleistocene. Horizon H7 is commonly observed onlapping and downlapping Horizon H5 at the ocean-sediment interface, and has been assigned an age of 0 Ma (modern). The total duration of Seismic Stratigraphic Unit 5 is 2.6 myr. Horizon H7 is observed at depths between 3.62 sec TWT and 7.15 sec TWT across the JAR and SENR.

Internal reflectors of Seismic Stratigraphic Unit 5 are interpreted to represent post-contourite-drift pelagic to hemipelagic and ice-rafted sediment accumulation during the Pleistocene. Drill cores from IODP Expedition 342 confirm that Seismic Facies G is primarily composed of clay, foraminiferal sand, and nannofossil ooze (Norris et al., 2014). Additionally, sediment cores yield isolated outsized clasts ranging in size from coarse sand to cobble that are interpreted to be ice-rafted detritus (Norris et al., 2014). Erosional scours are interpreted to be a result of increased bottom current intensity, and sedimentary deposits are interpreted to be a mix of ice-rafted debris and sediment deposited by oceanic currents. Increased contribution from ice-rafted debris combined with glaciogenic hemipelagic sedimentation complicates the signature of bottom current-controlled sedimentation.

5.2 Isochron Mapping and Depositional Interpretation

Isochron mapping of the aforementioned seismic stratigraphic units indicates distinct changes in contourite depocenters and morphology through time (Figure 11). Seismic Stratigraphic Unit 1 spans an age from 115 to 93.53 Ma, and displays a maximum thickness of 400 ms TWT on the SENR in close proximity to the seamounts. Toward the west, over the JAR, are two distinct accumulations with thicknesses below ~250 ms TWT. There is an isolated occurrence of Seismic Facies B observed solely in Seismic Line L049 south of the SENR seamounts that displays a thickness equivalent to accumulations observed on the JAR (Figure 11). Isochron mapping determines that Seismic Stratigraphic Unit 1 covers an area of ~14,500 km^2, making this seismic stratigraphic unit the least spatially extensive (Figure 11).

Isochron mapping of Seismic Stratigraphic Unit 2, which spans from 93.53 to 50.31 Ma, shows an increase in the spatial distribution of sediment to the west, east, and south of the SENR seamounts (Figure 11). Maximum unit thickness (~400 ms TWT) occurs in the northern half of the study area in two locations that are in close proximity to

the SENR seamounts (Figure 11). The areal extent of Seismic Stratigraphic Unit 2 exceeds that of Seismic Stratigraphic Unit 1 three-fold, spanning an area of ~44,500 km^2. Seismic Stratigraphic Unit 2 is thinly developed or absent in the south central portion of the study area.

Seismic Stratigraphic Unit 3 has a maximum unit thickness of ~1000 ms TWT, 2.5 times the maximum thickness of either Seismic Stratigraphic Unit 2 or Seismic Stratigraphic Unit 1 (Figure 11). Seismic Stratigraphic Unit 3 depocenters occur over the SENR along the southeastern boundary of the study area (Figure 11). An isolated deposit, reaching nearly 900 ms TWT in thickness, occurs in the south below the SENR seamounts and connects with the southeastern depocenter through a subtle northwest-southeast trending belt (Figure 11). Sediment thickness decreases toward the north and south perpendicular to the northwest-southeast trend of this belt. This sedimentary belt terminates at the eastern extent of the SENR (Figure 11). Basement highs observed in seismic-reflection profiles are commonly associated with locations of non-deposition. During this time interval, between 50.31 and 30.22 Ma, the spatial distribution of sediment cover is the most extensive, reaching an area of ~60,000 km^2 (Figure 11).

Seismic Stratigraphic Unit 4 spans from 30.22 to 2.6 Ma, covers an area of ~49,000 km^2, and yields a maximum unit thickness of ~1100 ms TWT, which makes it the thickest mapped seismic stratigraphic unit in this study (Figure 11). Sedimentation occurs in a well-defined bathymetric contour-parallel belt, which displays an east-west trend over the SENR, and gently curves toward a northwest-southeast trend between the SENR and JAR (Figure 11). Five isolated depocenters occur along this belt, and sediment thickness decreases perpendicular to trend. There are a few isolated deposits of Seismic Stratigraphic Unit 4 that are composed entirely of Seismic Facies F in close proximity to the SENR seamounts (Figure 11). Few localized points of non-deposition correspond to bathymetric highs (Figure 11).

Deposition of Seismic Stratigraphic Unit 5 occurred from 2.6 Ma to present and is focused in the northern half of the study area (Figure 11). Maximum sediment thickness is documented at ~400 ms TWT in two depocenters; one along the northern extent of the seismic grid and the other along the eastern limit of the seismic grid. Several localized accumulations of sediment with thickness <350 ms TWT are observed around the SENR

seamounts (Figure 11). To the southeast of the depocenter located along the eastern extent of the seismic grid is a ~75 km long and ~25 km wide location where Seismic Stratigraphic Unit 5 is absent, which corresponds to a bathymetric high (Figure 11). Along the southern extent of the seismic grid, in the center of the study area, is a location of sediment accumulation with a maximum thickness of ~350 ms TWT that does not follow the dominant trend of northern-focused deposition during Seismic Stratigraphic Unit 5 (Figure 11). Sediment accumulations thin and eventually pinch out over the JAR toward the west. Seismic Stratigraphic Unit 5 covers a spatial distribution of ~35,700 km^2.

Seismic Stratigraphic Unit 1 and Seismic Stratigraphic Unit 2 represent pre-contourite-drift accumulations of marine sediments. The presence of depocenters in close proximity to the SENR seamounts, along with the lack of spatial distribution in the south, suggest that deposition of Seismic Stratigraphic Units 1 and 2 were focused in the northern half of the study area. The boundary between Seismic Stratigraphic Unit 2 and Seismic Stratigraphic Unit 3 represents the onset of drift accumulation. At this boundary, depocenter thickness increased by over 250%, spatial coverage reached its maximum, and the depocenters shifted toward the southeastern boundary of the seismic grid (Figure 11). Interpretations of 2-D seismic-reflection profiles indicate that the transition from Seismic Stratigraphic Unit 3 to Seismic Stratigraphic Unit 4 represents a shift in focus of deposition and, thus, bottom current activity, from shallower to deeper depths (Figure 7). The decreased spatial distribution of Seismic Stratigraphic Unit 4 compared to Seismic Stratigraphic Unit 3, the well-defined belt-like morphology of Seismic Stratigraphic Unit 4, and the lack of sediment deposition around the SENR seamounts, corroborates the interpretation of a shift in focus of bottom current activity toward the south. The boundary between Seismic Stratigraphic Unit 4 and Seismic Stratigraphic Unit 5 marks a transition of deposition back toward shallower depths in the northern half of the study area (Figure 11). The boundary between Seismic Stratigraphic Unit 4 and Seismic Stratigraphic Unit 5 represents a shift from dominantly bottom current-controlled sedimentation to a combination of fine-grained glacial outwash and ice-rafted detritus from the Newfoundland and Nova Scotia margin with continued bottom-current-influenced sedimentation.

5.3 Volumetric and Mass Accumulation Rates

Linear sediment accumulation rates determined from sediment core are biased to the sedimentary record recovered at specific drill sites. Interpretations based on linear rates alone can be misleading in systems where locations of sedimentation change through time, such as those under the influence of bathymetric contour parallel currents. Volumetric accumulation rates (VARs) and mass accumulation rates (MARs) yield a more complete representation of sedimentation within a dynamic system. Isochron mapping along with shipboard measured physical property data allow for the determination of VARs and MARs for each seismic stratigraphic unit. VARs and MARs have been summarized in Table 4, and in Figure 12.

The boundary between Seismic Stratigraphic Unit 2 and Seismic Stratigraphic Unit 3 displays a five-fold increase in VARs and MARs, which has been associated with the onset of contourite drift formation (Figure 12). The transition from Seismic Stratigraphic Unit 3 to Seismic Stratigraphic Unit 4 displays a slight decrease of ~7% in VARs (Figure 12). Linear sedimentation rates suggest that the transition between Seismic Stratigraphic Unit 3 and Seismic Stratigraphic Unit 4 represents a sharp decline in sedimentation (Figure 10) (Norris et al., 2014). The transition from Seismic Stratigraphic Unit 4 to Seismic Stratigraphic Unit 5 is characterized by an approximately two-fold increase in VARs and MARs (Figure 12); however, linear sedimentation rates suggest little to no sedimentation at several drill sites during this period (Figure 10) (Norris et al., 2014).

6. DISCUSSION

6.1 Sediment Accumulation Phases

Three primary phases of sedimentation have been identified over the SENR and JAR through seismic stratigraphic mapping. These three phases are here termed 1) Pre-Contourite-Drift Phase, 2) Active-Contourite-Drift Phase, and 3) Post-Contourite-Drift Phase, and described below. Seismic Stratigraphic Unit 1 and Seismic Stratigraphic Unit 2, which are characterized by moderate- to high-amplitude semi-continuous reflectors, represent the Pre-Contourite-Drift Phase (115 to 50.31 Ma). Drill cores from IODP Expedition 342 show that Seismic Stratigraphic Unit 1 and Seismic Stratigraphic Unit 2

are composed of interbedded hemipelagic to pelagic sediments dominated by calcareous chalk/ooze and radiolarian-rich claystone/clay (Norris et al., 2014). Depocenters during the Pre-Contourite-Drift Phase are located in the north within close proximity to the SENR seamounts (Figure 11). During the deposition of Pre-Contourite-Drift Phase sediments the basaltic basement composing the SENR and JAR was warmer and more buoyant due to its young age. Consequently, these positive bathymetric features were exposed to shallower water depths, and likely above the Carbonate Compensation Depth (CCD) at this time.

The second phase of sedimentation is the Active-Contourite-Drift Phase (50.31 to 2.6 Ma), which consists of a composite contourite drift body, and is composed of Seismic Stratigraphic Unit 3 and Seismic Stratigraphic Unit 4. Lithologic data show that these units are composed of nannofossil ooze, biosiliceous ooze, and clay, which generally become less calcareous in the younger parts of the drift complex (Norris et al., 2014). Seismic-reflection profiles display diagnostic slope-parallel mounded features along with a gradational contact between transparent reflectors of Seismic Facies D and the wavy reflectors of Seismic Facies E (Figure 7; Figure 8). Internal wavy reflectors are also observed to abruptly onlap Seismic Stratigraphic Unit 3 toward the north in the up-slope direction (Figure 7).

Active-Contourite-Drift Phase accumulations form belt-like features, which parallel bathymetric contour parallel currents, and show thicknesses decreasing perpendicular to the major trend of these features (Figure 11). Rebesco and Stow (2001) interpreted drift elongation to generally occur in a down-current direction, suggesting that the Newfoundland Ridge drift complex was deposited under a general east-west trending current regime (Figure 11). Isolated mounded deposits of Seismic Facies F, within Seismic Stratigraphic Unit 4, provide evidence toward smaller-scale shifting and localized build-ups in close proximity to the SENR seamounts (Figure 11). These smaller-scale features may be a result of bathymetric contour current dynamics, such as eddies, that generally produce features that occur at scales below the resolution of the seismic-reflection data. Accumulations deposited during the Active-Contourite-Drift Phase are more spatially extensive and depocenters had shifted toward the southern half of the study area relative to the Pre-Contourite-Drift Phase deposits (Figure 11).

The third and final phase of sedimentation is the Post-Contourite-Drift Phase (2.6 Ma to present), which is represented solely by Seismic Stratigraphic Unit 5. Seismic-reflection profiles show Post-Contourite-Drift Phase accumulations are composed of continuous high-amplitude parallel reflectors. Internal reflectors are commonly observed onlapping and draping over Active-Contourite-Drift Phase packages, as well as infilling depressions (Figure 7; Figure 8; Figure 9). Deposits of Seismic Stratigraphic Unit 5 form mound-like morphologies in close proximity to the SENR seamounts that represent a minor component of Post-Contourite-Drift Phase sediment. Lithologic descriptions from core data show that this unit is composed of clay, foraminiferal sand, nannofossil ooze, and to a lesser extent ice-rafted debris (Norris et al., 2014). Accumulation of Post-Contourite-Drift Phase sediment is less spatially extensive than Active-Contourite-Drift sediments, and deposition has shifted back toward the north, in close proximity to the SENR seamounts (Figure 11). The paucity of depositional features diagnostic of contourite drifts in Seismic Stratigraphic Unit 5 leads to the definition of the Post-Contourite-Drift Phase. However, the full extent by which Post-Contourite-Drift Phase sediments are reworked by the DWBC remains uncertain.

6.2. Onset of Drift Accumulation and Deep-Water Circulation

The transition from Pre-Contourite-Drift Phase sedimentation to Active-Contourite-Drift Phase sedimentation, and hence the onset of drift accumulation, is represented by Horizon H3. Age-depth plots (Figure 10) show that Horizon H3 commonly is associated with a hiatal surface and linear sedimentation rates <1 cm/kyr (Norris et al., 2014). Regional unconformities have been documented at the base of contourite drift accumulations elsewhere and are interpreted to reflect significant intensification of, or changes to, oceanic circulation patterns (Faugères et al., 1999; Rebesco and Stow, 2001; Molina et al., 2008). Horizon H3 has been dated in this study to 50.31 ± 3.39 Ma and is interpreted to define the onset of significant bottom current activity and, thus, deep-water driven by thermohaline circulation in the North Atlantic Ocean. Hohbein et al. (2012) suggested that deep-water formed in the Norwegian-Greenland Sea began to spill over the Greenland-Scotland Ridge as early as 50-49 Ma based on seismic stratigraphic evidence recorded within the Judd Falls Drift. Modern

deep-water formed in the Norwegian-Greenland Sea constitutes a significant component of the Deep Western Boundary Current (Pickart, 1992; Hansen and Østerhus, 2000). It is hypothesized here that the contribution of Norwegian-Greenland outflow water into the North Atlantic Ocean played a role in the reorganization of oceanic circulation patterns represented by Horizon H3.

The reorganization of oceanic circulation associated with Horizon H3 correlates temporally with a period of long-term elevated global temperatures known as the early Eocene Climatic Optimum (EECO) (53-51 Ma) (Figure 12) (Greenwood and Wing, 1995; Zachos et al., 2001; 2004; 2008; Hyland and Sheldon; 2013). Elevated temperatures during the EECO have been linked to increased volcanic and metamorphic outgassing of CO_2 and other greenhouse gasses related to the Himalayan orogeny (Kent and Muttoni, 2008). A long-term (~19 myr) global cooling trend initiated at the end of the EECO, and marks a transition period from greenhouse to icehouse conditions (Bohaty and Zachos, 2003; Jovane et al., 2007). The causal relationship between long-term cooling and oceanic circulation at ~50 Ma remains uncertain; however, there is a strong temporal correlation between the onset of deep-water formation driven by thermohaline circulation and the overall cooling trend that initiated at the end of the EECO and lasted through the Cenozoic (Zachos et al., 2001; 2008).

6.3 Deepening and Intensification of the Deep Western Boundary Current

Horizon H4 (30.22 ± 4.23 Ma) marks the transition from Seismic Stratigraphic Unit 3 to Seismic Stratigraphic Unit 4, and represents an increase in current energy and focus, along with a deepening of the current path, all of which persisted until 2.6 Ma (Figure 7). The boundary between Seismic Stratigraphic Unit 3 and Seismic Stratigraphic Unit 4 is commonly gradational (Figure 8). This gradational contact between these two seismic stratigraphic units represents a transition from transparent reflectors of Seismic Facies D to the wavy reflectors of Seismic Facies E, and therefore is interpreted as an increase in current energy. Internal reflectors of Seismic Facies E abruptly onlap Horizon H4 in the up-slope direction over the SENR and suggests a deepening of current path toward the south (Figure 7). This shift in current path and intensity is also observed in isochron maps, where deposition of Seismic Stratigraphic Unit 4 shifts toward the south

away from the SENR seamounts (Figure 11). This interpreted shift in current path is synchronous with the formation of a well-developed sediment belt (Figure 11). It is uncertain if the abrupt boundary between Seismic Stratigraphic Unit 3 and Seismic Stratigraphic Unit 4 (Figure 7) represents an erosional surface, a shift in the depth of the CCD, or a combination of factors.

Horizon H4 (30.22 ± 4.23 Ma) corresponds closely to the Eocene-Oligocene boundary (~34 Ma) (Figure 12), which marks the beginning of Cenozoic icehouse conditions, the formation of southern hemisphere continental ice-sheets (DeConto and Pollard, 2003; Zachos and Kump, 2005; Lie et al., 2009), and the opening of the Tasmania-Antarctic and Drake passageways (Zachos et al., 2001; Scher and Martin, 2006). South of the Newfoundland Ridge Drift Complex, increased bottom current intensity at the Eocene-Oligocene boundary has been associated with a widespread deep-sea unconformity that, in some areas of the continental rise off the eastern United States, removed older strata by erosion (Tucholke, 1981; Mountain and Tucholke, 1985). Additionally, during this time interval the ocean experienced high magnitude fluctuations in eustatic sea level (Miller et al., 2005) and a ~1 km deepening of the CCD (Diester-Haass and Zahn, 1996). This evidence suggests that controls driving the deepening and intensification of the DWBC affected sedimentation across the North Atlantic, and were not restricted to the SENR and JAR.

6.4 Regional Implications

Seismic horizons that are continuous across contourite drift complexes represent changes in the structure of thermohaline circulation (Faugères et al., 1999). Previous seismic stratigraphic studies in the North Atlantic Ocean have documented the presence of prominent seismic horizons in sedimentary deposits influenced by bottom currents and have related their formation to thermohaline forcings (Table 5) (Tucholke, 1981; Mountain and Tucholke 1985; Arthur et al., 1989; Davies et al., 2001; Hohbein et al., 2012; Müller-Michaelis et al., 2013). These studies focused on areas north and south of the Newfoundland Ridge Drift Complex and, as such, this research allows for a correlation between these other studies and facilitates a more robust understanding of the sedimentary evolution of the North Atlantic Ocean Basin. Here, we investigate to what

extent Horizons H3, H4, and H5/H6 fit into an established framework of the evolution of the North Atlantic from other seismic stratigraphic studies (Table 5).

Horizon H3 (50.31 ± 3.39 Ma) is identified in seismic-reflection profiles as a continuous moderate- to high-amplitude reflector. Sediment cores obtained during IODP Expedition 342 show that Horizon H3 correlates with a chert-rich interval, and age-depth plots show a correlation with a hiatus that spans up to 7.5 Ma (Norris et al., 2014) (Figure 10). This boundary represents a transition from Seismic Facies C, which is composed of nannofossil ooze and biosiliceous ooze commonly interbedded with chert, to Seismic Facies D, which is composed of nannofossil clay, nannofossil ooze, and biosiliceous ooze. Horizon A^C identified by Tucholke (1981) and Mountain and Tucholke (1984), south of the JAR and SENR, is associated with a chert bed that dates from the early to middle Eocene (Tucholke, 1981; Mountain and Tucholke 1985; Muttoni and Kent, 2007). North of the JAR and SENR in the Faroe-Shetland Channel, Hohbein et al. (2012) documented the presence of the Intra-Eocene Unconformity (IEU), a prominent seismic horizon, and assigned the IEU an age of 50-49 Ma in the Judd Falls Drift. Hohbein et al. (2012) also discussed the possible correlation of the IEU with the I-Lutetian 3 horizon identified by Smallwood (2004) in the Faroe-Shetland Channel. A close temporal correlation of Horizon H3 with the IEU, I-Lutetian 3, and A^C, along with both Horizon H3 and A^C being associated with a chert horizon, leads to the conclusion that these four horizons were formed under the same shift in the structure of thermohaline circulation (Table 5).

Horizon H4 (30.22 ± 4.23 Ma) is mapped at the boundary between Seismic Stratigraphic Unit 3 and Seismic Stratigraphic Unit 4. Age-depth models determine that Horizon H4 represents a relatively condensed section with sedimentation rates less than 1 cm/kyr over its age range (Figure 10) (Norris et al., 2014). South of the SENR and JAR a seismic horizon, Horizon A^U, has been dated as early Oligocene and has been associated with an unconformable surface that resulted from a swifter, more erosive bottom current (Tucholke, 1981; Mountain and Tucholke, 1985). North of the study area in the Faroe-Shetland Basin, Davies et al. (2001) identified a seismic horizon, Horizon TE, as early Oligocene and associated this horizon with the onset of current-controlled deposition recorded in the Southeast Faroes Drift. Horizon H4, A^U, and TE have similar dates

assigned to their formation, and represent the beginning of a period of increased bottom current activity (Table 5). The formation of these three horizons most likely resulted from the same event of bottom current intensification driven by the intensification of thermohaline circulation. Differences in the characteristics of these horizons are interpreted to be the result of local variations in sedimentary processes associated with this event. However, unlike most areas in the North Atlantic, there is localized early Oligocene sediment accumulation and, thus, a rarely preserved Eocene-Oligocene section on the Newfoundland Ridge, discovered at Site U1411 (Norris et al., 2014).

Horizon H5/H6 (2.6 Ma) represents the upper boundary of Seismic Stratigraphic Unit 4, the base of Seismic Facies G, and is commonly marked with erosional features. Internal reflectors of Seismic Facies G are observed onlapping or draping underlying units, and are primarily composed of clay, foraminiferal sand, and nannofossil ooze, with a lesser concentration of ice-rafted debris. The closing of the Isthmus of Panama near the Pliocene-Pleistocene boundary has been linked with an intensification of Atlantic Ocean thermohaline circulation (Driscoll and Haug, 1998), and at the same time Northern Hemisphere ice sheets significantly expanded (Zachos et al., 2001). A seismic horizon, Horizon R1, has been identified in the Erik Drift (Arthur et al., 1989; Müller-Michaelis et al., 2013), and Gloria Drift (Arthur et al., 1989) north of the JAR and SENR in the Labrador Sea. Horizon R1 has been temporally constrained to the Pliocene-Pleistocene boundary, and is commonly associated with the first appearance of ice-rafted debris, and erosional features (Arthur et al., 1989; Müller-Michaelis et al., 2013). Similarities between Horizon H5/H6 and R1 are interpreted to be the result of the same reorganization of thermohaline circulation in the North Atlantic (Table 5). IODP Expedition 342 drill cores did not penetrate horizon H5/H6, and the hypothesized age of 2.6 Ma for these horizons was inferred from ages assigned to R1 (Arthur et al., 1989; Müller-Michaelis et al., 2013). The boundary between Seismic Stratigraphic Unit 4 and Seismic Stratigraphic Unit 5 marks a decrease in the presence of diagnostic contourite drift features from Active-Contourite-Drift Phase accumulations, suggesting that the reorganization of thermohaline circulation associated with Horizon H5/H6, which has persisted from 2.6 Ma to present, breached a threshold needed for the formation of significant accumulations of contourite drifts.

6.5 Dynamics and Depositional Evolution of Contourite Drifts

Bathymetric contour parallel currents change their path, focus, and intensity through time. Stratigraphic units and their bounding surfaces documented in this study reveal the spatial distribution and associated dynamic depositional evolution of drift deposits (Figure 5). The boundary between Seismic Stratigraphic Unit 2 and Seismic Stratigraphic Unit 3 marks the onset of drift formation over the SENR and JAR. Isochron maps show a poorly defined sediment belt in Seismic Stratigraphic Unit 3, which suggests a broadly focused current path. Seismic-reflection profiles suggest that the transition from Seismic Stratigraphic Unit 3 to Seismic Stratigraphic Unit 4 represents a deepening of current path, and an increase in current intensity. A well-defined sediment belt formed south of the SENR seamounts, and little deposition occurred in close proximity to the SENR seamounts during Seismic Stratigraphic Unit 4 (Figure 11). This shift from Seismic Stratigraphic Unit 3 to Seismic Stratigraphic Unit 4 indicates current path shifted toward the south, while its intensity and focus increased.

Sedimentary systems deposited under the influence of thermohaline-driven currents have morphologies that evolve with changes in global circulatory patterns. When using the sedimentary archive recorded in contourite drifts it is important to consider the dynamic evolution of the system, otherwise conclusions inferred from their sedimentary record may be misleading. For example, initial findings of IODP Expedition 342 show that linear sedimentation rates are commonly the greatest in the center, and decrease toward the flanks of mounded sedimentary drift bodies (Norris et al., 2014). Therefore, linear sedimentation rates obtained from cores represent a history of deposition at a specific site, and are not necessarily representative of the entire system. Thus, if contourite drift complexes are to be drilled as sedimentary archives of paleoceanographic change, their spatial distribution and internal architecture must be considered. Combining seismic stratigraphic interpretation, isochron mapping, and sediment core data allows for more accurate interpretations of the evolution of contourite drift systems.

7. CONCLUSIONS

An integrated dataset containing 2-D seismic-reflection profiles along with temporal and sedimentological data obtained from IODP Expedition 342 drill cores

provides insight toward the evolution of deep-water formation driven by thermohaline circulation and deep-sea sedimentary processes over the J-Anomaly (JAR) and Southeast Newfoundland Ridges (SENR). Results of this study indicate that Horizon H3 (50.31 ± 3.39 Ma) marks the onset of drift accumulation over the JAR and SENR, which is correlative to the onset of long-term global cooling following the Early Eocene Climatic Optimum. Horizon H3 is related to several other seismic stratigraphic horizons identified throughout the North Atlantic and is closely related to the earliest evidence of a deep-water contribution from the Norwegian-Greenland Sea into the North Atlantic Ocean (Hohbein et al., 2012).

Horizon H4 (30.22 ± 4.23 Ma) represents a shift in bottom current path toward greater depths along with an increase in current focus and intensity. The Eocene-Oligocene boundary, expansion of Antarctic ice sheets, and the opening of southern ocean gateways all correspond closely to Horizon H4. Seismic horizons identified in other seismic stratigraphic studies conducted in the North Atlantic temporally correspond to Horizon H4. These horizons display variable characteristics all of which reflect an increase in bottom current intensity and change in path, and are interpreted to represent individual signatures of the same reorganization of circulation dynamics.

Horizon H5/H6 (2.6 Ma) represent a shift in bottom current path from deeper to shallower depths and a decrease in the presence of diagnostic contourite drift morphologies from underlying sedimentary units. Consequently, the extent to which bottom currents reworked these sediments is uncertain. The onset of northern hemisphere glaciation and the coincident closing of the Isthmus of Panama correspond closely with Horizon H5/H6 and are associated with a reorganization of thermohaline circulation.

Sedimentary packages deposited under the influence of bottom current activity display unique seismic-reflection characteristics related to the dynamic evolution of thermohaline circulation. Variations in drift morphologies and calculated accumulation rates correspond closely to key climatic events during the Cenozoic, however the causal relationship between these events and thermohaline circulation remains poorly understood. Our observations from the Newfoundland Ridge Drift Complex correlate to events observed in other North Atlantic seismic stratigraphic studies, suggesting that these events played a significant role in the shaping of the North Atlantic Basin.

REFERENCES

Arthur, M.A., Sirvastava, S.P., Kaminski, M., Jarrard, R., Osler, J., 1989. Seismic stratigraphy and history of deep circulation and sediment drift development in Baffin bay and the Labrador sea. Proceedings of the Ocean Drilling Program, Scientific Results 105, 957- 988

Blum, P., 1997. Physical properties handbook. ODP Tech. Note 26. doi:10.2973/odp.tn.26.1997

Bohaty, S.M., Zachos, J.C., 2003. Significant Southern Ocean warming event in the late middle Eocene. Geology 31, 1017-1020

Bower, A.S. Hunt, H.D., 2000. Lagrangian observations of the Deep Western Boundary Current in the North Atlantic Ocean. Part I: Large-scale pathways and spreading rates, WHOI contribution number 9805. Journal of Physical Oceanography 30, 764 - 783

Broecker, W.S., 1997. Thermohaline Circulation. The Achilles Heel of Our Climate System: Will Man-Made CO_2 Upset the Current Balance?. Science 28, 1582- 1588

Broecker, W.S., Peacock, S.L., Walker, S., Weiss, R., Fahrbach, E., Schroeder, M., Mikolajewicz, U., Heinze, C., Key, R., Peng, T.H., Rubin, S., 1998. How much water is formed in the Southern Ocean?. Journal of Geophysical Research 103-C8, 15833-15843

Clark, P.U., Pisias, N.G., Stocker, T.F., Weaver, A.J., 2002. The role of the thermohaline circulation in abrupt climate change. Nature 415, 863-869

Davies, R., Cartwright, J., Pike, J., Line, C., 2001. Early Oligocene initiation of North Atlantic Deep Water formation. Nature 410, 917-920

DeConto, R.M., Pollard, D., 2003. Antarctica induced by declining atmospheric CO_2. Nature 421, 245-249

Diester-Haass, L., Zahn, R., 1996. Eocene-Oligocene transition in the Southern Ocean: history of water mass circulation and biological productivity. Geology 24, 163-166

Driscoll, N.W., Haug, G.H., 1998. A short circuit in thermohaline circulation: a cause for Northern Hemisphere glaciation. Science 282, 436-438

Expedition 342 Scientists., 2012, Paleogene Newfoundland sediment Drifts. IODP Prel.

Rept., 342, 1-263. doi:10.2204/iodp.pr.342.2012.

Faugères, J.-C., Stow, D.A.C., Imbert, P., Viana, A., 1999. Seismic features diagnostic of contourite drifts. Marine Geology 162, 1-38

Fine, R.A., Molinari, R.L., 1988. A continuous deep western boundary current between Abaco (26.5°N) and Barbados (13°N). Deep-sea Research 35, 1441-1450

Graber, K.K., Pollard, E., Jonasson, B., Schulte, E. (Eds.), 2002. Overview of ocean drilling program engineering tools and hardware. ODP Tech. Note, 31. doi:10.2973/odp.tn.31.200.

Greenwood, D.R., Wing, A.L., 1995. Eocene continental climates and latitudinal temperature gradients. Geology 23, 1044-1048

Hansen, B., Østerhus, S., 2000. North Atlantic-Nordic Seas exchanges. Progress in Oceanography 45, 109-208

Heezen, B.C., Hollister, C., 1964. Deep-sea current evidence from abyssal sediments. Marine Geology 1, 141-174

Hernández-Molina, F.L., Llave, E., Stow, D.A.V., 2008 Continental Slope Contourites. In: Rebesco, M., Camerlenghi, A., (Eds), Contourites: Developments in Sedimentology, 60. Elsevier, 397-408

Hohbein, M.W., Sexton, P.R., Cartwright, J.A., 2012. Onset of North Atlantic Deep Water production coincident with inception of the Cenozoic global cooling trend. Geology 40, 255-258

Hyland, E.G., Sheldon, N.D., 2013. Coupled CO_2-climate response during the Early Eocene Climatic optimum. Palaeogeography, Palaeoclimatology, Palaeoecology 369, 125-135

Jovane, L., Florindo, F., Coccioni, R., Dinarès-Turell, J., Marsili, A., Monechi, S., Roberts, A.P., Sprovieri, M., 2007. The middle Eocene climatic optimum event in the Contessa Highway section, Umbrian Apennines, Italy. Geological Society of America Bulletin 119, 413-427

Keigwin, L.D., Jones, G.A., 1989. Glacial-Holocene stratigraphy, chronology, and paleoceanographic observations on some North Atlantic sediment drifts. Deep-Sea Research 36, 845-867

Kent, D.V., Muttoni, G., 2008. Equatorial convergence of India and early Cenozoic climate trends. PNAS 105, 16065-16070

Kuhlbrodt, T., Rahmstorf, S., Zickfeld, K., Vikebø F.B., Sundby, S., Hofmann, M., Link, P.M., Bondeau, A., Cramer, W., Jaeger, C., 2009. An Integrated Assessment of changes in the thermohaline circulation. Climatic Change 96, 489-537

Liu, Z., Pagani, M., Zinniker, D., DeConto, R., Huber, M., Brinkhuis, H., Shah, S.R., Leckie, R.M., Pearson, A., 2009. Global cooling during the Eocene-Oligocene climate transition. Science 323, 1187- 1190

Miller, K.G., Tucholke, B.E., 1983. Development of Cenozoic abyssal circulation south of the Greenland-Scotland Ridge. In: Bott, M.H.P., (Eds), Structure and Development of the Greenland-Scotland Ridge, Nato Conference Series, 8, 549-589

Miller, G.G., Kominz, M.A., Browning, J.V., Wright, J.D., Mountain, G.S., Katz, M.E., Sugarman, P.J., Cramer, B.S., Christie-Blick, N., Pekar, S.E., 2005. The Phanerozoic record of global sea-level change. Science 310, 1293-1298

Mountain, G.S., Tucholke, B.E., 1985. Mesozoic and Cenozoic geology of the U.S. Atlantic continental slope and rise. In: Poag, C.W., (Eds), Geologic evolution of the United States Atlantic Margin. Van Nostrand Reinhold Company Inc., 293-341

Müller-Michaelis, A., Uenzelmann, G., Stein, R., 2013. A revised Early Miocene age for the instigation of the Eirik Drift, offshore southern Greenland: Evidence from high-resolution seismic-reflection data. Marine Geology 340, 1-15

Norris, R.D., Wilson, P.A., Blum, P., Expedition 342 Scientists, 2014. Expedition 342 Summary. Proceedings of the Integrated Ocean Drilling Program, 342, 1- 149

Palter, J.B., Lozier, M.S., Lavender K.L., 2008. How does Labrador Sea Water enter the Deep Western Boundary Current?. Journal of Physical Oceanography 39, 968-983

Pe-Piper, G., Piper, D.J.W., de Jonge, A., 2007. Early Cretaceous opening of the North Atlantic Ocean: Implications of the petrology and tectonic setting of the Fogo Seamounts off the SW Grad Banks, Newfoundland. GSA Bulletin 119, 712-714

Pickart, R.S., 1992. Water mass components of the North Atlantic deep western boundary

current. Deep-Sea Research 39, 1553-1572

Rahmstorf, S., 2000. The thermohaline ocean circulation: A system with dangerous thresholds. Climatic Change 46, 247-256

Rahmstorf, S., 2003. The current climate. Nature 421, 699

Rahmstorf, S., 2006. Thermohaline Ocean Circulation. In: Elias, S.A., (Eds), Encyclopedia of Quaternary Sciences, Elsevier, 1-10

Rebesco, M., Stow. D., 2001. Seismic expression of contourites and related deposits: a preface. Marine Geophysical Researches 22, 303-2001

Rebesco, M., Hernández-Molina, F.J., Rooij, D.V., Wåhlin, A., in press. Contourites and associated sediments controlled by deep-water circulation processes: state-of-the-art and future considerations. Marine Geology, 1- 147

Richardson, M.J., Wimbush, M, Mayer, L., 1981. Exceptionally Strong Near-Bottom Flows on the Continental Rise of Nova Scotia. Science 213, 887-888

Ryan, W.B.F., Carbotte, S.M., Coplan, J.O., O'Hara, S., Melkonian A., Arko, R., Weissel, R.A., Ferrini, V., Goodwillw, A., Nitsche, F., Bonczkowski, J., Zemsky, R., 2009. Global Multi-Resolution Topography synthesis. Geochemistry Geophysics Geosystems 10, doi:10.1029/2008GC002332.

Sangree, J.B., Widmier, J.M., 1978. Seismic Stratigraphy and Global Changes of Sea Level, Part 9: Seismic Interpretation of Clastic Depositional Facies. AAPG Bulletin 62, 752-771

Scher, H.D., Martin, E.E., 2006. Timing and climatic consequences of the opening of Drake Passage. Science 312, 428-430

Smallwood, J.R., 2004. Tertiary inversion in the Faroe-Shetland Channel and the development of major erosional scarps, In: Davies et al., (Eds) 3D seismic technology: applications to the exploration of sedimentary basins. The Geological Society of London Memoirs, 29, 197-198

Stocker, M.S., Praeg, D., Hjelstuen, B.O., Laberg, J.S., Nielsen, T., Shannon, P.M., 2005. Neogene stratigraphy and the sedimentary and oceanographic development of the NW European Atlantic margin. Marine and Petroleum Geology 22, 977-1005

Stow, D.A.V., Faugères, J., Howe, J.A., Pudsey, C.J., Viana. A.R., 2002. Bottom currents, contourites and deep-sea sediment drifts: current state-of-the-art.

Geological Society of London Memoirs 22, 7-20

Stow, D.A.V., Faugères J.-C., 2008. Contourite facies and the facies model. In: Rebesco, M., Camerlenghi, A., (Eds), Contourites: Developments in Sedimentology 60. Elsevier, 397-408

Sullivan, K.D., Keen, C.E., 1978. On the nature of the crust in the vicinity of the Southeast Newfoundland Ridge. Canadian Journal of Earth Science 15, 1462-1471

Tucholke, B.E., Vogt, P.R., Murdmaa I.O., Rothe, P., Houghton, R.L., Galehouse, J.S., Kaneps, K., McNulty, C.L. Jr., Okada, H., Kendrick, J.W., Demars, K.R., McCave, I.N., 1979. Initial reports of the Deep Sea Drilling Project. Washington (US Government Printing Office), 107-154

Tucholke, B.E., 1981. Geologic significance of Seismic reflectors in the deep western North Atlantic Basin. SEPM Special Publication 32, 23-37

Tucholke, B.E., Ludwig, W.J., 1982. Structure and origin of the J Anomaly Ridge, Western North Atlantic Ocean. Journal of Geophysical Research 87, 9389-9407

Tucholke, B.E., 1985. Geologic significance of seismic reflectors in the deep western North Atlantic Basin. SEPM Special Publication 32, 23-37

Tucholke, B.E., Austin, J.A. jr., Uchup, E., 1989. Crustal structure and rift-drift evolution of the Newfoundland Basin. In: Tankard, A.J., Balkwill, H.R., (Eds), Extensional tectonics and stratigraphy of the North Atlantic Margin. AAPG Memoir 46, 247-263

Tucholke, B.E., Sawyer, D.S., Sibuet, J.C., 2007. Breakup of the Newfoundland-Iberia rift. Geological Society of London, Special Publications 282, 9-46. doi:10.1144/SP282.2

Zachos, J., Panganis, M., Sloan, L., Thomas, E., Billups, K., 2001. Trends, rhythms, and aberrations in global climate 65 Ma to present. Science 292, 686-693

Zachos, J.C., Wara, M.W., Bohaty, S., Delaney, M.L., Petrizzo, M.R., Brill, A., Bralower, T.J., Premoli-Silva, I., 2003. A transient rise in tropical sea surface temperature during the Paleocene-Eocene thermal maximum. Science 302, 1551-1554

Zachos, J.C., Kroon, D., Blum, P., et al., 2004. Leg 208 Summary. Proceedings of the

Ocean Drilling Program, Initial Reports 208, 1- 112

Zachos, J.C., Kump, L.R., 2005. Carbon cycle feedbacks and the initiation of Antarctic glaciation in the earliest Oligocene. Global and Planetary Change 47, 51-66

Zachos, J.C., Dickens, G.R., and Zeebe, R.E., 2008. An early Cenozoic perspective on greenhouse warming and carbon-cycle dynamics. Nature 45, 279-283

FIGURES

Figure 1. Shaded bathymetric relief map of the J-Anomaly Ridge and Southeast Newfoundland Ridge, offshore Newfoundland Canada. Thick red lines depict the modern path of the Deep Western Boundary Current. Thinner black lines show seismic-reflection transects collected by the Integrated Ocean Drilling Program on the R.V. Knorr in 2004. Bathymetry data from GeoMapApp (http://www.geomapapp.org).

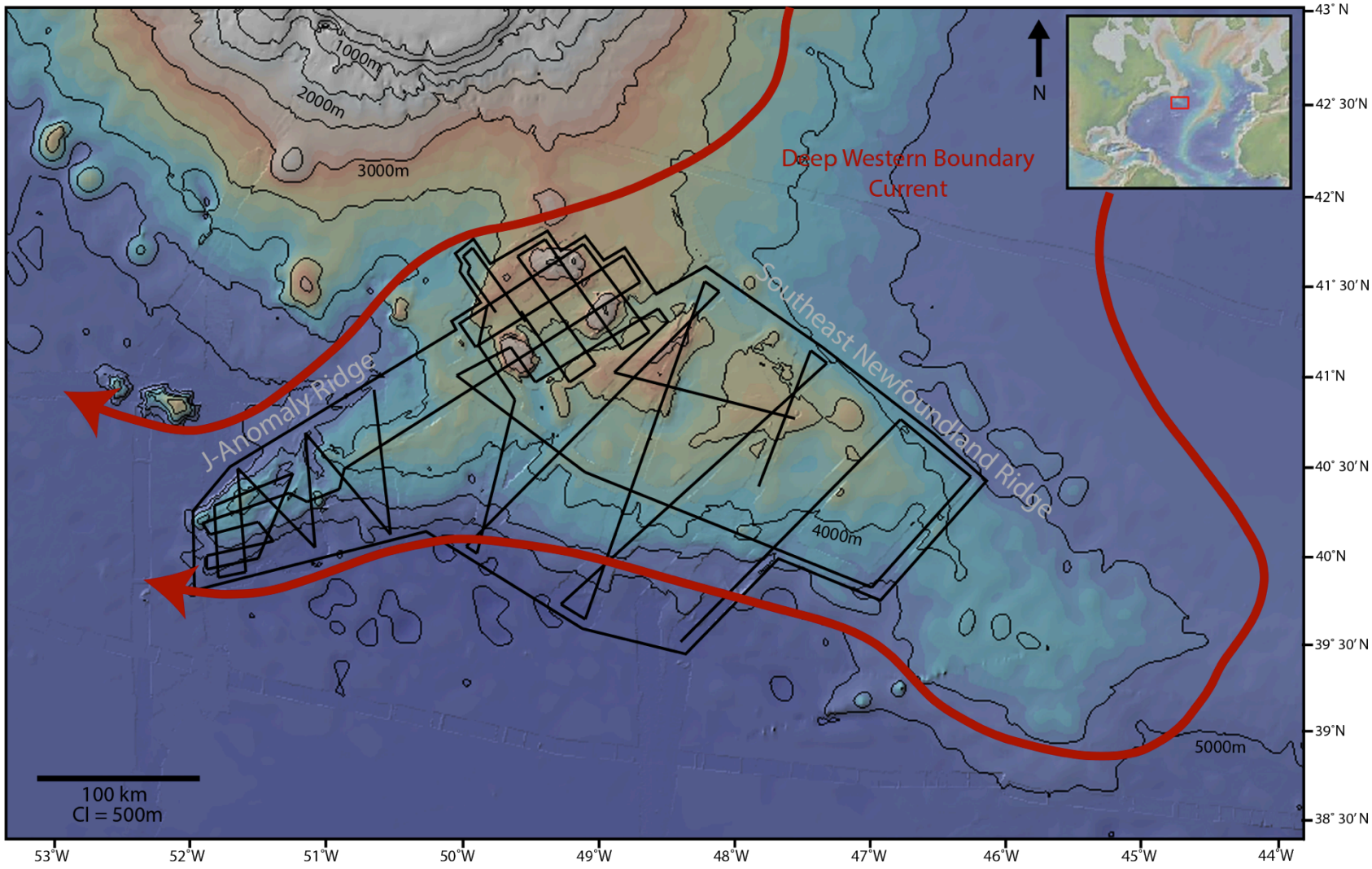
1000m
2000m
3000m
4000m
5000m
Deep Western Boundary Current
J-Anomaly Ridge
Southeast Newfoundland Ridge
N
100 km
CI = 500m
43° N
42° 30'N
42°N
41° 30'N
41°N
40° 30'N
40°N
39° 30'N
39°N
38° 30'N
53°W
52°W
51°W
50°W
49°W
48°W
47°W
46°W
45°W
44°W

Figure 2: Shaded bathymetric relief map showing seismic-reflection profiles collected in 2004 by the Integrated Ocean Drilling Program on the R.V. Knorr 179-1 (thin black lines). Drill sites from IODP Expedition 342 are shown with red points with yellow centers, and DSDP site 384 is represented with a black and red star. Segments of line L05, L020, and L037 are displayed in this paper and shown with thick red lines. Bathymetry from GeoMapApp (http://www.geomapapp.org).

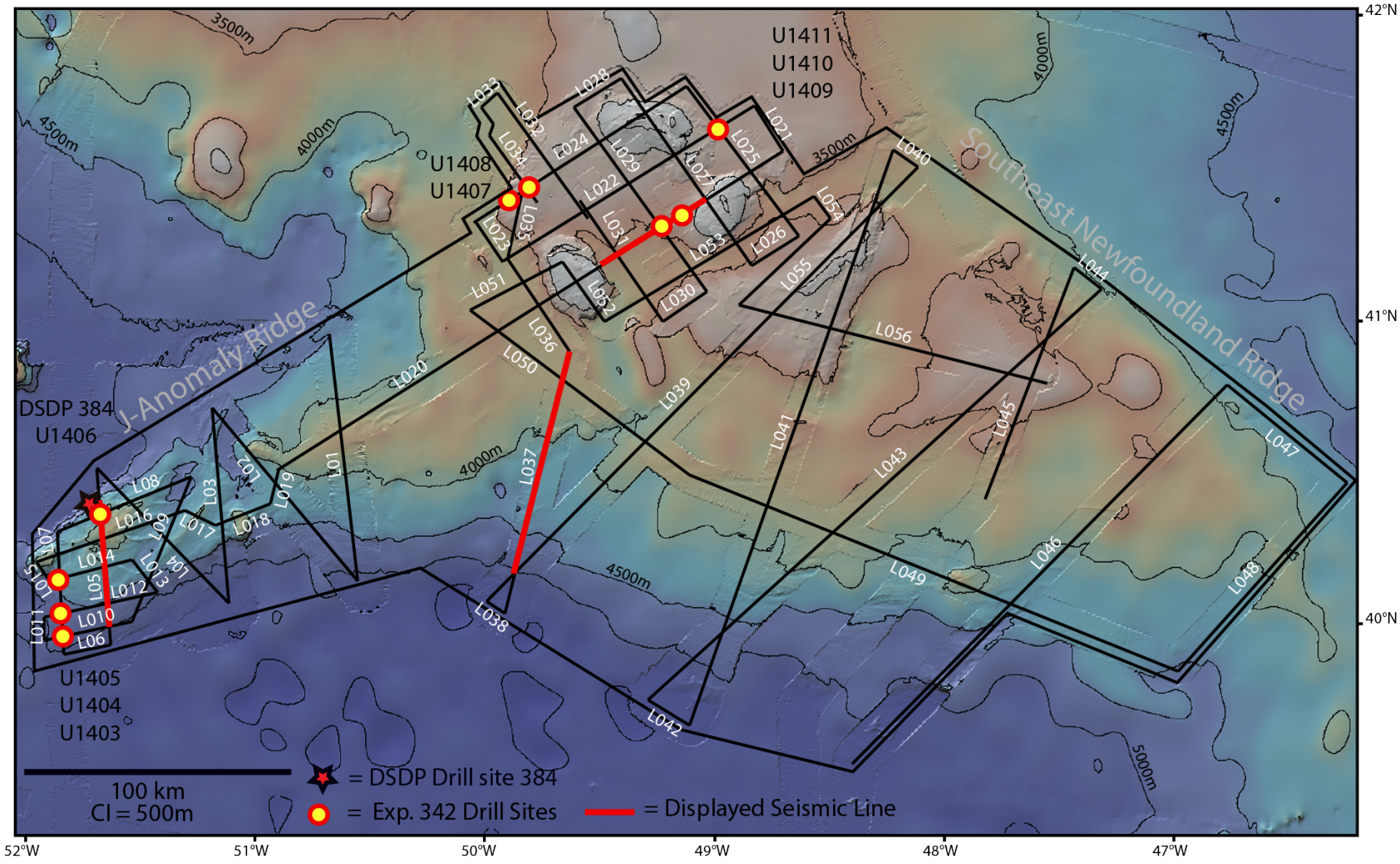
U1411
U1410
U1409
U1408
U1407
DSDP 384
U1406
U1405
U1404
U1403
J-Anomaly Ridge
Southeast Newfoundland Ridge
3500m
4000m
4500m
5000m
42°N
41°N
40°N
52°W
51°W
50°W
49°W
48°W
47°W
100 km
CI = 500m
= DSDP Drill site 384
= Exp. 342 Drill Sites
= Displayed Seismic Line

Figure 3: Spatial distribution and penetrative depths of IODP Expedition 342 drill sites over the J-Anomaly Ridge. Sites U1403, U1404, U1405 on seismic line L07, and sites U1406 and DSDP site 384 on seismic line L05.

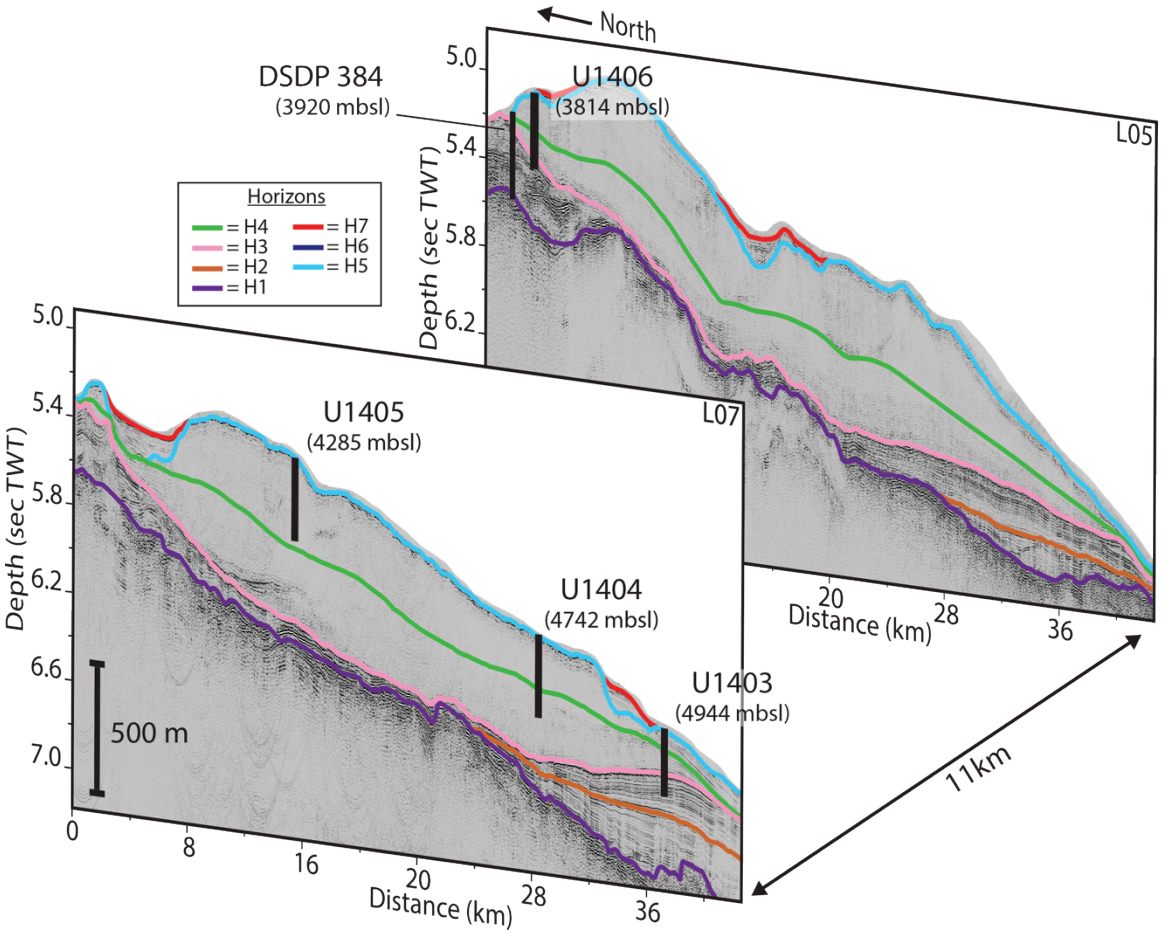

Figure 4: Spatial distribution and penetrative depths of IODP Expedition 342 drill sites over the Southeast Newfoundland Ridge. Site U1407 and U1408 on seismic line L024, sites U1409 and U1410 on seismic line L020, and site U14011 on seismic line L020.

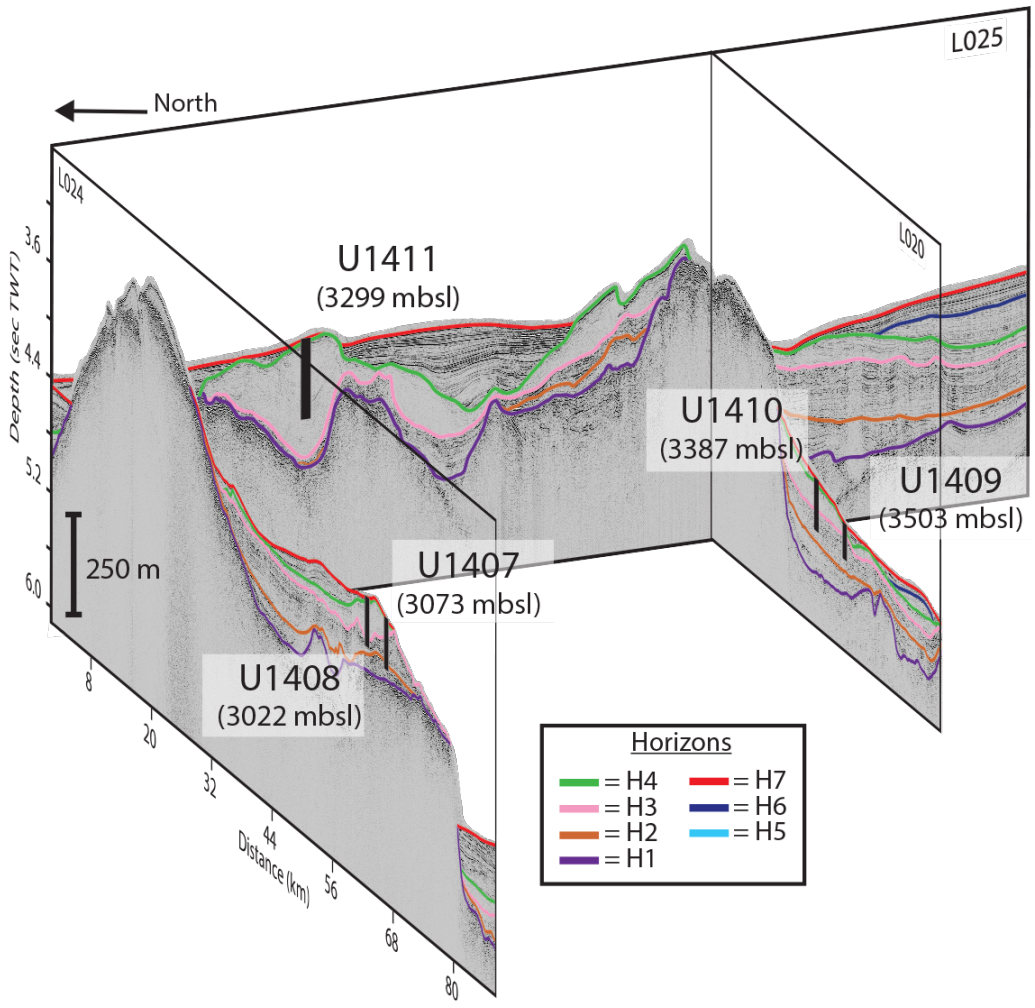

Figure 5: A.) Characteristics and interpretations of seismic facies. Seismic facies are grouped into seismic stratigraphic units separated by mappable and datable boundaries. B.) Criteria used for the identification and mapping of seismic horizons.

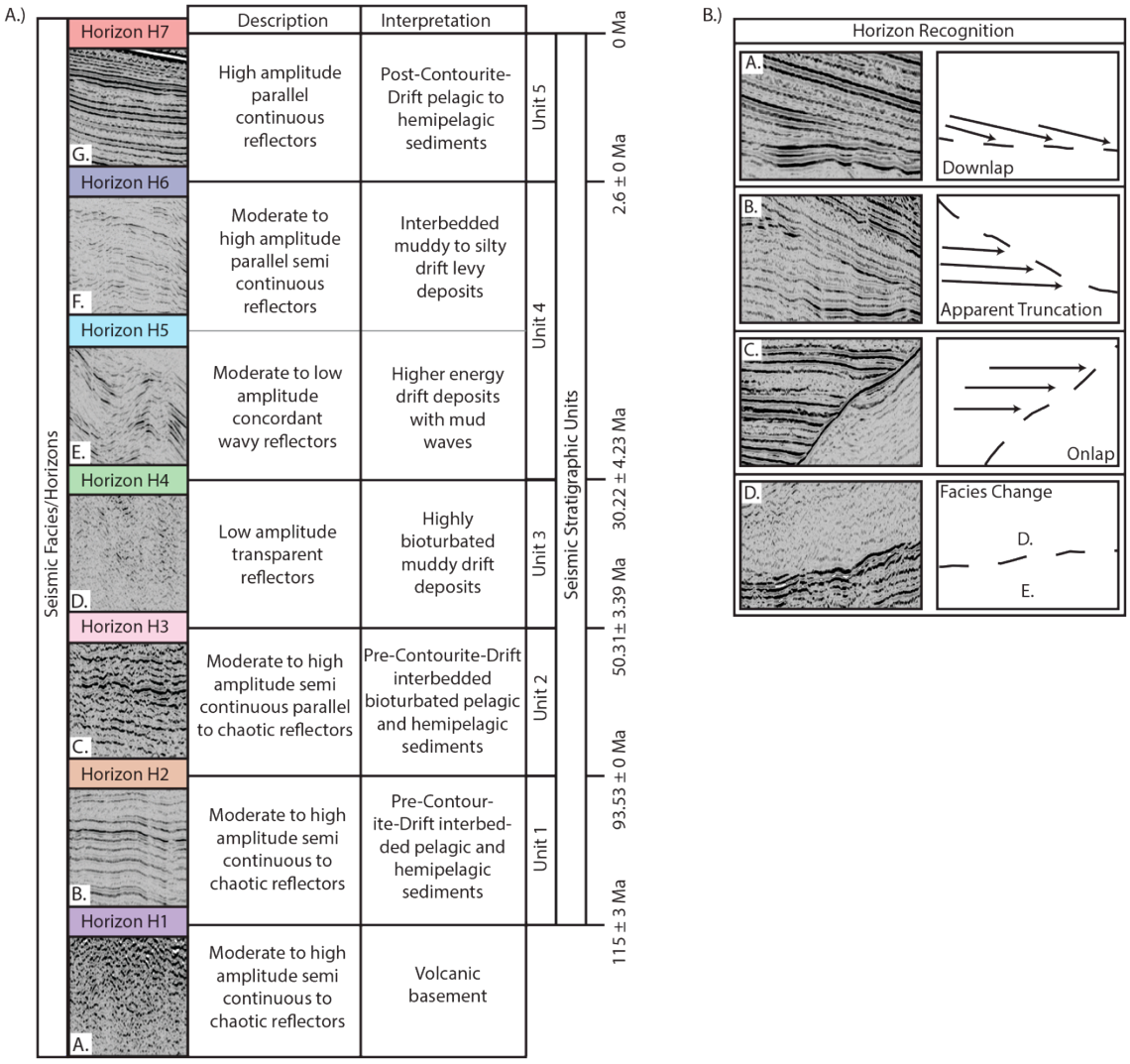

Figure 6: Acoustic impedance logs generated from shipboard measured physical property data for the eight IODP Expedition 342 drill sites that penetrated mappable seismic horizons. See Appendix 1 for velocity and density data.

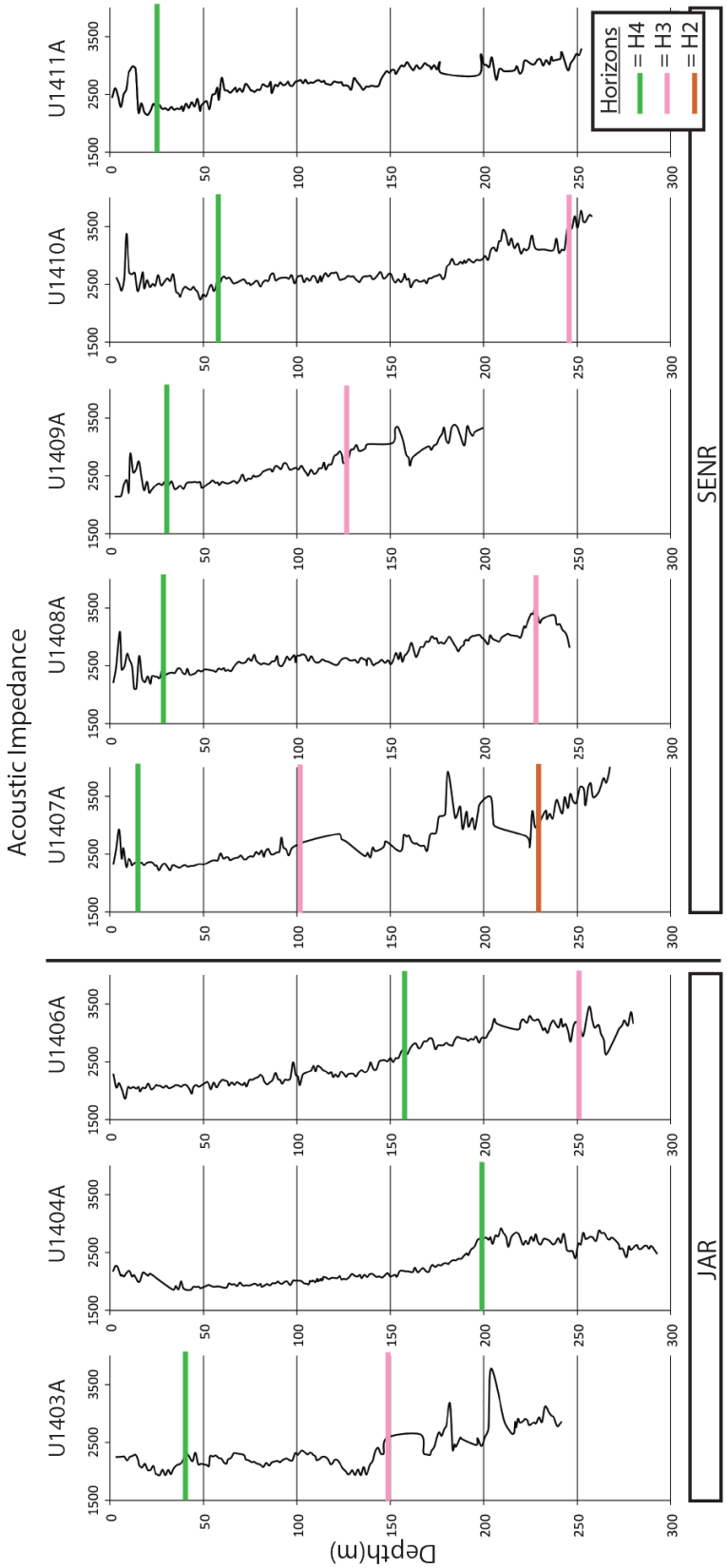
Acoustic Impedance
Depth(m)
U1403A
U1404A
U1406A
U1407A
U1408A
U1409A
U1410A
U1411A
JAR
SENR
Horizons
= H4
= H3
= H2

Figure 7: Seismic-reflection profile L037 displaying seismic-reflection character typical of sediment cover over the Southeast Newfoundland Ridge. A.) Un-interpreted seismic-reflection profile, B.) Seismic-reflection profile overlain with seismic stratigraphic interpretations and annotated observations, C.) Line-drawing diagram highlighting seismic stratigraphic interpretations and observations. See Figure 2 for location of profile.

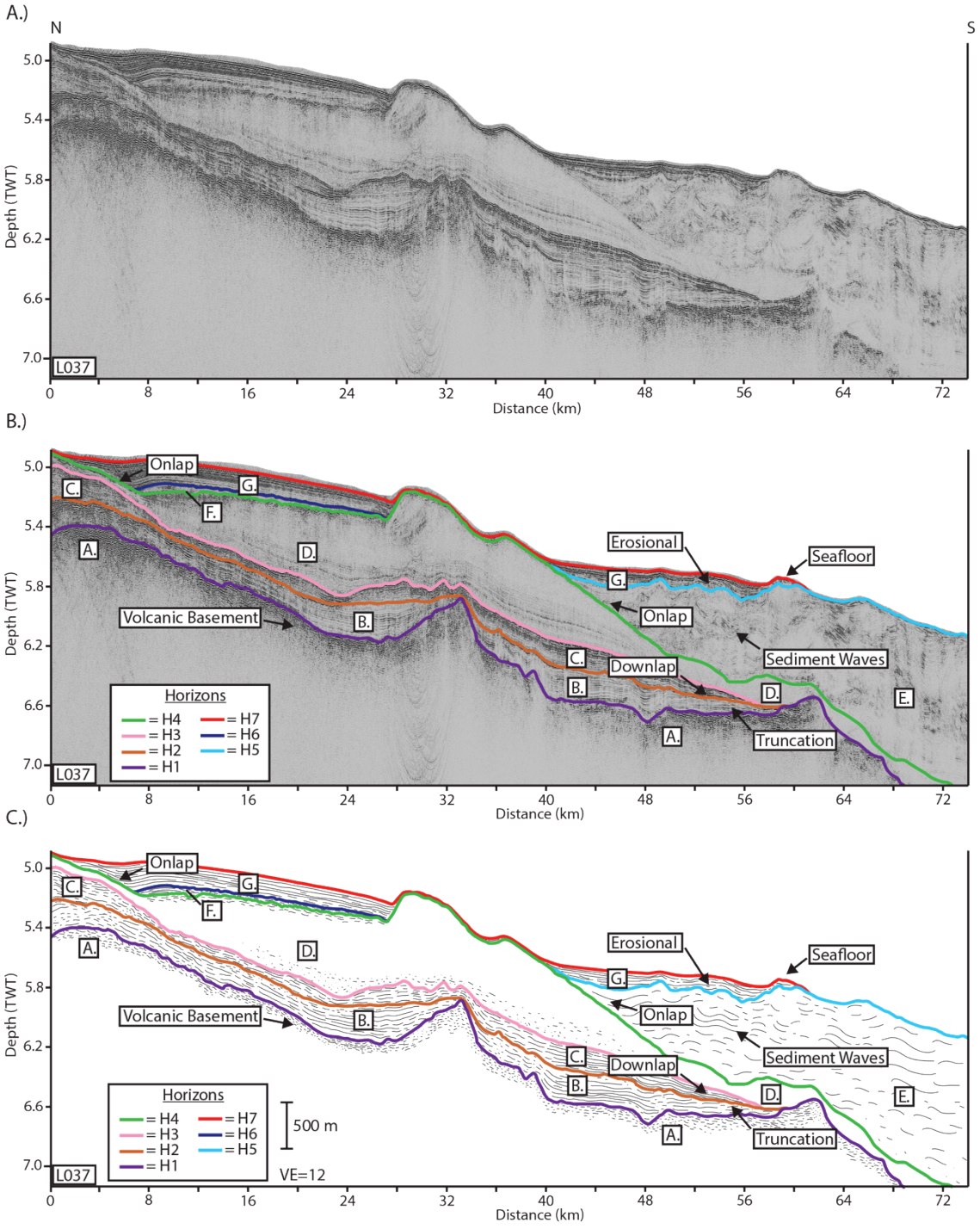
A.)
N
S
Depth (TWT)
5.0
5.4
5.8
6.2
6.6
7.0
L037
0
8
16
24
32
40
48
56
64
72
Distance (km)
B.)
Onlap
C.
G.
F.
A.
D.
Erosional
Seafloor
G.
Onlap
Volcanic Basement
B.
Sediment Waves
C.
Downlap
B.
D.
E.
A.
Truncation
Horizons
= H4
= H7
= H3
= H6
= H2
= H5
= H1
C.)
Onlap
C.
G.
F.
A.
D.
Erosional
Seafloor
G.
Onlap
Volcanic Basement
B.
Sediment Waves
C.
Downlap
B.
D.
E.
A.
Truncation
Horizons
= H4
= H7
= H3
= H6
= H2
= H5
= H1
500 m
VE=12

Figure 8: Seismic-reflection profile L05 displaying seismic-reflection character typical of sediment cover over the J-Anomaly Ridge. A.) Un-interpreted seismic-reflection profile, B.) Seismic-reflection profile overlain with annotated seismic stratigraphic interpretations, and C.) Line-drawing diagram highlighting seismic stratigraphic interpretations and observations. See Figure 2 for location of profile.

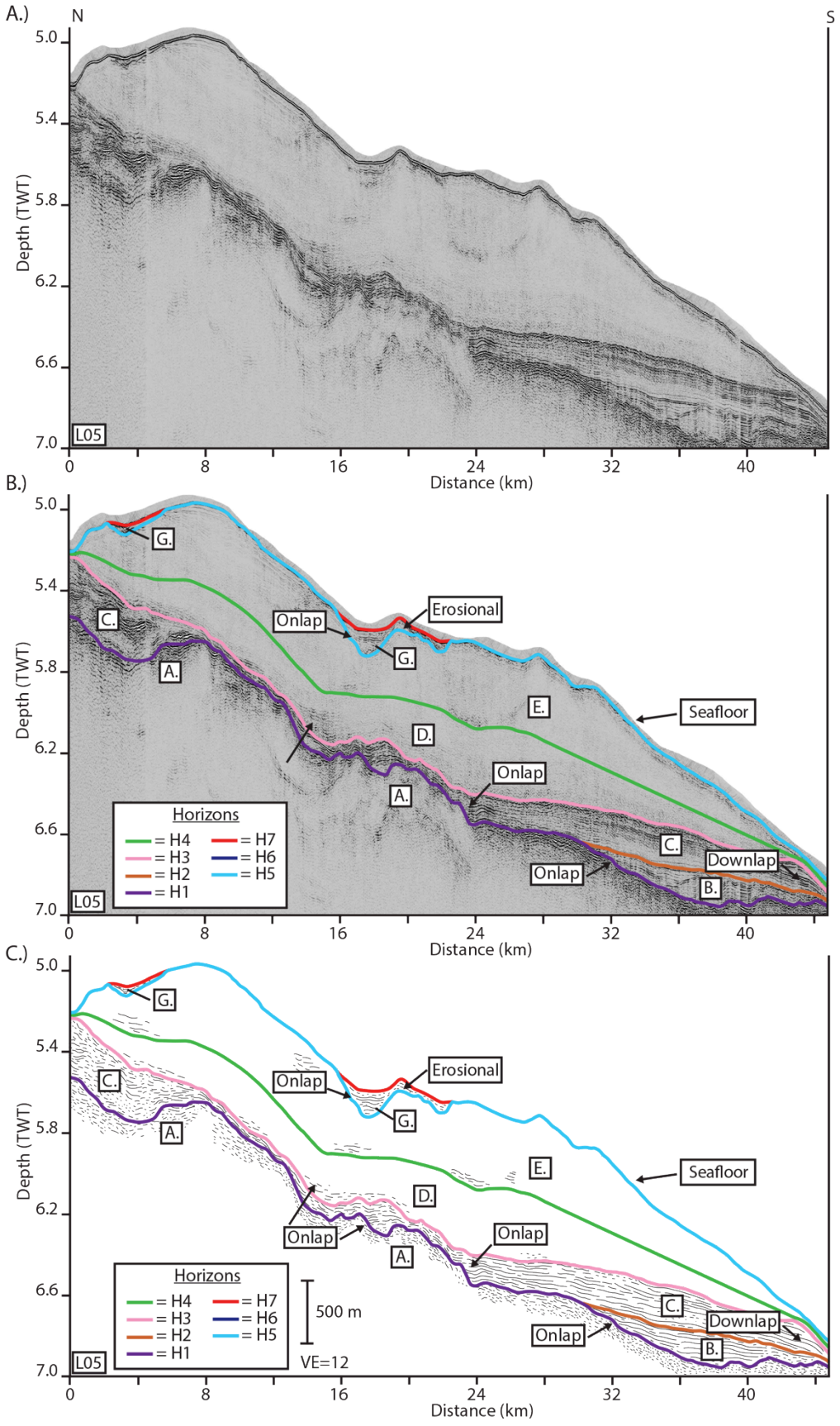
A.)
N
S
5.0
5.4
5.8
6.2
6.6
7.0
Depth (TWT)
L05
0
8
16
24
32
40
Distance (km)
B.)
G.
C.
A.
Onlap
Erosional
G.
E.
Seafloor
D.
Onlap
A.
C.
Downlap
Onlap
B.
Horizons
= H4
= H3
= H2
= H1
= H7
= H6
= H5
C.)
500 m
VE=12

Figure 9: Seismic-reflection profile L020 displaying seismic-reflection character typical of sediment cover in close proximity to the Southeast Newfoundland Ridge seamounts. A.) Un-interpreted seismic-reflection profile, B.) Seismic-reflection profile overlain with seismic stratigraphic interpretations and annotated observations, C.) Line-drawing diagram highlighting seismic stratigraphic interpretations and observations. See Figure 2 for location of profile.

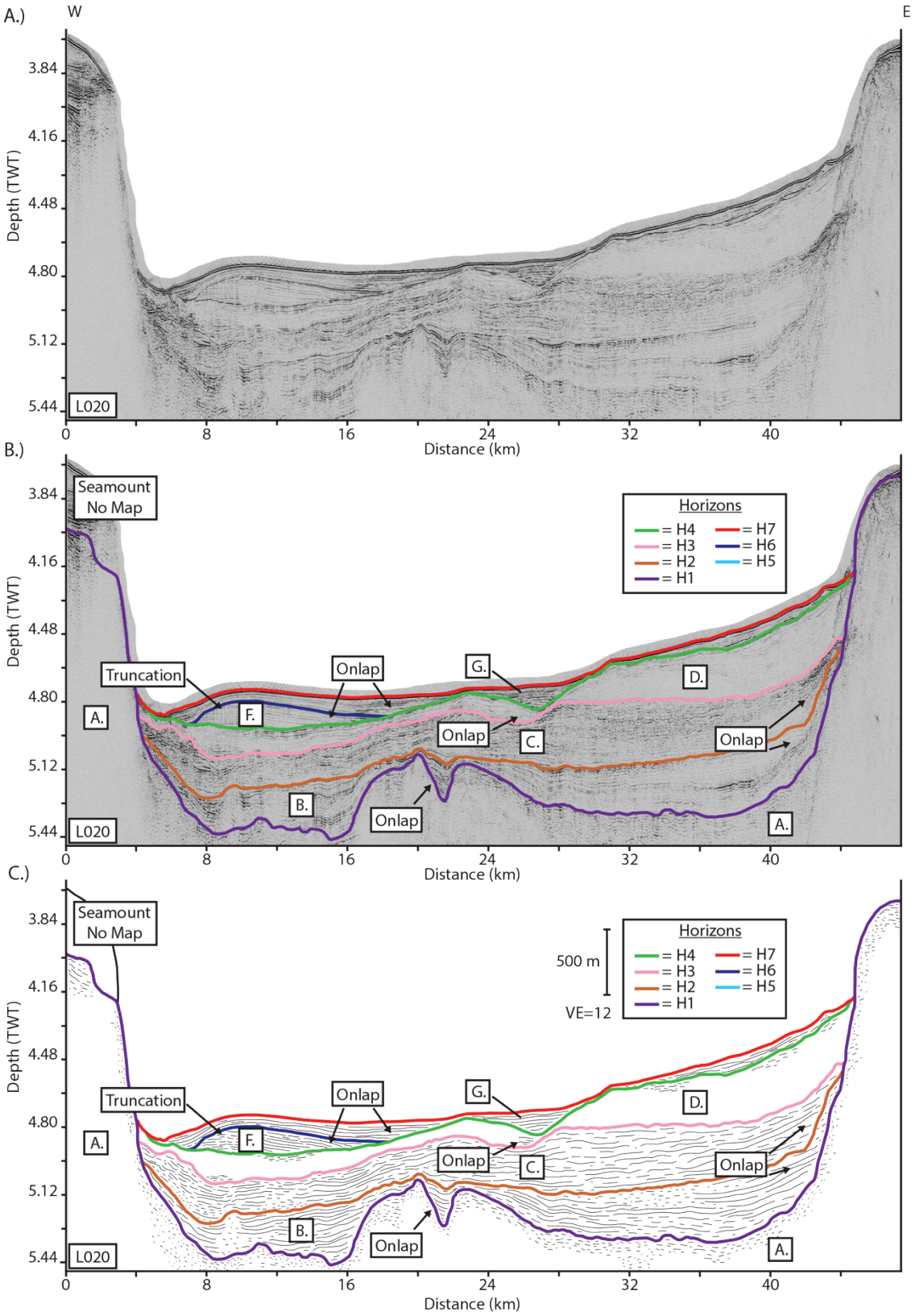
A.)
W
E
Depth (TWT)
3.84
4.16
4.48
4.80
5.12
5.44
L020
0
8
16
24
32
40
Distance (km)
B.)
Seamount
No Map
Horizons
= H4
= H7
= H3
= H6
= H2
= H5
= H1
Truncation
Onlap
G.
D.
F.
A.
Onlap
C.
Onlap
B.
Onlap
A.
C.)
Seamount
No Map
500 m
VE=12
Horizons
= H4
= H7
= H3
= H6
= H2
= H5
= H1
Truncation
Onlap
G.
D.
F.
A.
Onlap
C.
Onlap
B.
Onlap
A.

Figure 10: Age-depth models for the eight IODP expedition drill sites that penetrated mappable seismic horizons. Depth (m) is on the y-axis and Age (Ma) is on the x-axis, with slope of the curve representing linear sedimentation rates. Horizontal and near horizontal slopes represent intervals of low accumulation rates and hiatuses, and steep slopes represent higher sedimentation rates. Modified from Norris et al. (2014).

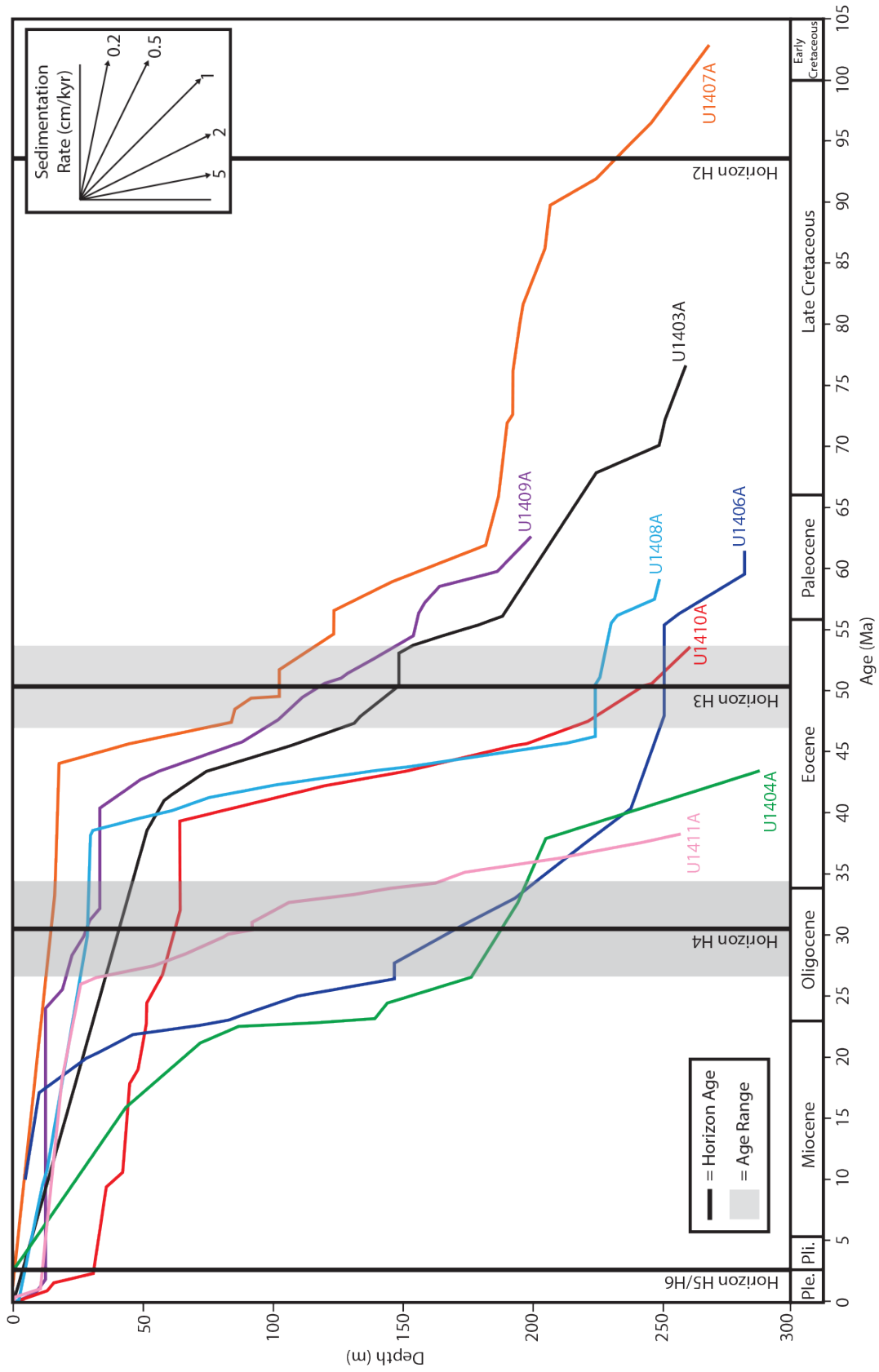
Depth (m)
0
50
100
150
200
250
300
Age (Ma)
0
5
10
15
20
25
30
35
40
45
50
55
60
65
70
75
80
85
90
95
100
105
Ple.
Pli.
Miocene
Oligocene
Eocene
Paleocene
Late Cretaceous
Early Cretaceous
Horizon H5/H6
Horizon H4
Horizon H3
Horizon H2
= Horizon Age
= Age Range
Sedimentation Rate (cm/kyr)
0.2
0.5
1
2
5
U1407A
U1403A
U1409A
U1408A
U1406A
U1410A
U1404A
U1411A

Figure 11: Isochron maps of seismic stratigraphic units with vertical domain displayed in Two Way Time (note scale changes). A.) Distribution of seismic data and mapping strategy, B.) Seismic Stratigraphic Unit 5 (2.6 Ma - Present), C.) Seismic Stratigraphic Unit 4 (30.22- 2.6 Ma), D.) Seismic Stratigraphic Unit 3 (50.31- 30.22 Ma), E.) Seismic Stratigraphic Unit 2 (93.53-50.31 Ma), and F.) Seismic Stratigraphic Unit 1 (115-93.53 Ma).

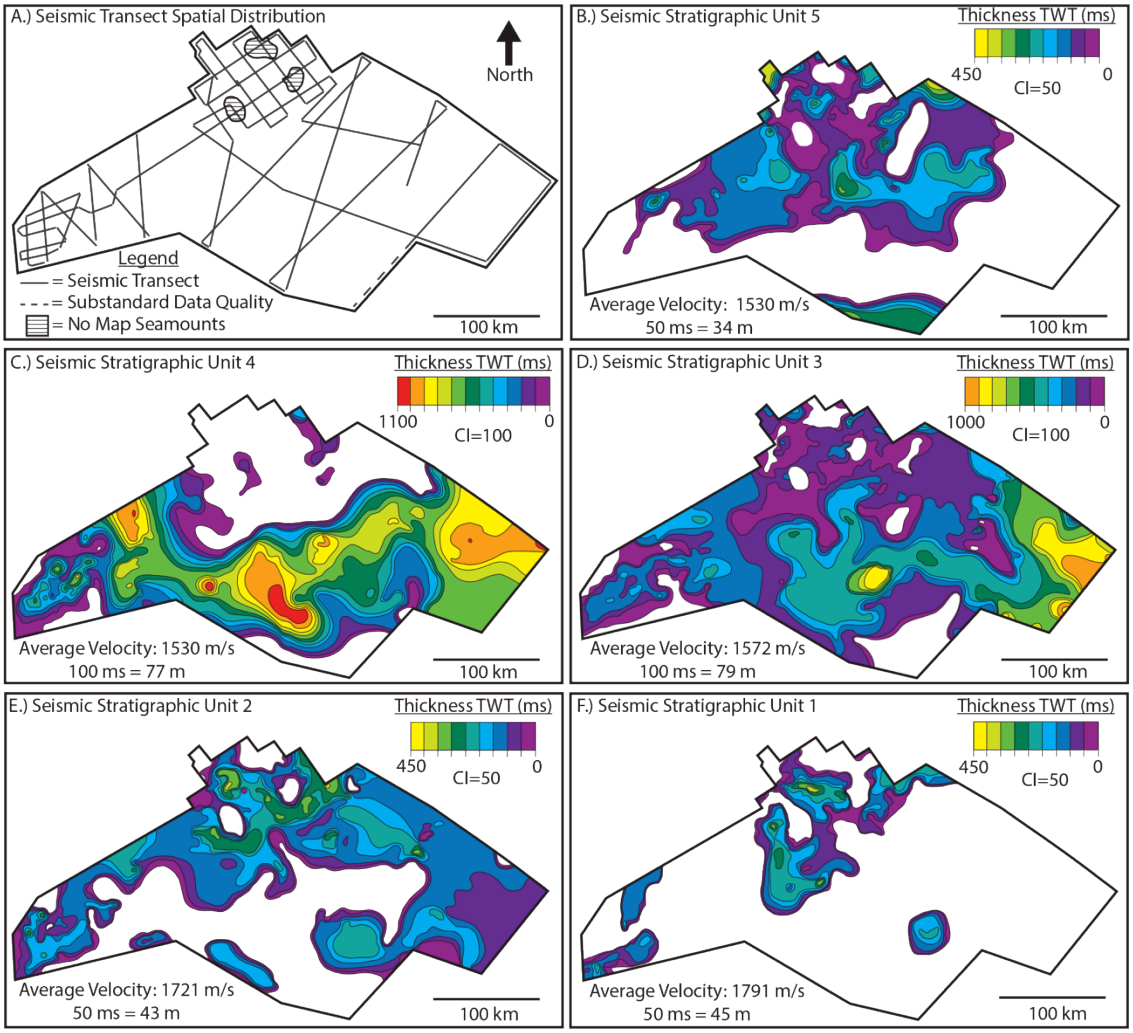

Figure 12: A.) Volumetric and mass accumulation rates for all five seismic stratigraphic units. B.) Oxygen isotope data modified from Zachos et al. (2008) with significant periods of climatic reorganization. Note that dates assigned to H5/H6 were inferred from other North Atlantic seismic stratigraphic studies, and were not determined from IODP Expedition 342 data.

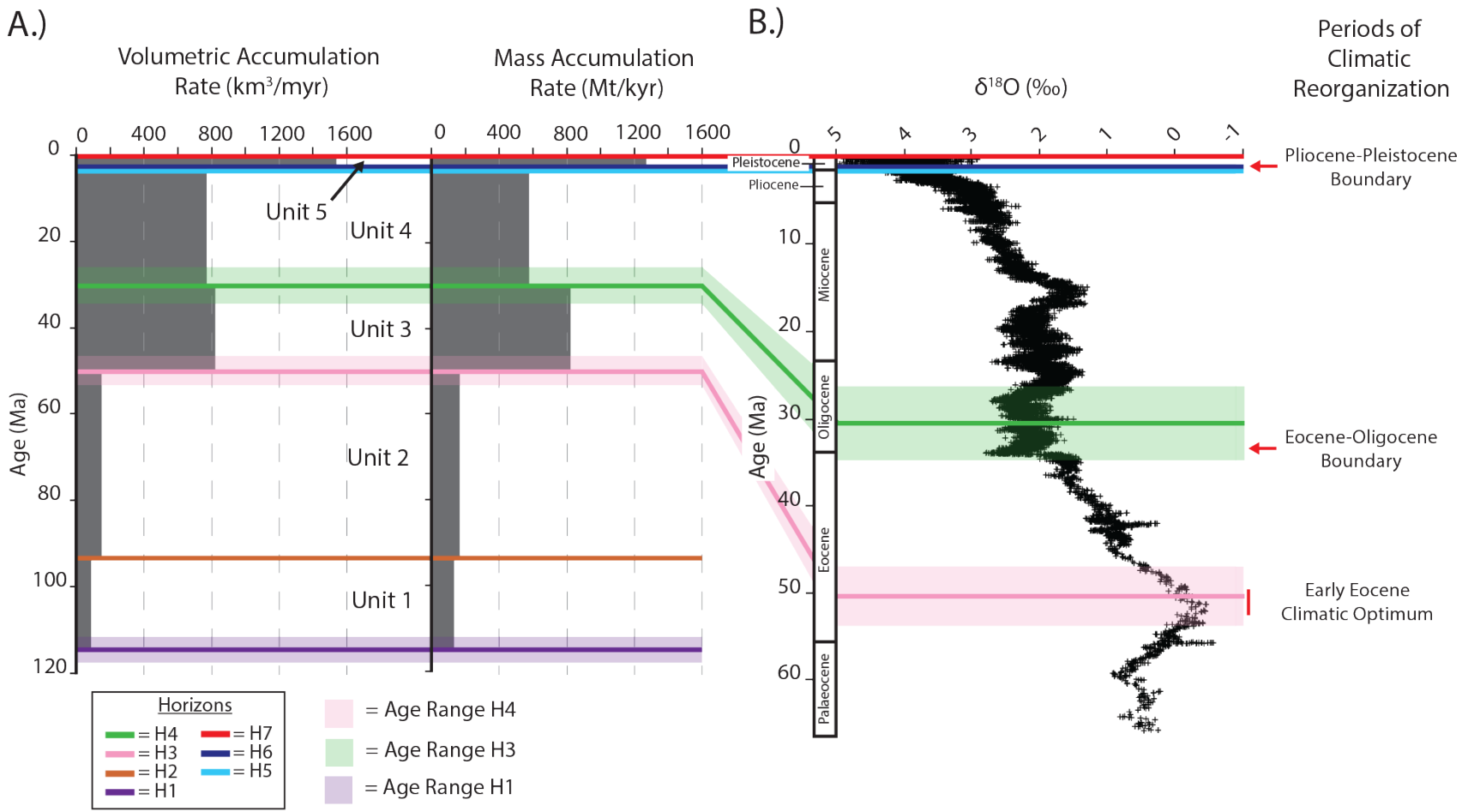
A.)
Volumetric Accumulation Rate (km³/myr)
Mass Accumulation Rate (Mt/kyr)
0
400
800
1200
1600
Age (Ma)
0
20
40
60
80
100
120
Unit 5
Unit 4
Unit 3
Unit 2
Unit 1
Horizons
= H4
= H3
= H2
= H1
= H7
= H6
= H5
= Age Range H4
= Age Range H3
= Age Range H1
B.)
δ¹⁸O (‰)
5
4
3
2
1
0
-1
Pleistocene
Pliocene
Miocene
Oligocene
Eocene
Palaeocene
Periods of Climatic Reorganization
Pliocene-Pleistocene Boundary
Eocene-Oligocene Boundary
Early Eocene Climatic Optimum

TABLES

Table 1: Depths at which IODP Expedition 342 drill cores penetrate interpreted seismic horizons. Drill cores do not penetrate all interpreted seismic horizons at each drill site.

TABLE 1: Borehole Penetration Depth to Seismic Horizons

Seismic Reflector	1403 Depth (m)	1404 Depth (m)	1405 Depth (m)	1406 Depth (m)	1407 Depth (m)	1408 Depth (m)	1409 Depth (m)	1410 Depth (m)	1411 Depth (m)
Horizon H7	Not penetrated	Not penetrated	Not penetrated	Not penetrated	Not penetrated	Not penetrated	Not penetrated	Not penetrated	Not penetrated
Horizon H6	Not penetrated	Not penetrated	Not penetrated	Not penetrated	Not penetrated	Not penetrated	Not penetrated	Not penetrated	Not penetrated
Horizon H5	Not penetrated	Not penetrated	Not penetrated	Not penetrated	Not penetrated	Not penetrated	Not penetrated	Not penetrated	Not penetrated
Horizon H4	40.54	198.23	Not penetrated	156.96	15.04	28.2	29.92	57.53	25.5
Horizon H3	147.97	Not penetrated	Not penetrated	250.78	101.96	227.45	126.1	245.07	Not penetrated
Horizon H2	Not penetrated	Not penetrated	Not penetrated	Not penetrated	228.72	Not penetrated	Not penetrated	Not penetrated	Not penetrated
Horizon H1	Not penetrated	Not penetrated	Not penetrated	Not penetrated	Not penetrated	Not penetrated	Not penetrated	Not penetrated	Not penetrated

Note: Drill site 1405 did not penetrate mapped horizons and has been excluded from this table.
Note: Depth to Horizon H2 and Horizon H3 was determined with Expedition 342 DESC Reports.
Note: Depth to Horizon H4 was pinpointed using seismic velocities and strengthened with Acoustic Impedance logs.

Table 2: Ages assigned to interpreted seismic horizons. Temporal constraint was determined with biostratigraphic data (i.e., calcareous nannofossils, radiolarians, foraminifera) and magnetochron boundary data of Norris et al. (2014). Drill cores do not penetrate all interpreted seismic horizons at each drill site.

TABLE 2: Seismic Horizon Age

Seismic Horizon	1403 Age (Ma)	1404 Age (Ma)	1406 Age (Ma)	1407 Age (Ma)	1408 Age (Ma)	1409 Age (Ma)	1410 Age (Ma)	1411 Age (Ma)	DSDP 384 Age (Ma)	Average Horizon Age (Ma)	Age Span (myr)
Horizon H7	Not penetrated	Not penetrated	Not penetrated	Not penetrated	0	0	0	0	Not penetrated	0	0
Horizon H6	Not penetrated	Not penetrated	Not penetrated	Not penetrated	Not penetrated	Not penetrated	Not penetrated	Not penetrated	Not penetrated	Not penetrated	Not penetrated
Horizon H5	0	0	0	0	Not penetrated	Not penetrated	Not penetrated	Not penetrated	0	2.6 (?)	0
Horizon H4	1.93-36.05	29.62-32.92	26.57-29.62	32.02-34.44	30.00-32.92	31.03- 33.71	26.84	25.99	?	30.22	8.45
Horizon H3	50.50 – 53.70	Not penetrated	46.92	49.47- 51.64	50.78-53.70	50.5	50.5	Not penetrated	Upper Lower Eocene	50.31	6.78
Horizon H2	Not penetrated	Not penetrated	Not penetrated	93.53	Not penetrated	Not penetrated	Not penetrated	Not penetrated	?	93.53	0
Horizon H1	Not penetrated	Not penetrated	Not penetrated	Not penetrated	Not penetrated	Not penetrated	Not penetrated	Not penetrated	~112-118 (?)	115 (?)	~6 (?)

Note: Drill site 1405 did not penetrate mapped horizons and has been excluded from this table.
Note: Depth to Horizon H2 and Horizon H3 was determined with Expedition 342 DESC Reports.
Note: Depth to Horizon H4 was pinpointed using seismic velocities and strengthened with Acoustic Impedance logs.

Table 3: Average P-wave velocities determined from shipboard measured physical property data for each seismic stratigraphic unit. All seismic stratigraphic units are not penetrated at each drill site. At all IODP Expedition 342 drill sites Seismic Stratigraphic Unit 5 is below the resolution of seismic-reflection data, and thus, the average velocity for this unit is based on P-wave velocities measured in the top 5 m of sediment cores. Drill cores do not always penetrate the entire thickness of seismic stratigraphic units and as such average p-wave velocities are calculated with available data.

TABLE 3: Seismic Stratigraphic Unit Velocity

Seismic Stratigraphic Unit	1403 velocity (m/s)	1404 velocity (m/s)	1406 velocity (m/s)	1407 velocity (m/s)	1408 velocity (m/s)	1409 velocity (m/s)	1410 velocity (m/s)	1411 velocity (m/s)	Average (m/s)
5	1507.3 ± 6.7	1505.1 ± 11.1	1537.8 ± 34.6	1550.7 ± 39.3	1585.7 ± 57.4	1543.0 ± 46.7	1555.4 ± 50.5	1593.4 ± 44.2	1545.6 ± 46.3
4	1512.5 ± 22.5	1518.9 ± 19.6	1532.9 ± 21.3	1540 ± 39.1	1540.9 ± 46.3	1527.7 ± 40.7	1529.8 ± 31.2	1543.4 ± 30.9	1530.1 ± 28.6
3	1537.2 ±16.8	Not penetrated	1636 ± 53.0	1526 ± 20.4	1574.6 ± 57.9	1540.0 ± 25.2	1598.1 ± 83.5	Not penetrated	1571.7 ± 65
2	Not penetrated	Not penetrated	Not penetrated	1721.2 ± 238	Not penetrated	Not Penetrated	Not penetrated	Not penetrated	1721.2 ± 238
1	Not penetrated	Not penetrated	Not penetrated	1790.9 ± 91.3	Not penetrated	Not Penetrated	Not penetrated	Not penetrated	1790.9 ± 91.3

Note: Drill site 1405 did not penetrate mapped horizon and has been excluded from this table.
Note: Average velocities were calculated through each isochron unit with shipboard measured PWC physical property data.
Note: Site 1407 did not penetrate the full thickness of Unit 1, limiting average velocities of this unit to penetration extent.

Table 4: Bulk volumetric and mass accumulation rates for each seismic stratigraphic unit, along with variables used in calculations.

TABLE 4: Volumetric and Mass Accumulation Rates

Unit	Average Age Span (myr)	Sediment volume (km^3)	Median Duration (myr)	Bulk Volumetric Accumulation Rate (km^3/myr)	Bulk Volume (m^3)	Bulk-Dry Density (kg/m^3)	Sed Mass (kg)	Sed Mas (tonnes)	Sed Mass (Mt)	Mass Accumulation Rate (Mt/myr)	Mass Accumulation Rate (Mt/kyr)
5	2.6-0	3939.36	2.60	1515.14	3.94E+12	834 ± 223	3.29E+15	3.29E+12	3285423.07	1263624.26	1263.62
4	30.22 - 2.6	20901.41	27.62	757.98	2.09E+13	760 ± 230	1.59E+16	1.59E+13	15885071.60	576067.87	575.13
3	50.31- 30.22	16317.61	20.09	810.41	1.63E+13	1010 ± 206	1.65E+16	1.65E+13	16480786.10	818514.33	820.35
2	93.53- 50.31	6321.08	43.22	146.25	6.32E+12	1091 ± 167	6.90E+15	6.90E+12	6896298.28	159562.66	159.56
1	115-93.53	1911.46	21.47	89.03	1.91E+12	1461 ± 124	2.79E+15	2.79E+12	2792643.17	130071.88	130.07

Note: Median duration was calculated using the median of the average horizon age in Table 2.
Note: Bulk-dry densities were calculated using IODP measured moisture and density (MAD) data.
Note: Drill core did not penetrate the entirety of unit 4, limiting Bulk-Dry density values to penetration depth.

Table 5: Correlation of seismic horizons identified in this study, with seismic horizons documented in other North Atlantic seismic stratigraphic studies.

TABLE 5: North Atlantic Seismic Horizon Correlation

Reflector Age	Reflector Name	Region	Reference
2.6 Ma	H5/H6	Newfoundland Ridge	This Study
2.5 Ma	R1	Erik Drift	Müller-Michaelis et al., 2013
Pliocene-Pleistocene	R1	Gloria Drift, Erik Drift	Arthur et al., 1989
30.2 ± 4.2 Ma	H4	Newfoundland Ridge	This Study
early Oligocene	TE	Southeast Faroes Drift	Davies et al., 2001
early Oligocene	A^U	Offshore Eastern United States	Tucholke, 1981; Mountain and Tucholke, 1985
50.3 ± 3.4 Ma	H3	Newfoundland Ridge	This Study
50-49 Ma	IEU	Judd Falls Drift	Hohbein et al., 2012
middle Eocene	I-Lutetian 3	Faroe-Shetland Channel	Smallwood, 2004
early Eocene	A^C	Offshore Eastern United States	Tucholke, 1981; Mountain and Tucholke, 1985

Appendix 1: P-wave Velocity and Density Logs

P-wave velocity and density logs measured shipboard from drill cores during IODP Expedition 342. Values displayed by these logs were used to generate acoustic impedance logs (Figure 4).

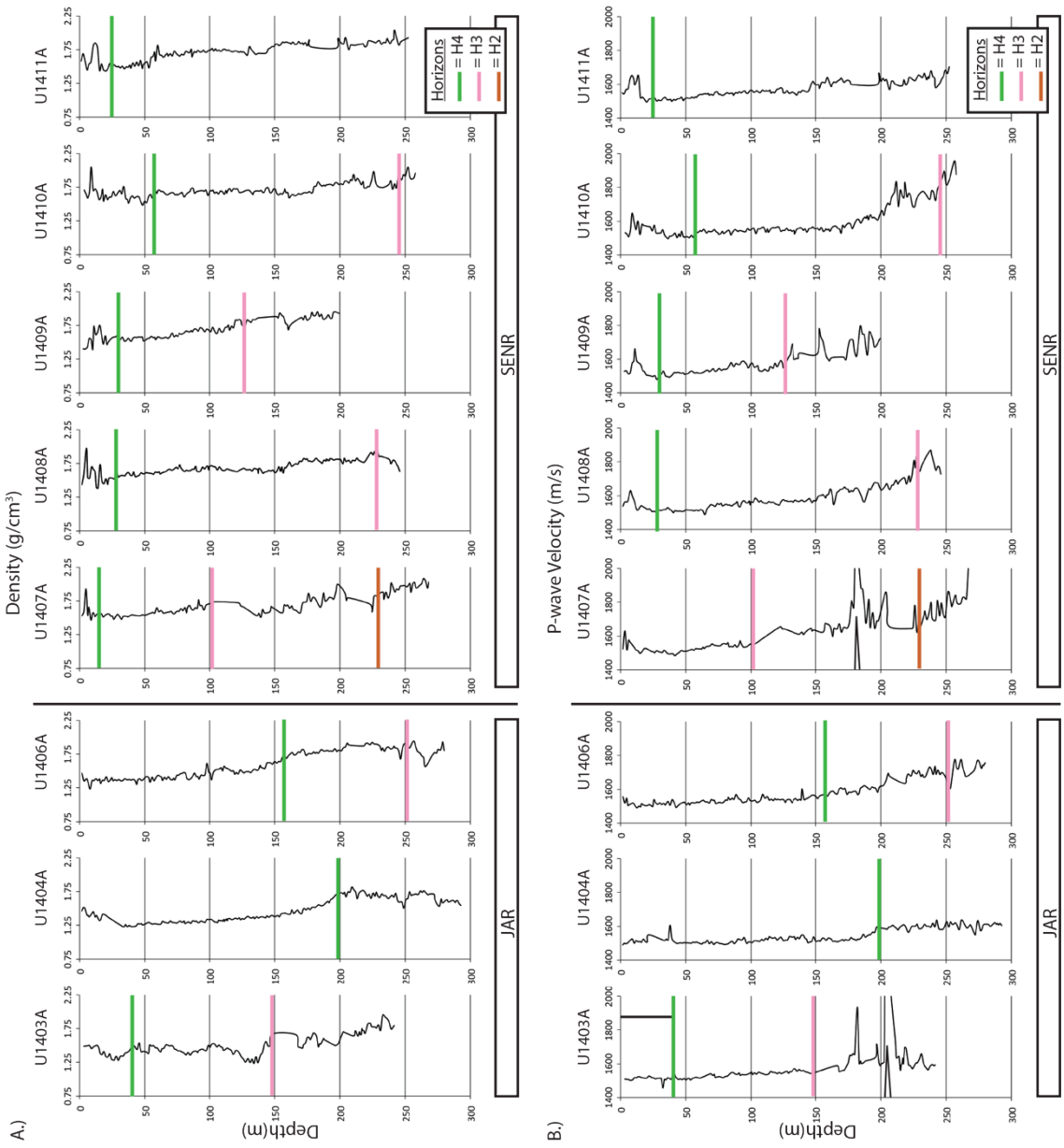
A.)
Density (g/cm³)
U1403A
U1404A
U1406A
U1407A
U1408A
U1409A
U1410A
U1411A
Horizons
= H4
= H3
= H2
JAR
SENR
Depth (m)
B.)
P-wave Velocity (m/s)

Appendix 2: RV Knorr 179-1 Seismic Transects

All 56 2-D seismic-reflection profiles collected in 2004 on the R.V. Knorr 179-1 displayed with seismic stratigraphic interpretations from this study. Seismic-reflection profiles are number L01-L056. Note changes in scales.

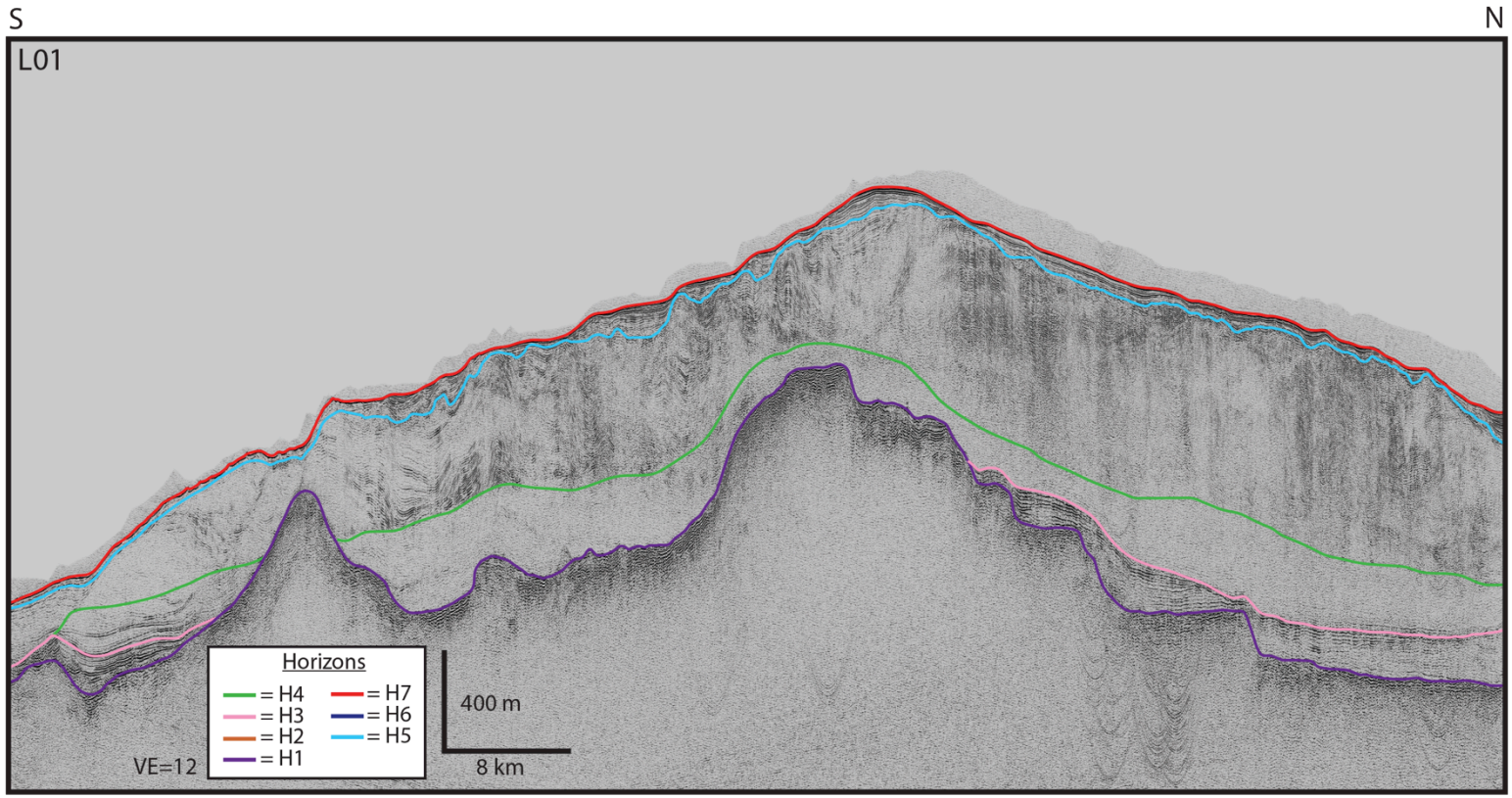
S
N
L01
Horizons
= H4
= H3
= H2
= H1
= H7
= H6
= H5
400 m
8 km
VE=12

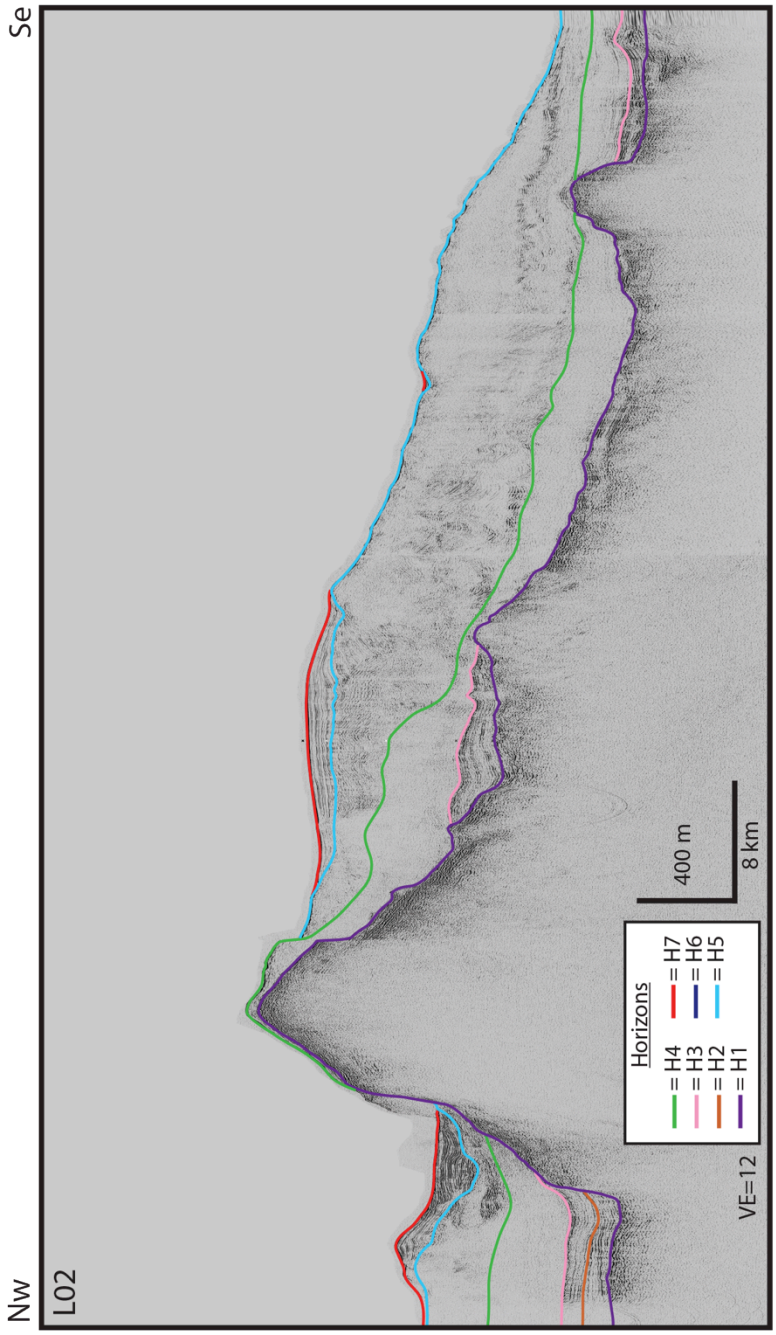
Se
Nw
L02
Horizons
= H4
= H3
= H2
= H1
= H7
= H6
= H5
400 m
8 km
VE=12

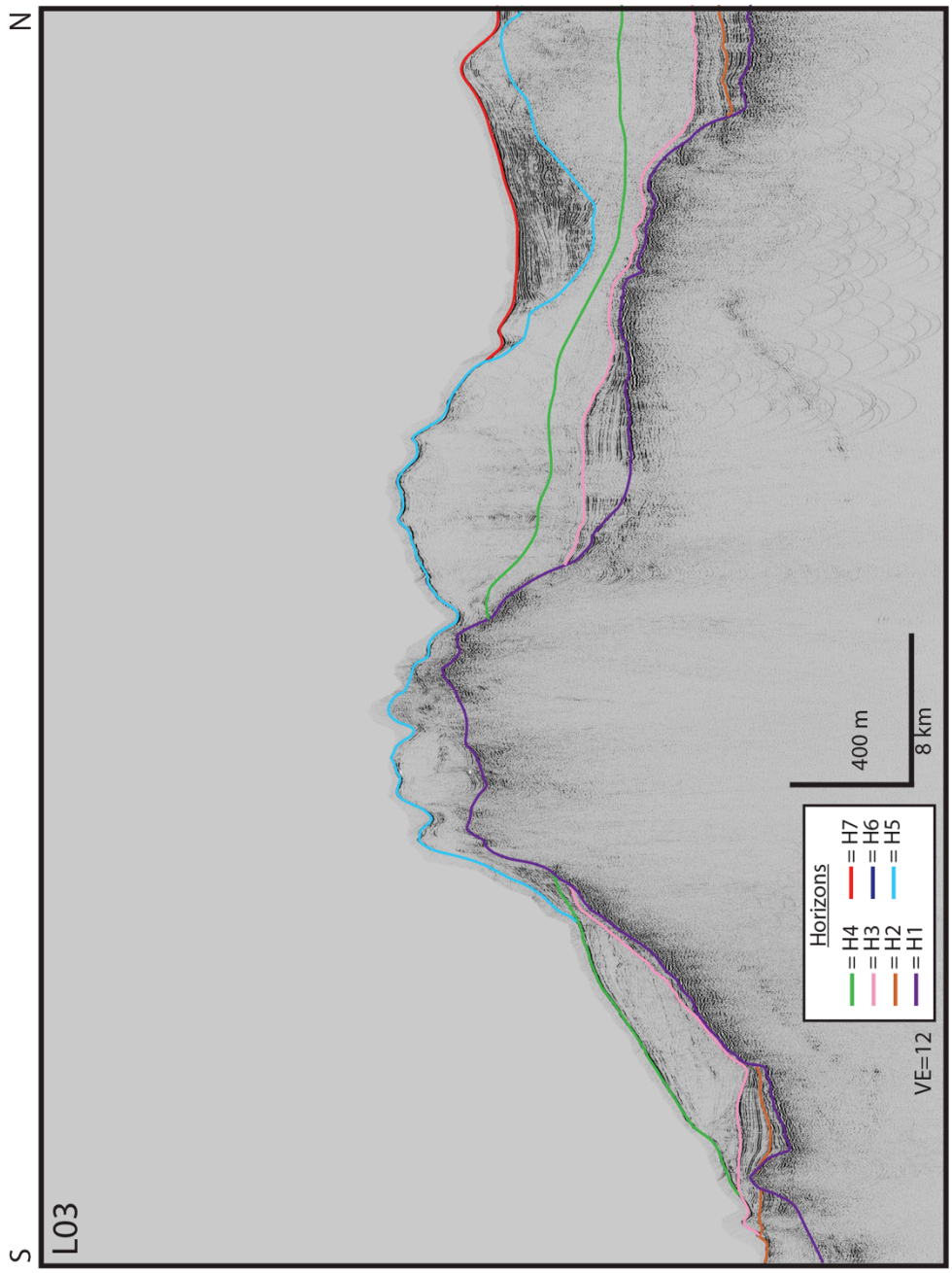
N
S
L03
Horizons
= H4
= H3
= H2
= H1
= H7
= H6
= H5
400 m
8 km
VE=12

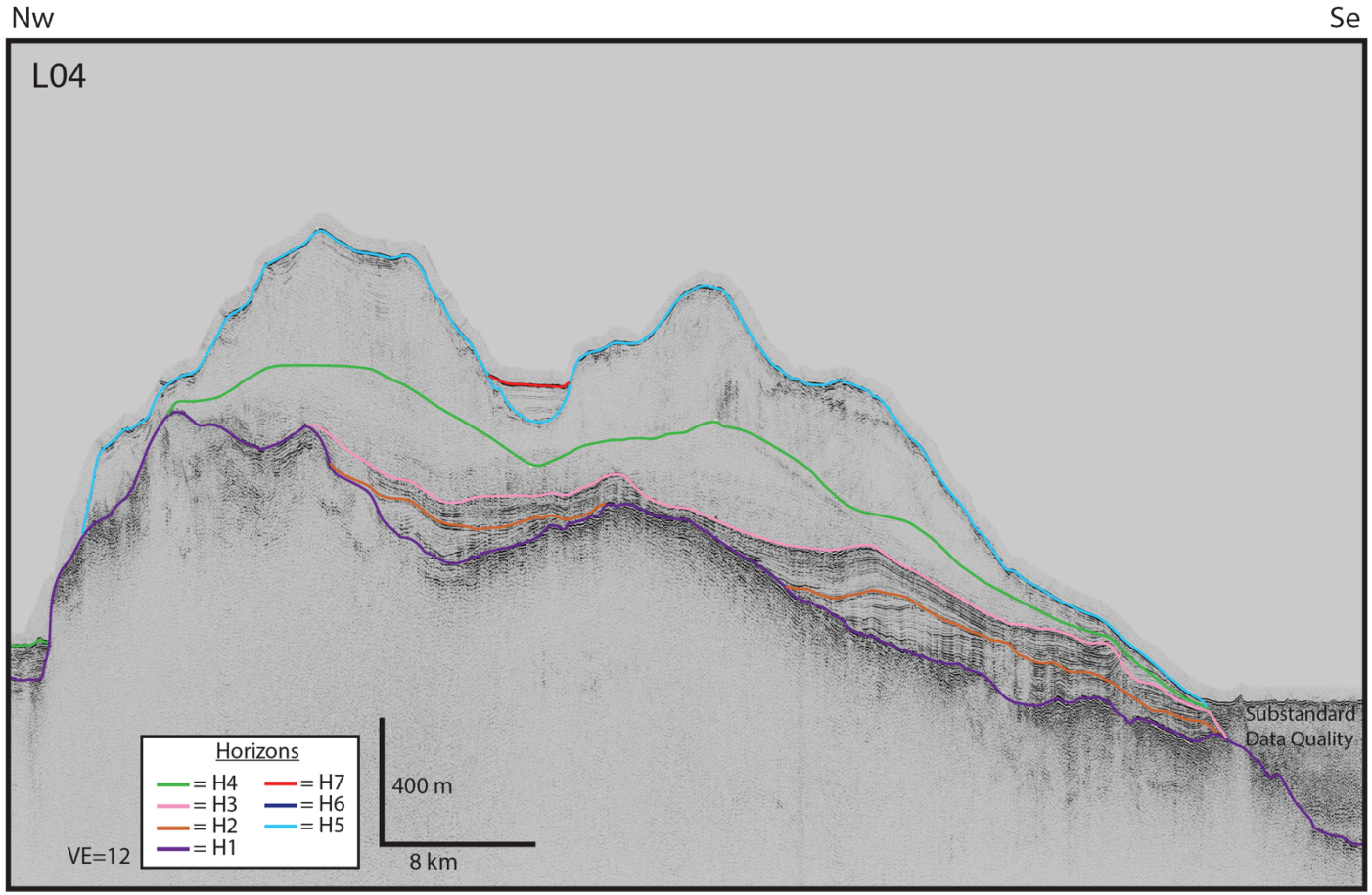
Nw
Se
L04
Horizons
= H4
= H3
= H2
= H1
= H7
= H6
= H5
VE=12
400 m
8 km
Substandard
Data Quality

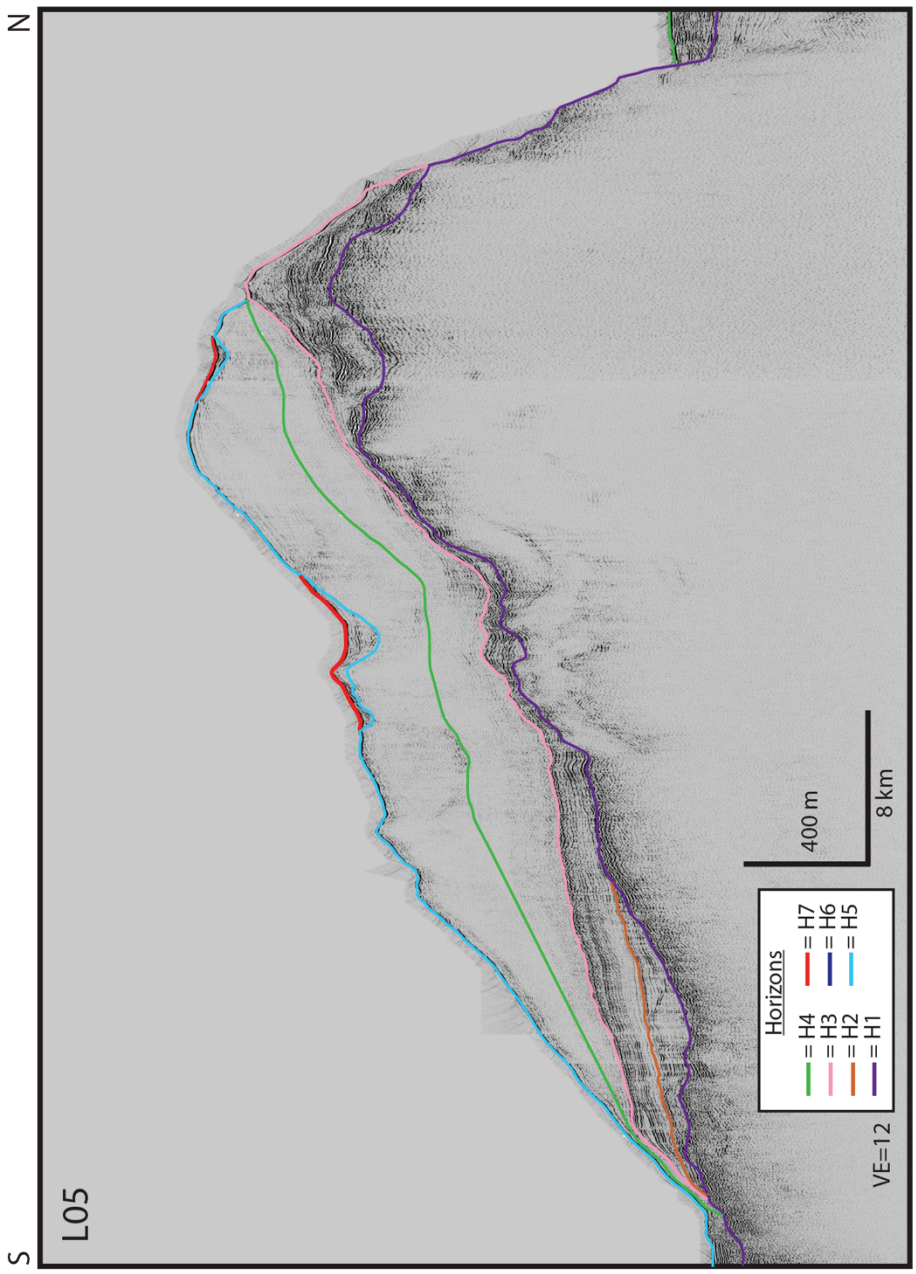
N
S
L05
Horizons
= H4
= H3
= H2
= H1
= H7
= H6
= H5
400 m
8 km
VE=12

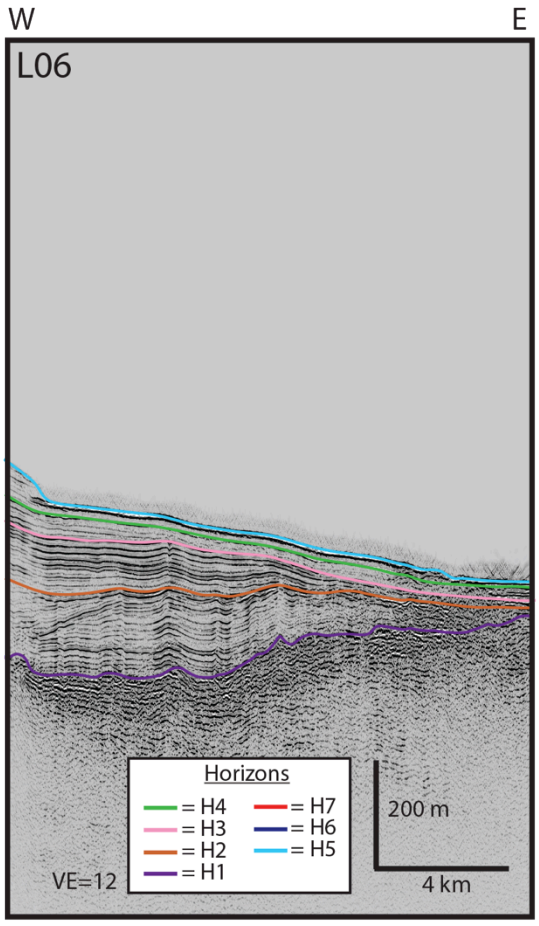
W
E
L06
Horizons
= H4
= H3
= H2
= H1
= H7
= H6
= H5
VE=12
200 m
4 km

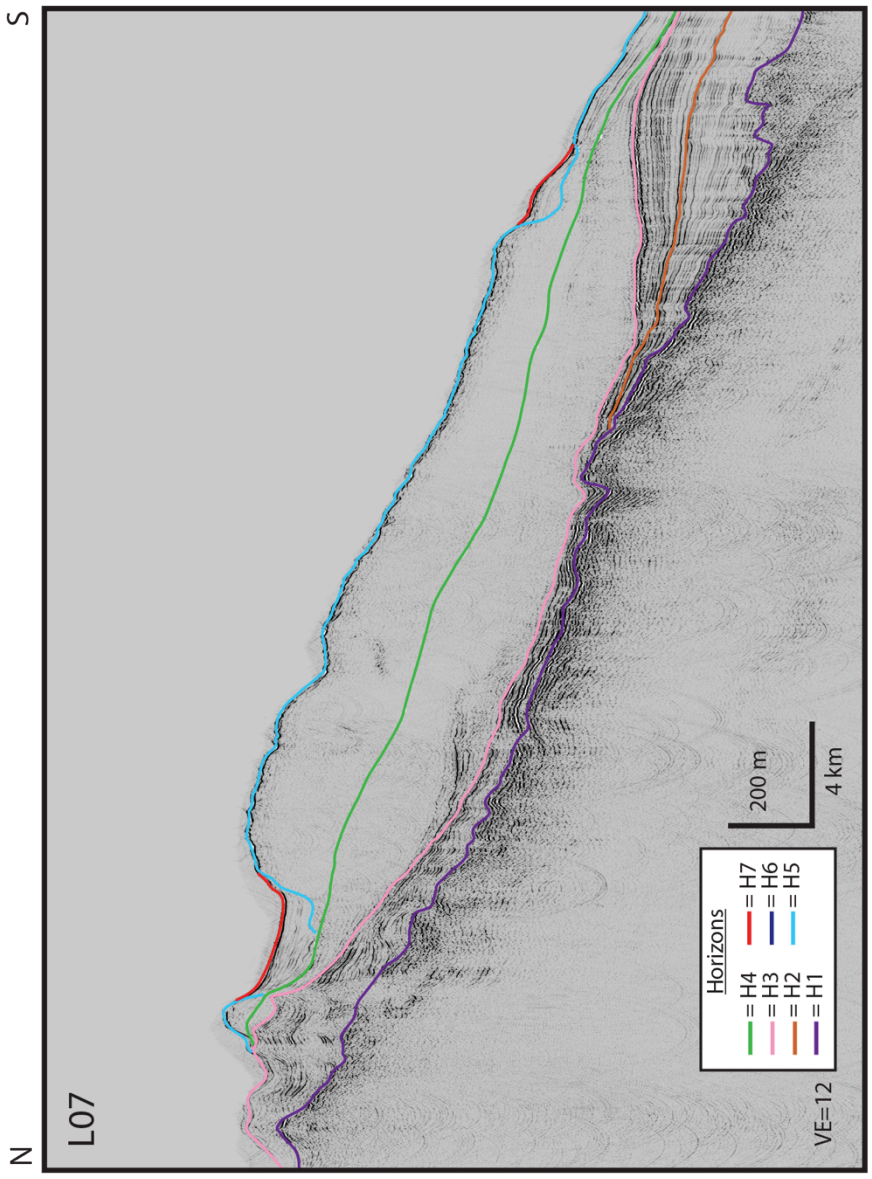
S
N
L07
Horizons
= H4
= H3
= H2
= H1
= H7
= H6
= H5
200 m
4 km
VE=12

W
E
L08
Substandard Data
Horizons
= H4
= H3
= H2
= H1
= H7
= H6
= H5
200 m
4 km
VE=12

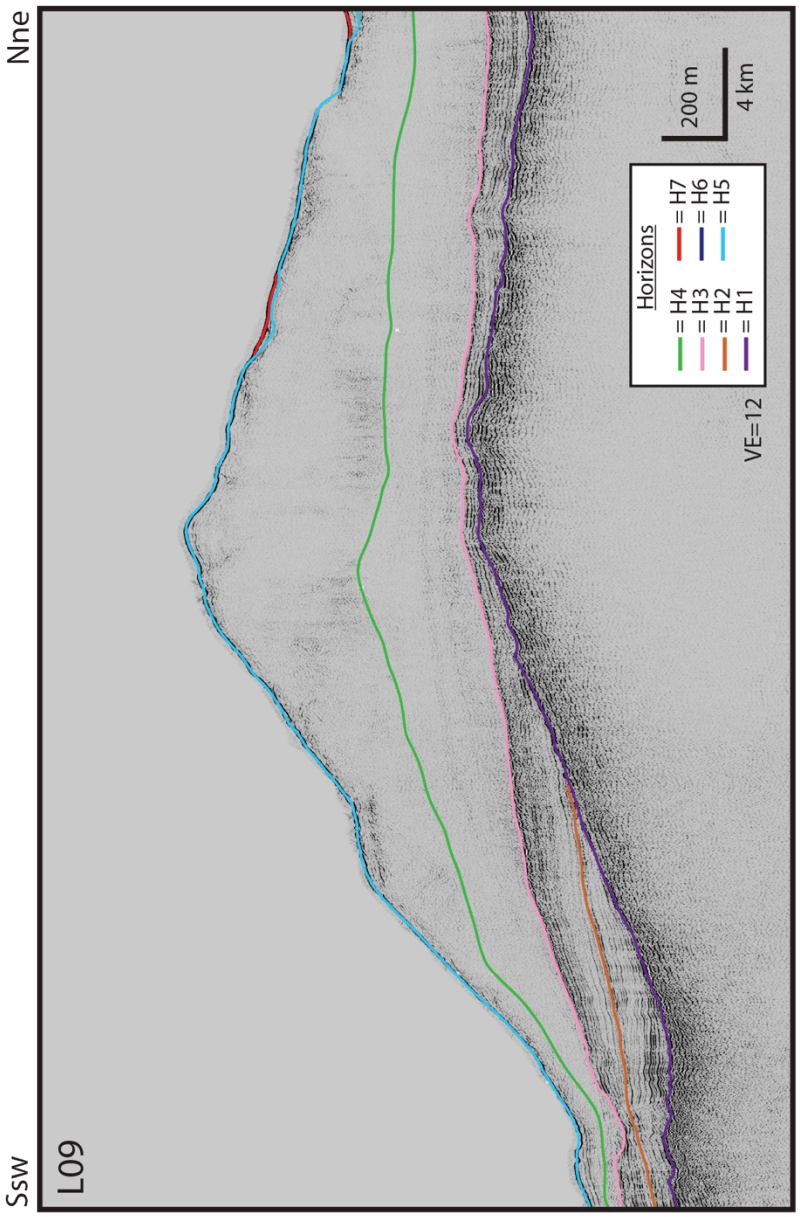
Ssw
Nne
L09
Horizons
H4
H3
H2
H1
H7
H6
H5
200 m
4 km
VE=12

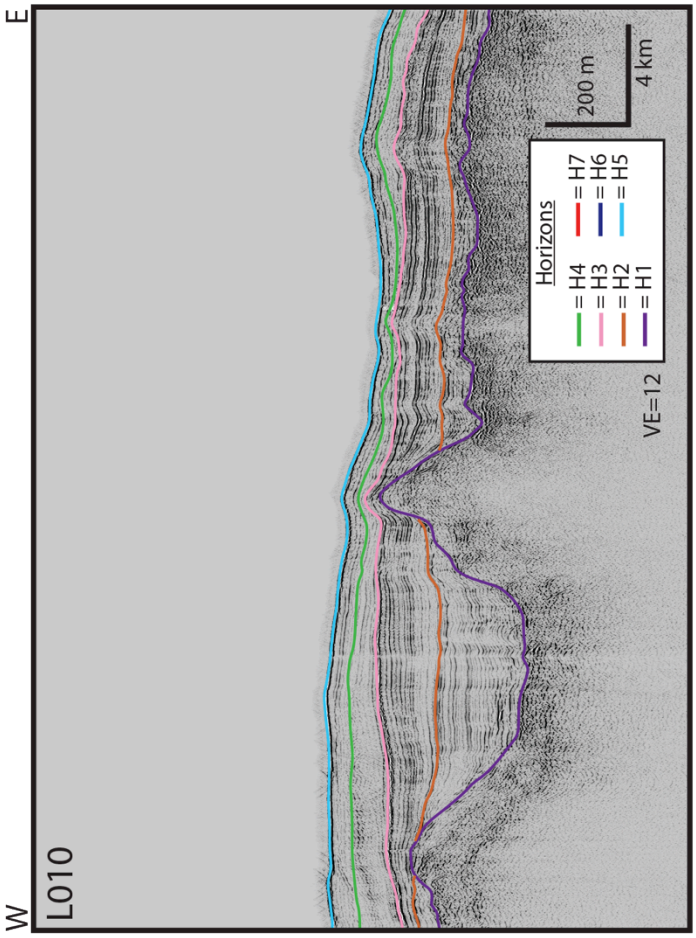
E
W
L010
200 m
4 km
Horizons
= H7
= H6
= H5
= H4
= H3
= H2
= H1
VE=12

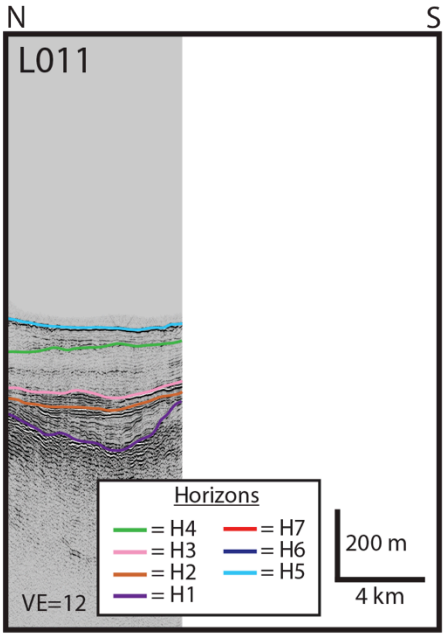
N
S
L011
Horizons
= H4
= H3
= H2
= H1
= H7
= H6
= H5
200 m
4 km
VE=12

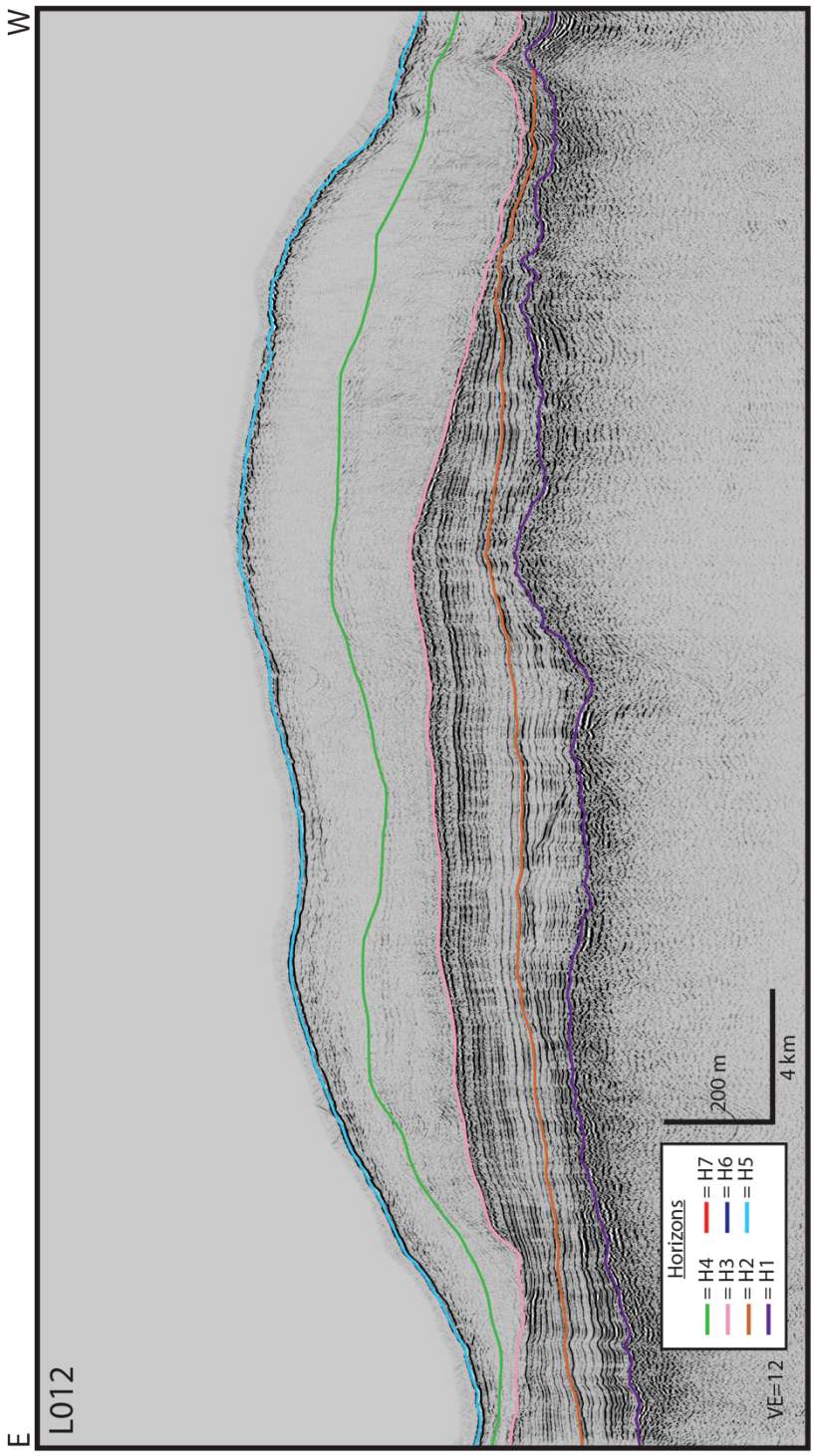
W
E
L012
Horizons
H4 = H7
H3 = H6
H2 = H5
H1
200 m
4 km
VE=12

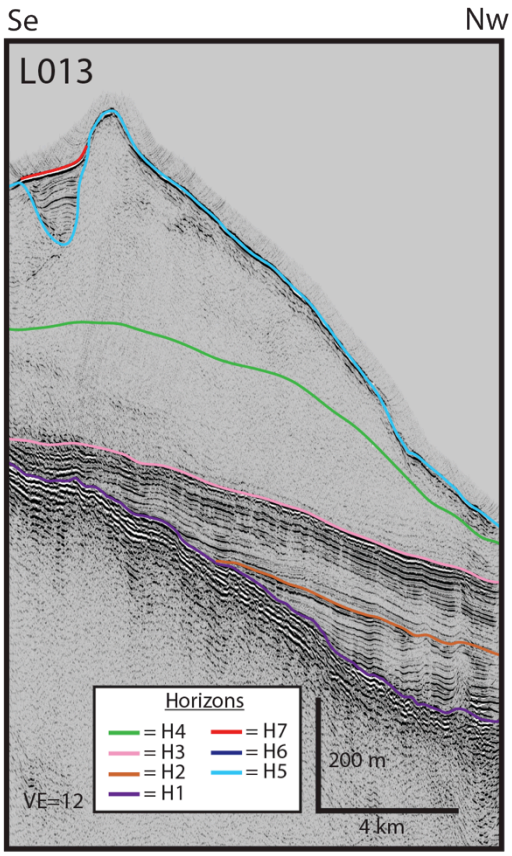
Se
Nw
L013
Horizons
= H4
= H3
= H2
= H1
= H7
= H6
= H5
200 m
4 km
VE=12

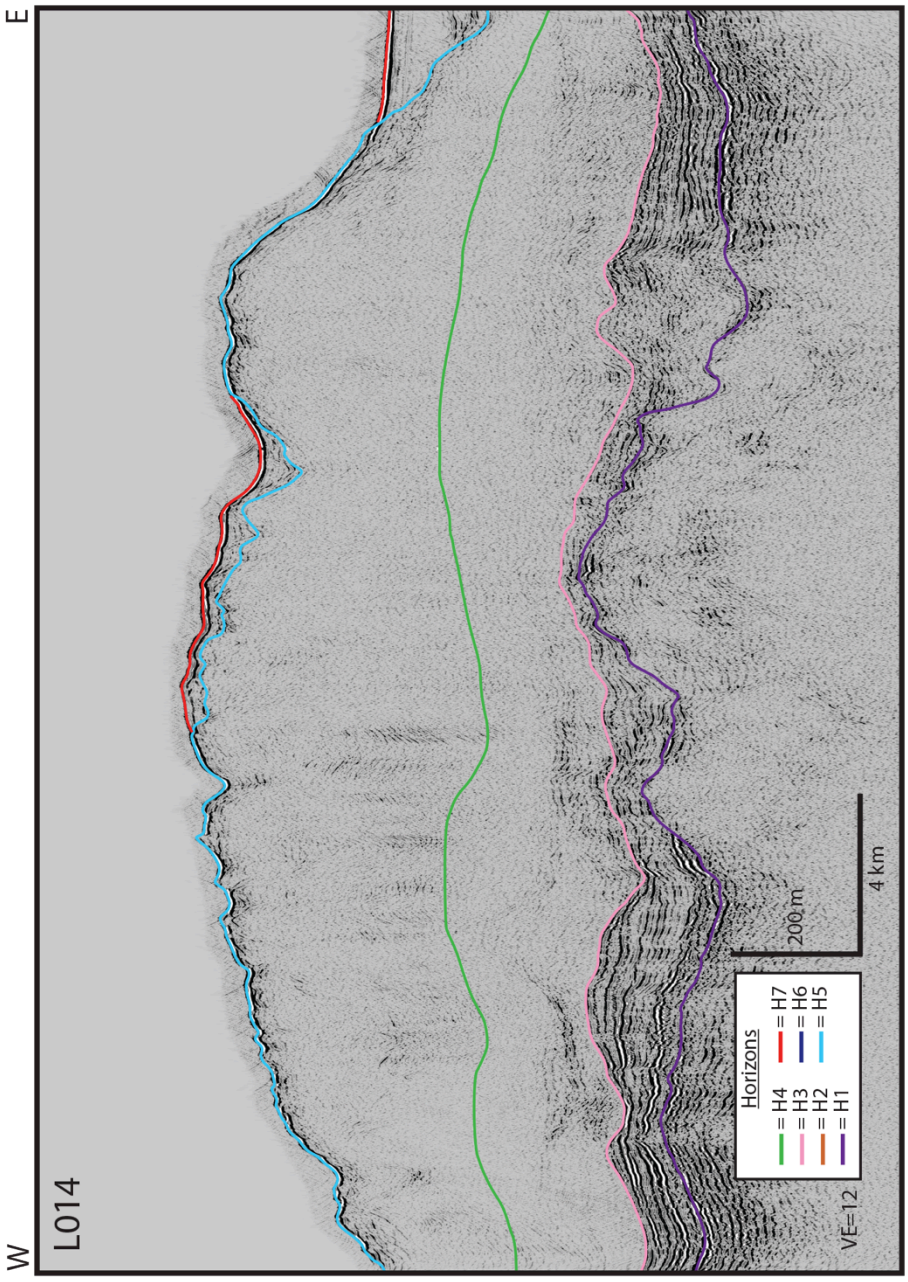
W
E
L014
Horizons
= H4
= H3
= H2
= H1
= H7
= H6
= H5
200 m
4 km
VE=12

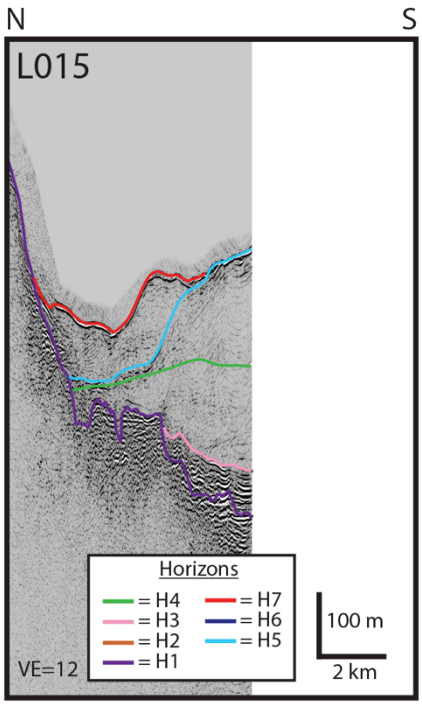
N
S
L015
Horizons
= H4
= H3
= H2
= H1
= H7
= H6
= H5
100 m
2 km
VE=12

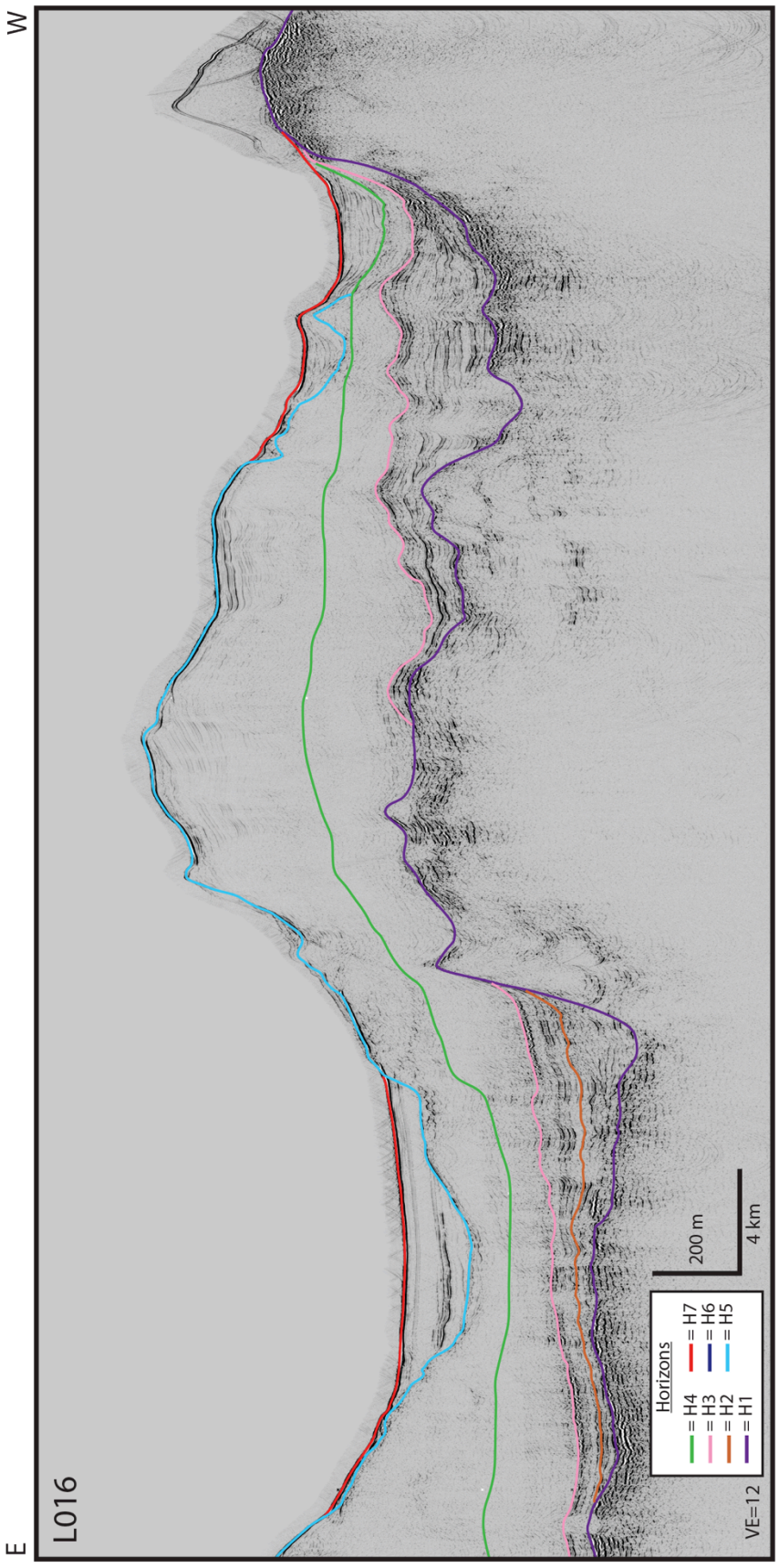
W
E
L016
Horizons
= H4
= H3
= H2
= H1
= H7
= H6
= H5
200 m
4 km
VE=12

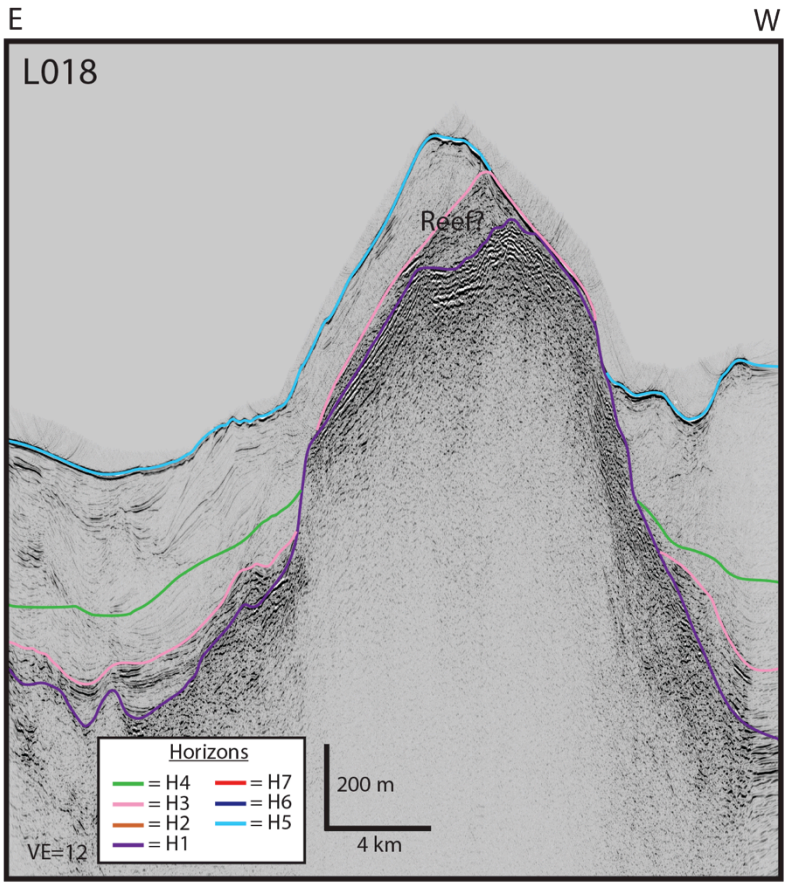
E
W
L018
Reef?
Horizons
= H4
= H3
= H2
= H1
= H7
= H6
= H5
200 m
4 km
VE=12

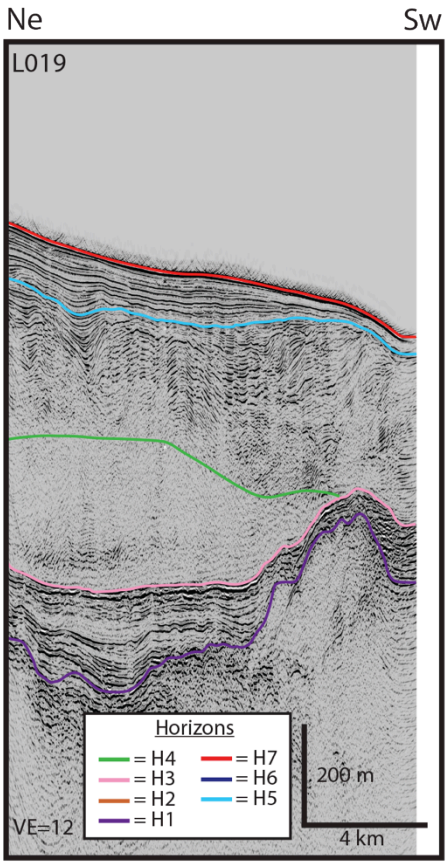
Ne
Sw
L019
Horizons
= H4
= H3
= H2
= H1
= H7
= H6
= H5
200 m
4 km
VE=12

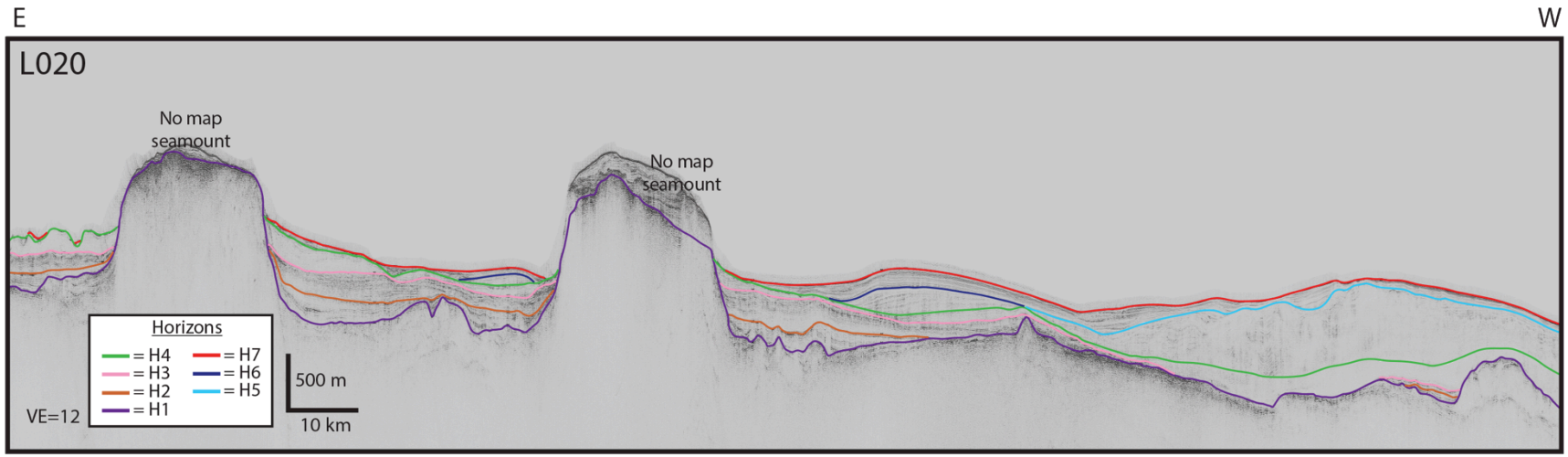
E
W
L020
No map seamount
No map seamount
Horizons
= H4
= H3
= H2
= H1
= H7
= H6
= H5
500 m
10 km
VE=12

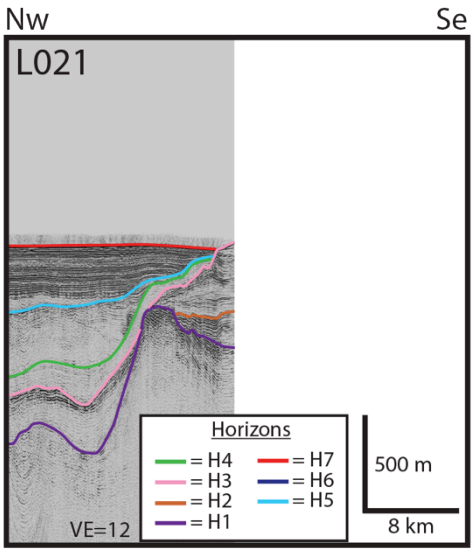
Nw
Se
L021
Horizons
= H4
= H3
= H2
= H1
= H7
= H6
= H5
500 m
8 km
VE=12

E
W
L022
Horizons
= H4
= H3
= H2
= H1
= H7
= H6
= H5
500 m
8 km
VE=12

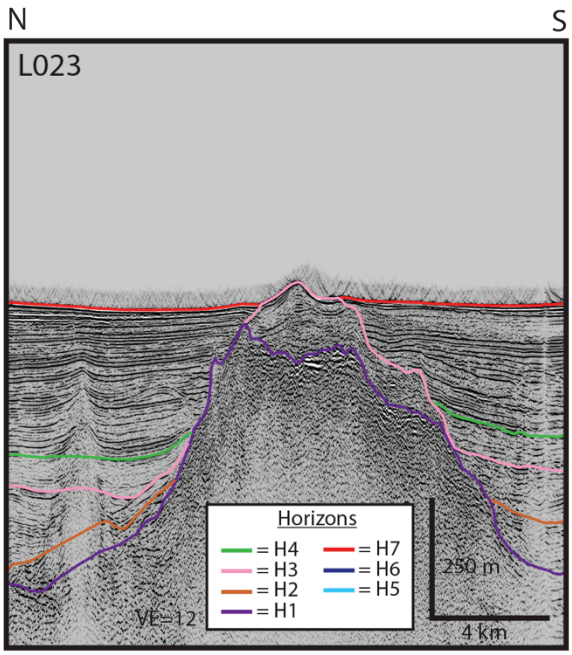
N
S
L023
Horizons
= H4
= H3
= H2
= H1
= H7
= H6
= H5
250 m
4 km
VE=12


W
E
L024
Horizons
= H4
= H3
= H2
= H1
= H7
= H6
= H5
500 m
8 km
VE=12

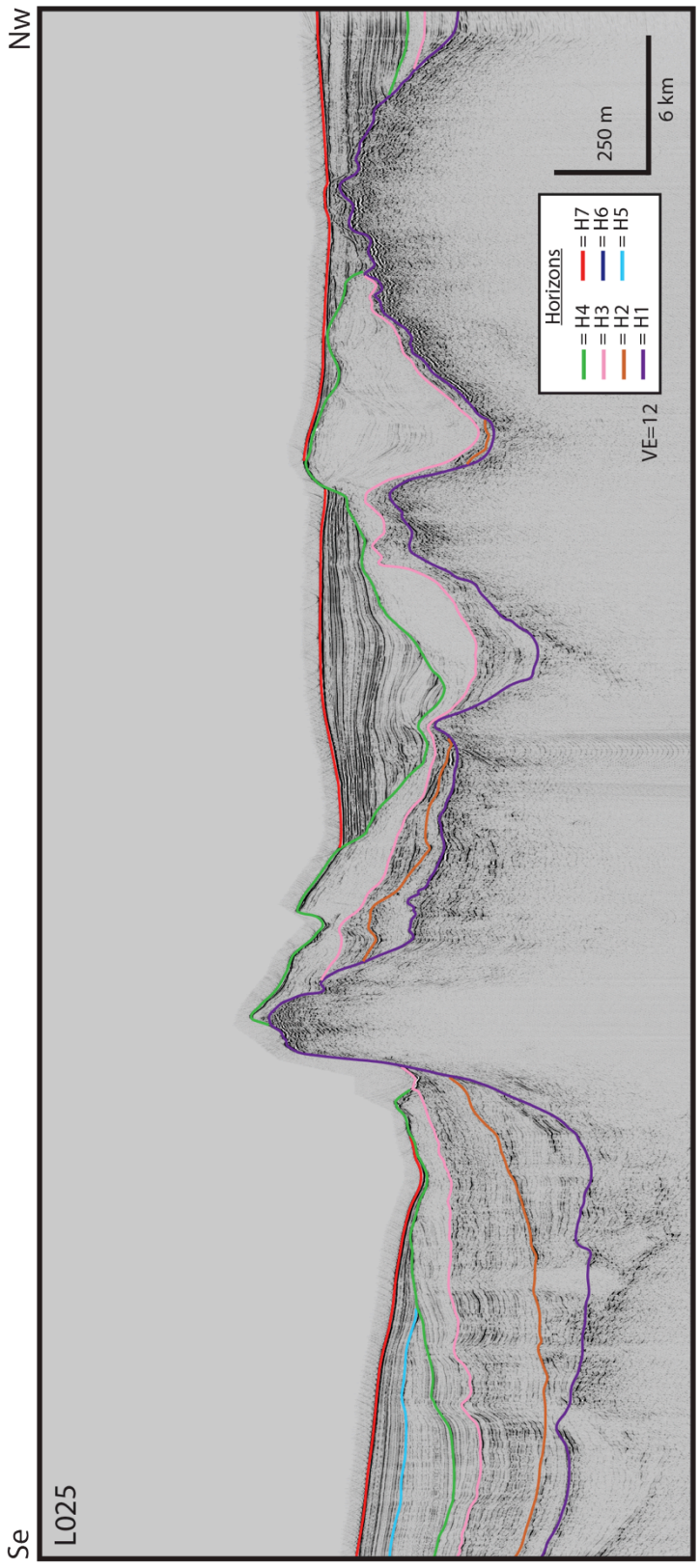
Nw
Se
L025
Horizons
H4
H3
H2
H1
H7
H6
H5
250 m
6 km
VE=12

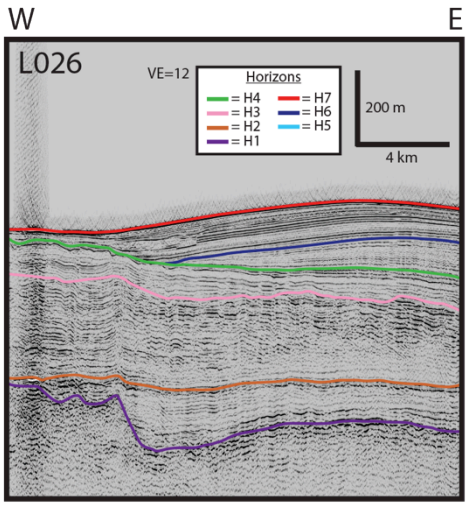
W
E
L026
VE=12
Horizons
= H4
= H3
= H2
= H1
= H7
= H6
= H5
200 m
4 km

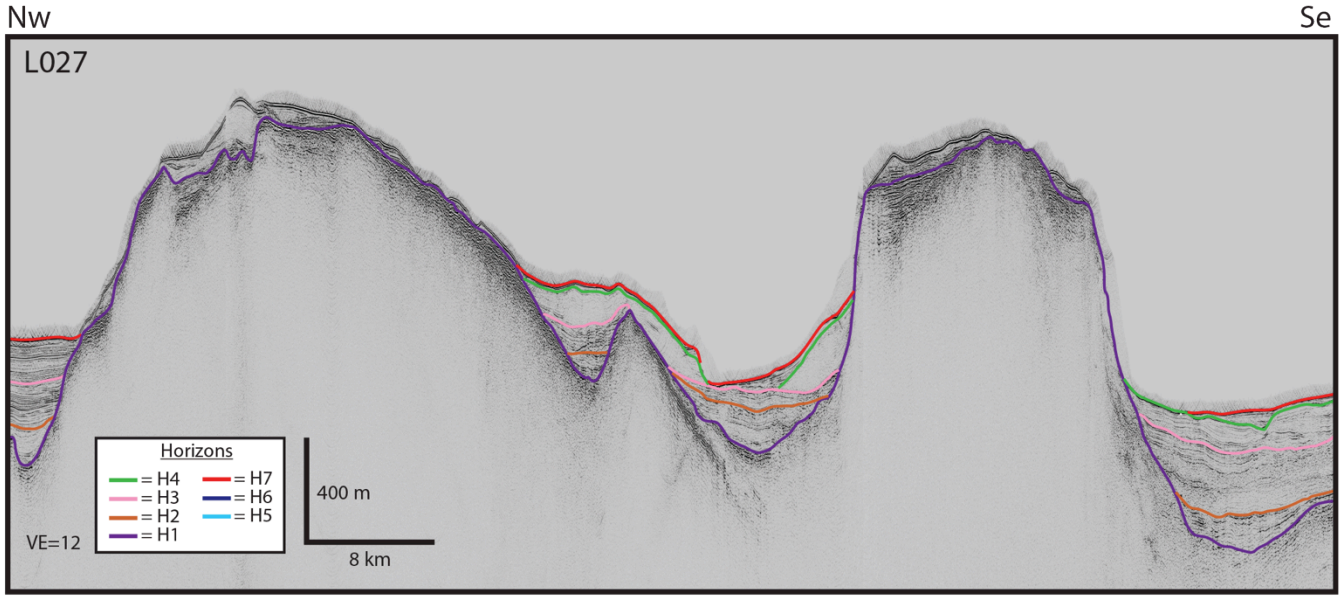
Nw
Se
L027
Horizons
= H4
= H3
= H2
= H1
= H7
= H6
= H5
400 m
8 km
VE=12

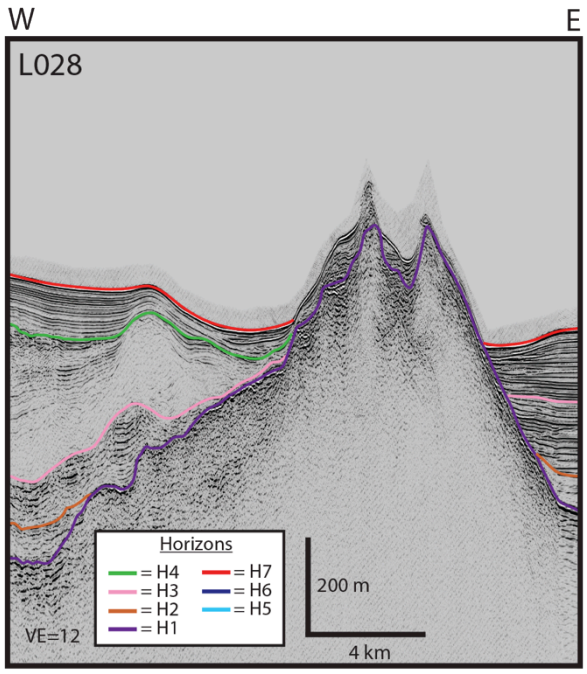
W
E
L028
Horizons
= H4
= H3
= H2
= H1
= H7
= H6
= H5
200 m
4 km
VE=12

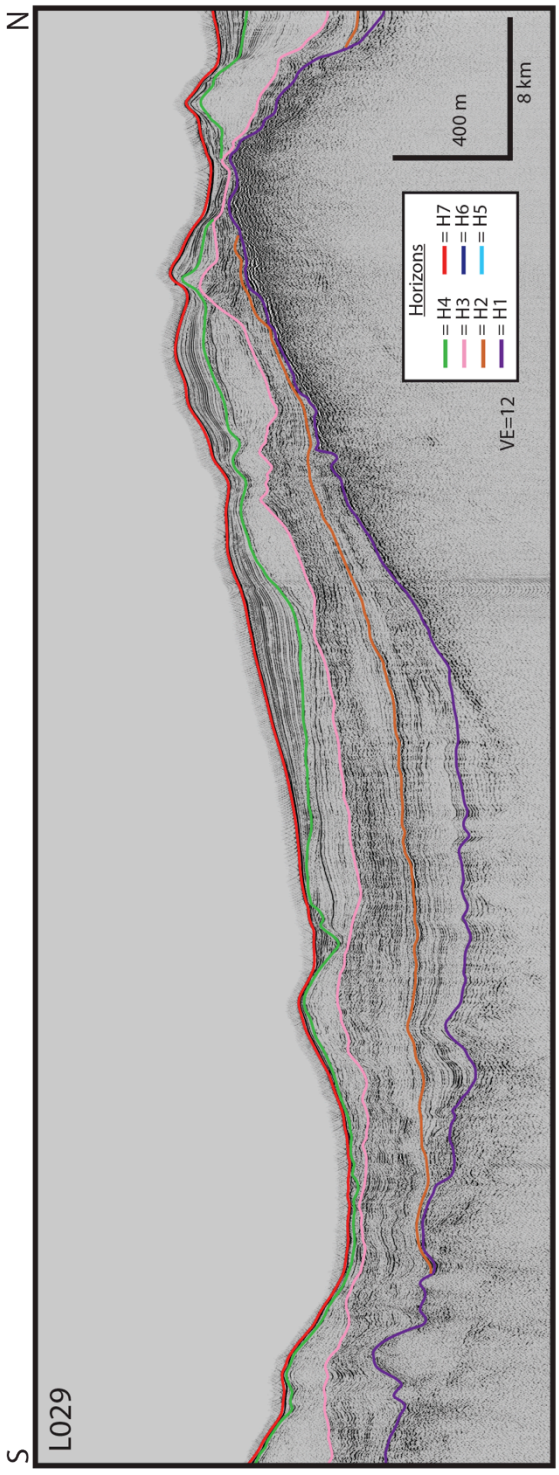
N
S
L029
Horizons
H4
H3
H2
H1
H7
H6
H5
400 m
8 km
VE=12

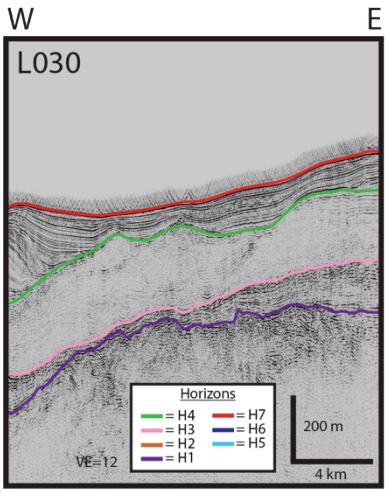
W
E
L030
Horizons
= H4
= H3
= H2
= H1
= H7
= H6
= H5
VE=12
200 m
4 km

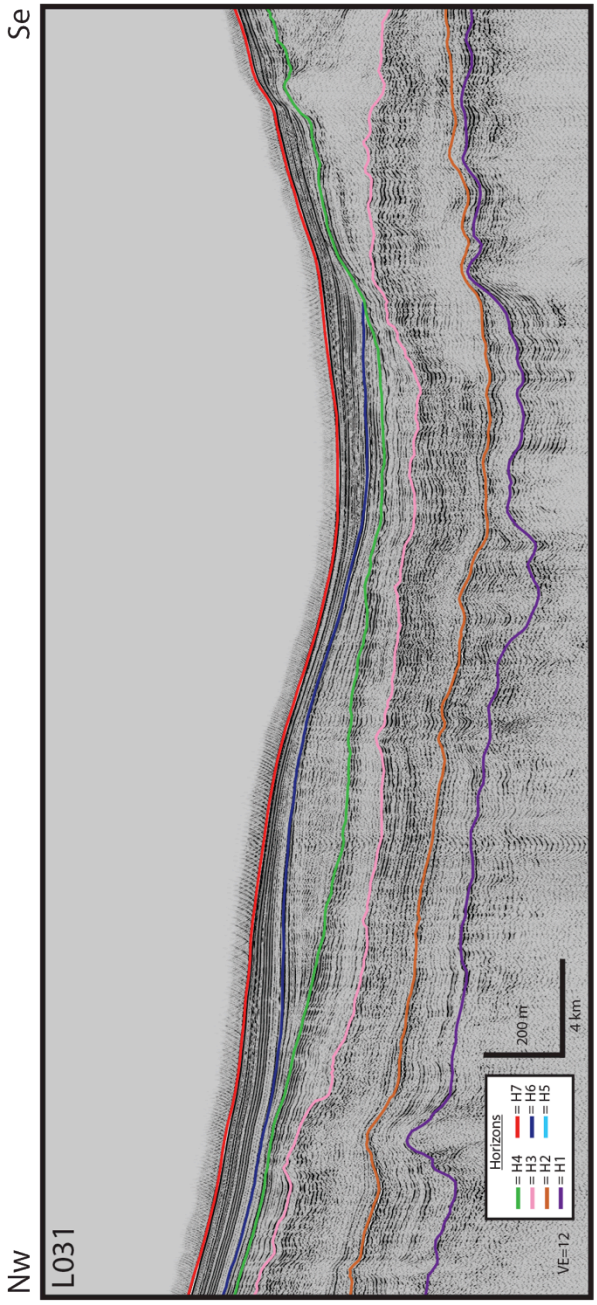
Se
Nw
L031
Horizons
H7
H6
H5
H4
H3
H2
H1
200 m
4 km
VE=12

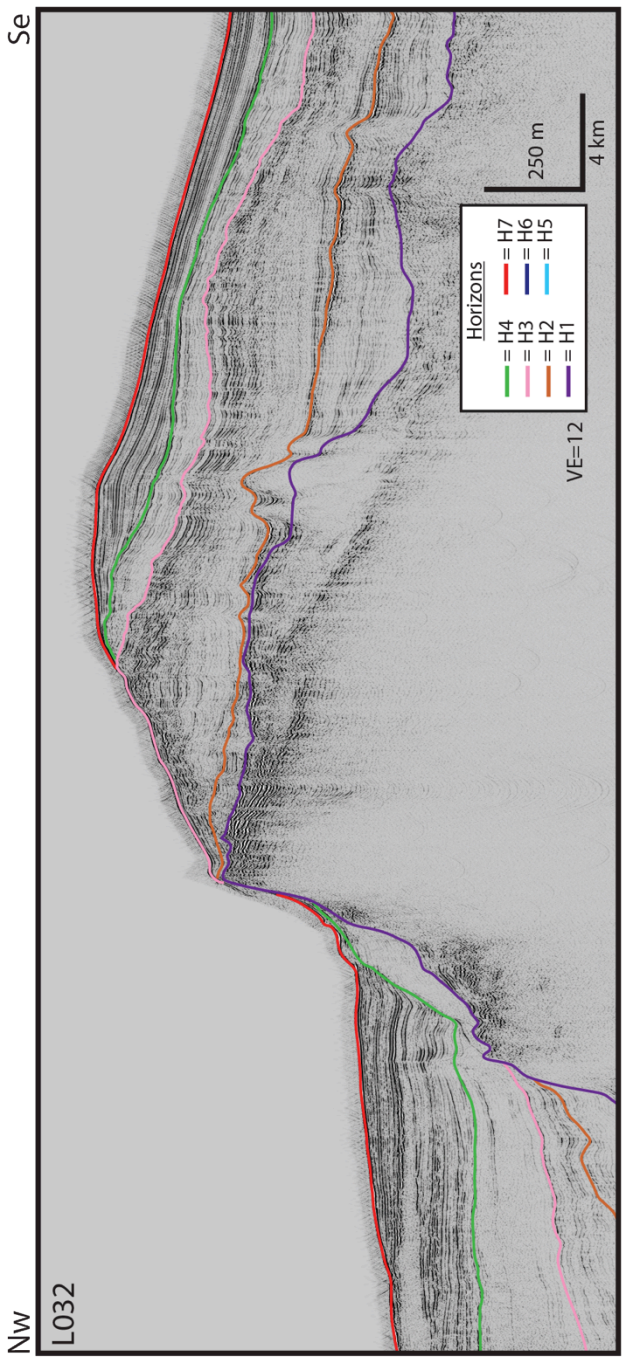
Se
Nw
L032
Horizons
= H4
= H3
= H2
= H1
= H7
= H6
= H5
250 m
4 km
VE=12

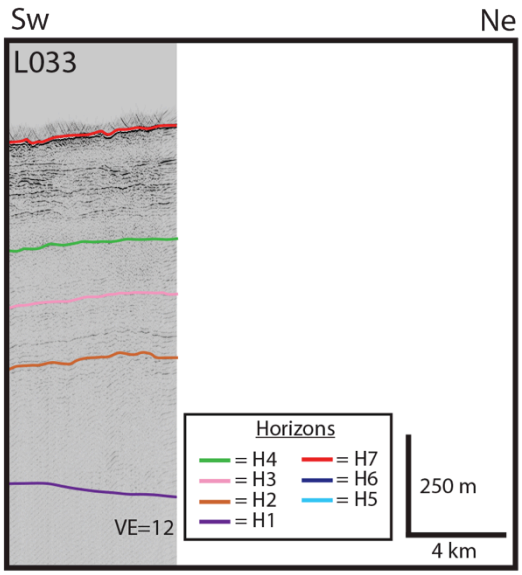
Sw
Ne
L033
Horizons
= H4
= H3
= H2
= H1
= H7
= H6
= H5
250 m
4 km
VE=12

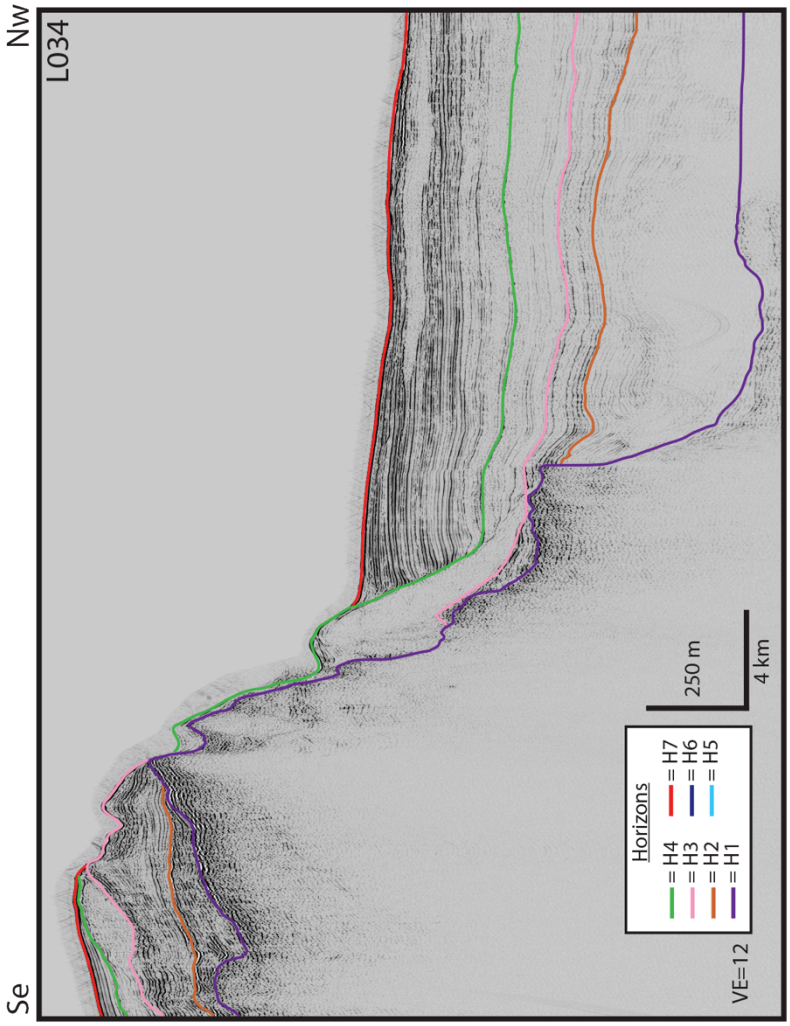
Nw
Se
L034
Horizons
= H4
= H3
= H2
= H1
= H7
= H6
= H5
250 m
4 km
VE=12

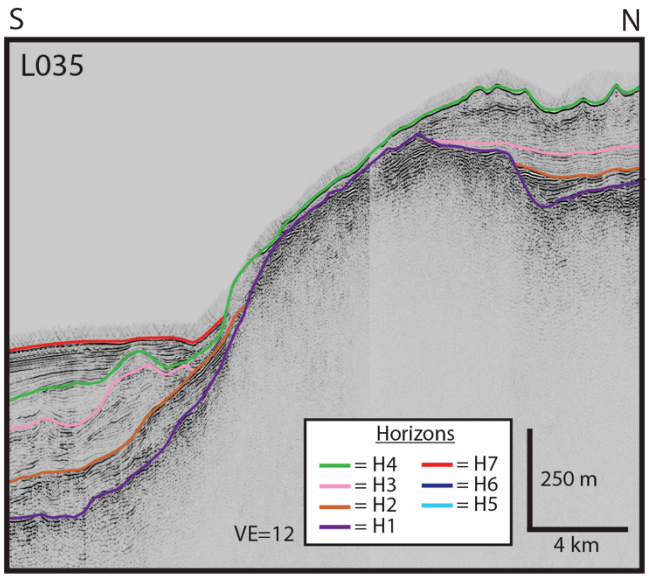
S
N
L035
Horizons
= H4
= H3
= H2
= H1
= H7
= H6
= H5
VE=12
250 m
4 km

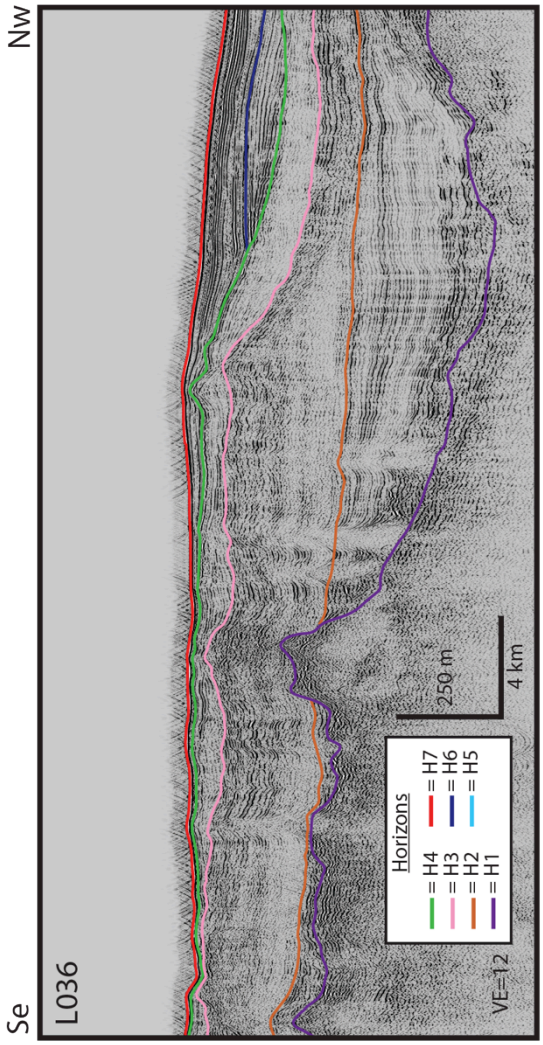
Nw
Se
L036
Horizons
= H4
= H3
= H2
= H1
= H7
= H6
= H5
VE=12
250 m
4 km

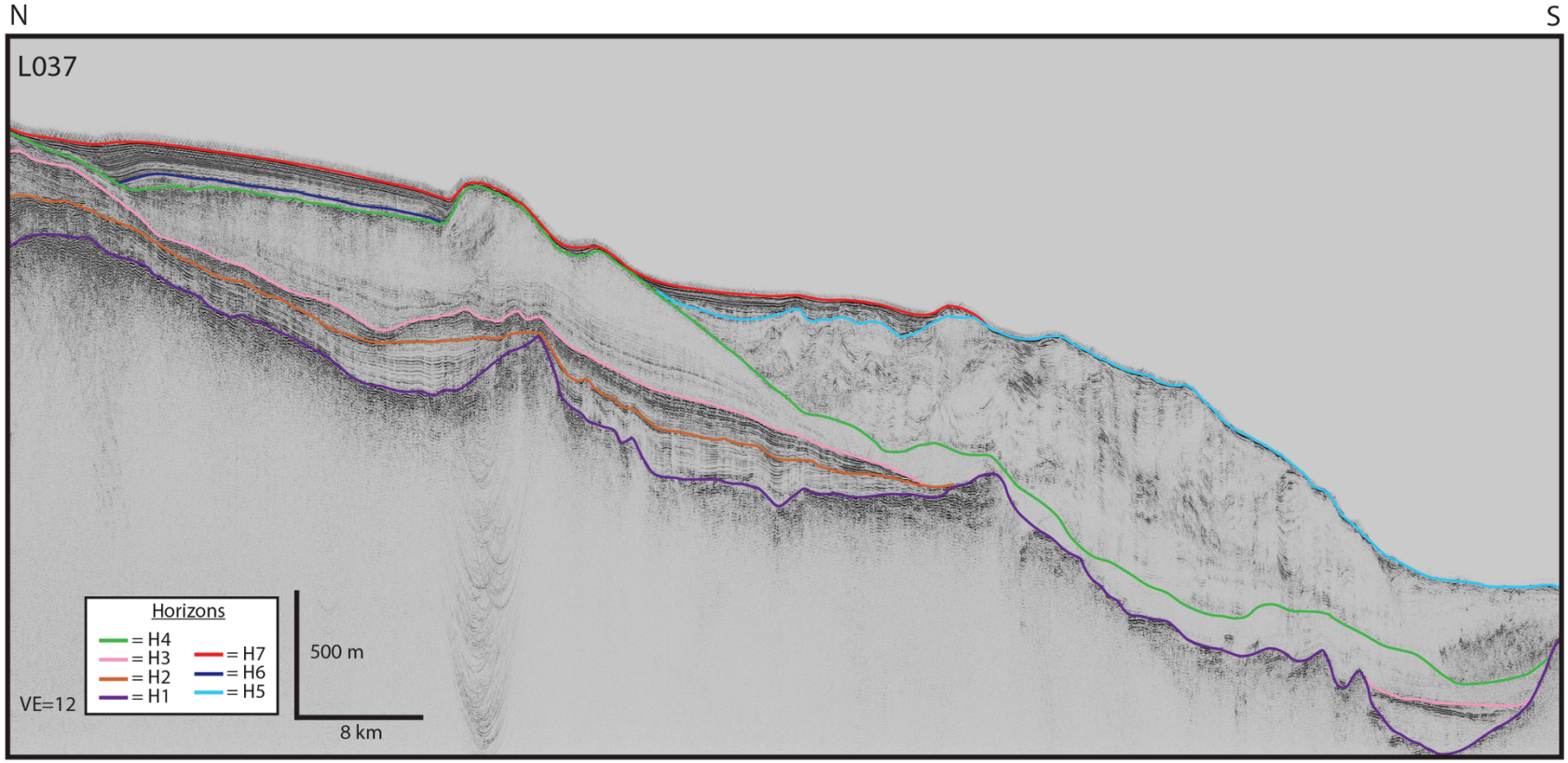
N
S
L037
Horizons
= H4
= H3
= H2
= H1
= H7
= H6
= H5
500 m
8 km
VE=12

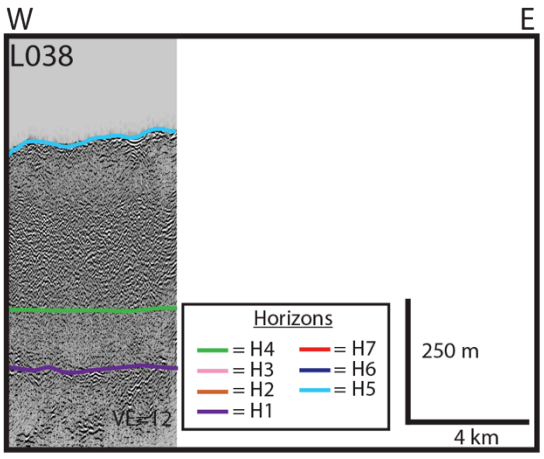
W
E
L038
Horizons
= H4
= H7
= H3
= H6
= H2
= H5
= H1
250 m
4 km
VE=12


Sw
Ne
L039
Horizons
= H4
= H3
= H2
= H1
= H7
= H6
= H5
1000 m
20 km
VE=12

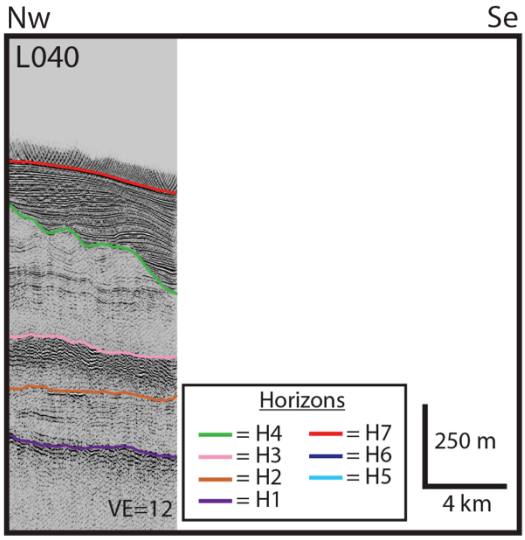
Nw
Se
L040
VE=12
Horizons
= H4
= H3
= H2
= H1
= H7
= H6
= H5
250 m
4 km

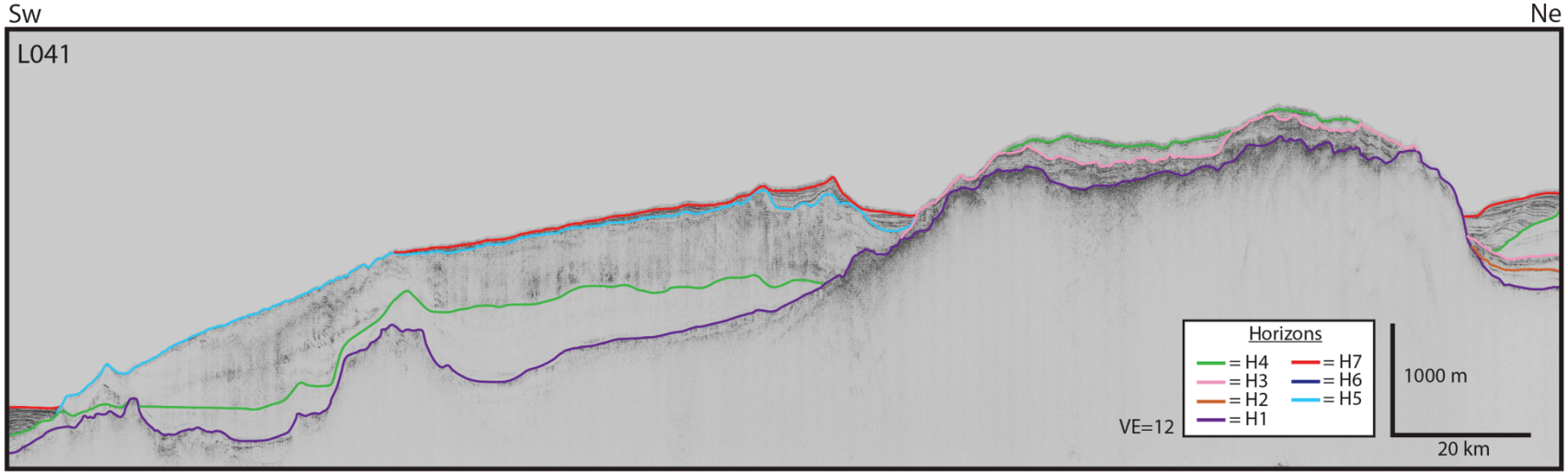
Sw
Ne
L041
Horizons
= H4
= H7
= H3
= H6
= H2
= H5
= H1
VE=12
1000 m
20 km

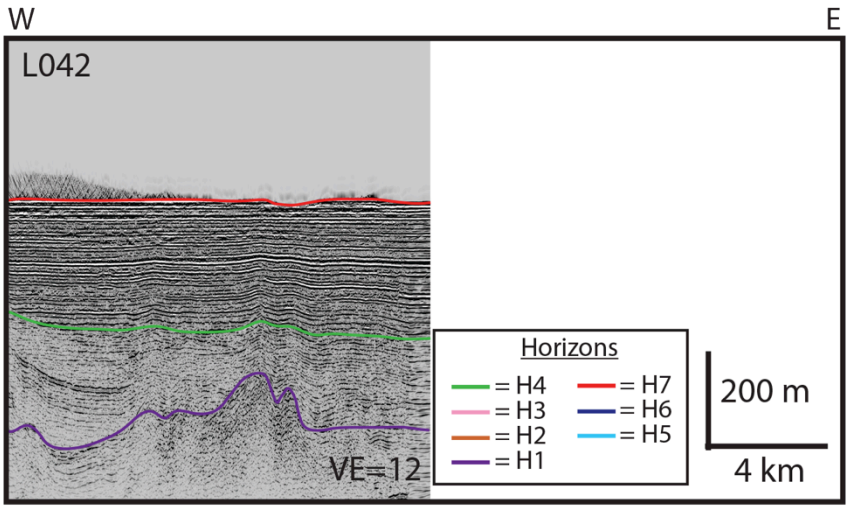
W
E
L042
VE=12
Horizons
= H4
= H3
= H2
= H1
= H7
= H6
= H5
200 m
4 km

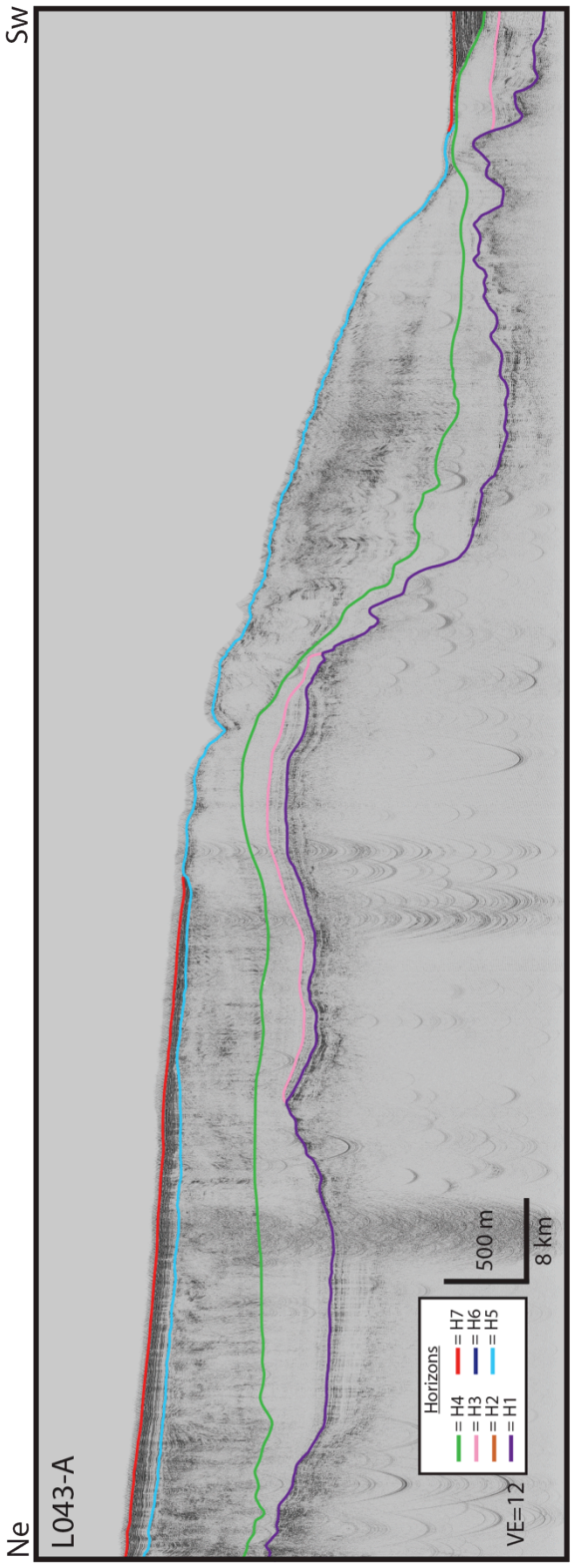
Sw
Ne
L043-A
Horizons
= H4
= H3
= H2
= H1
= H7
= H6
= H5
500 m
8 km
VE=12

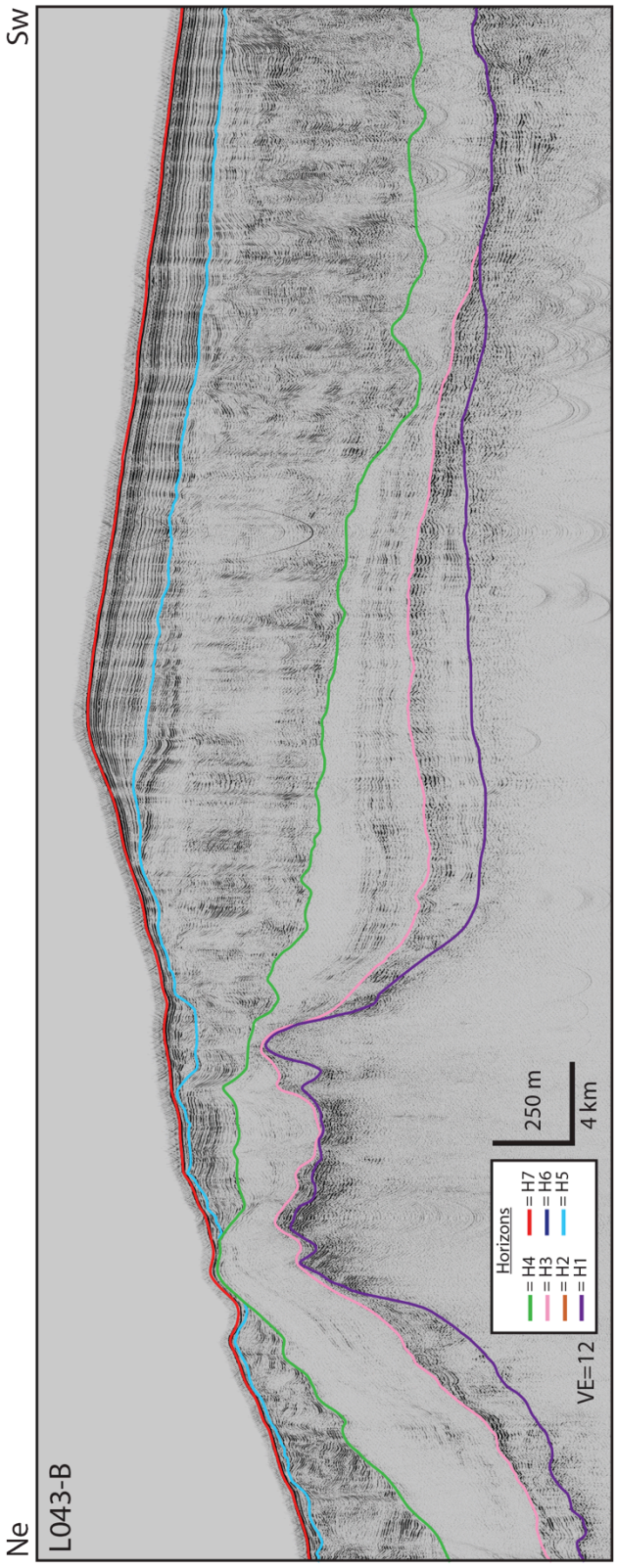
Sw
Ne
L043-B
Horizons
H4
H3
H2
H1
H7
H6
H5
250 m
4 km
VE=12

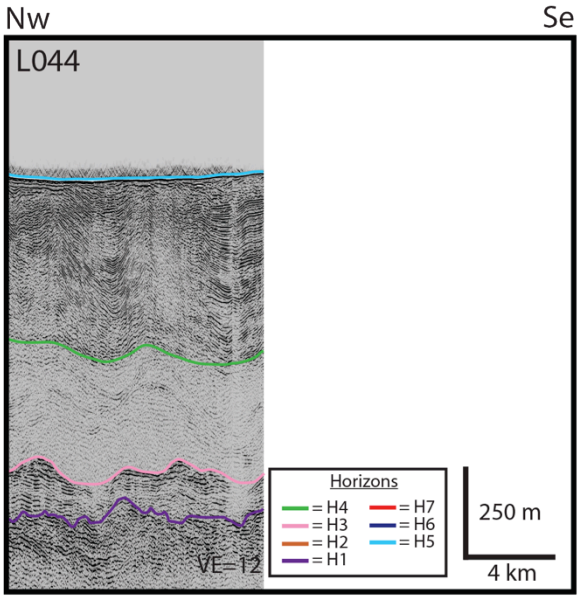
Nw
Se
L044
VE=12
Horizons
= H4
= H3
= H2
= H1
= H7
= H6
= H5
250 m
4 km

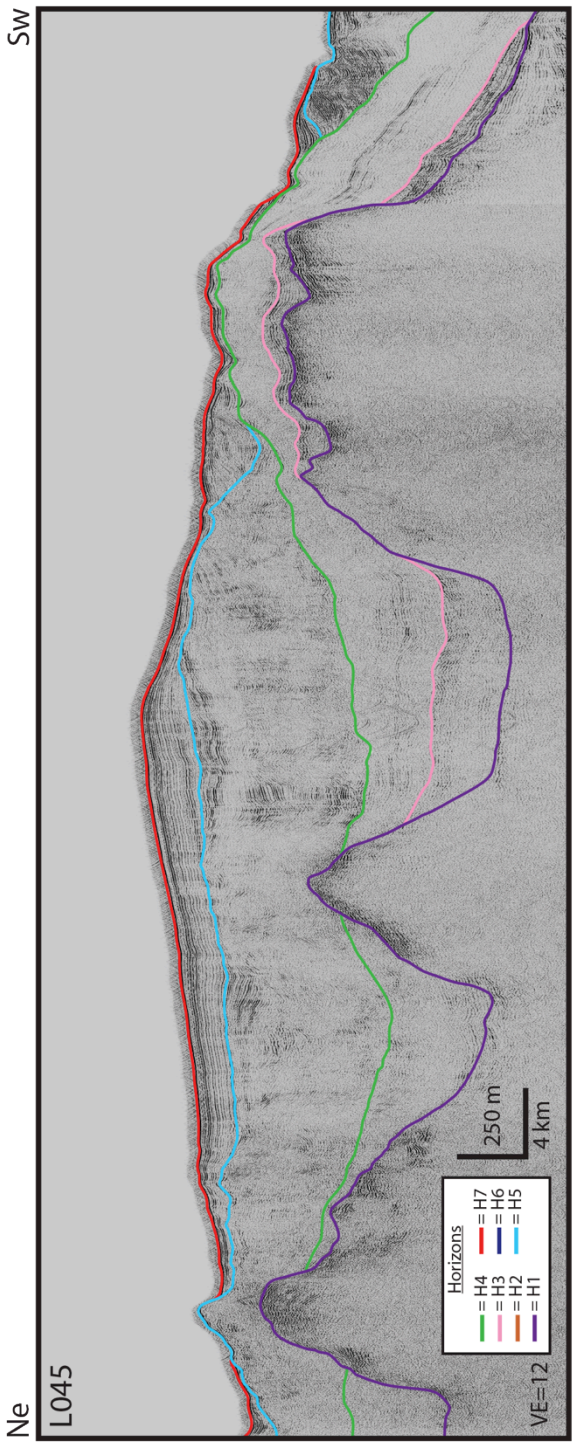
Sw
Ne
L045
Horizons
= H4
= H3
= H2
= H1
= H7
= H6
= H5
250 m
4 km
VE=12

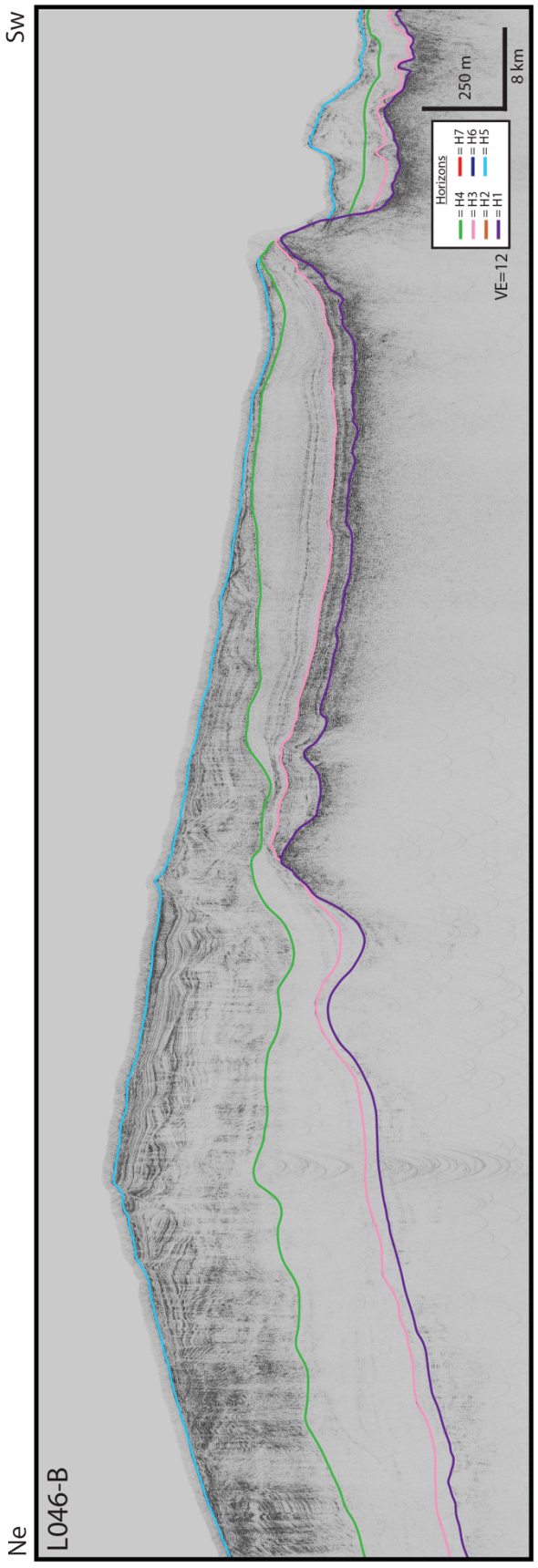
Sw
Ne
L046-B
Horizons
H7
H6
H5
H4
H3
H2
H1
250 m
8 km
VE=12

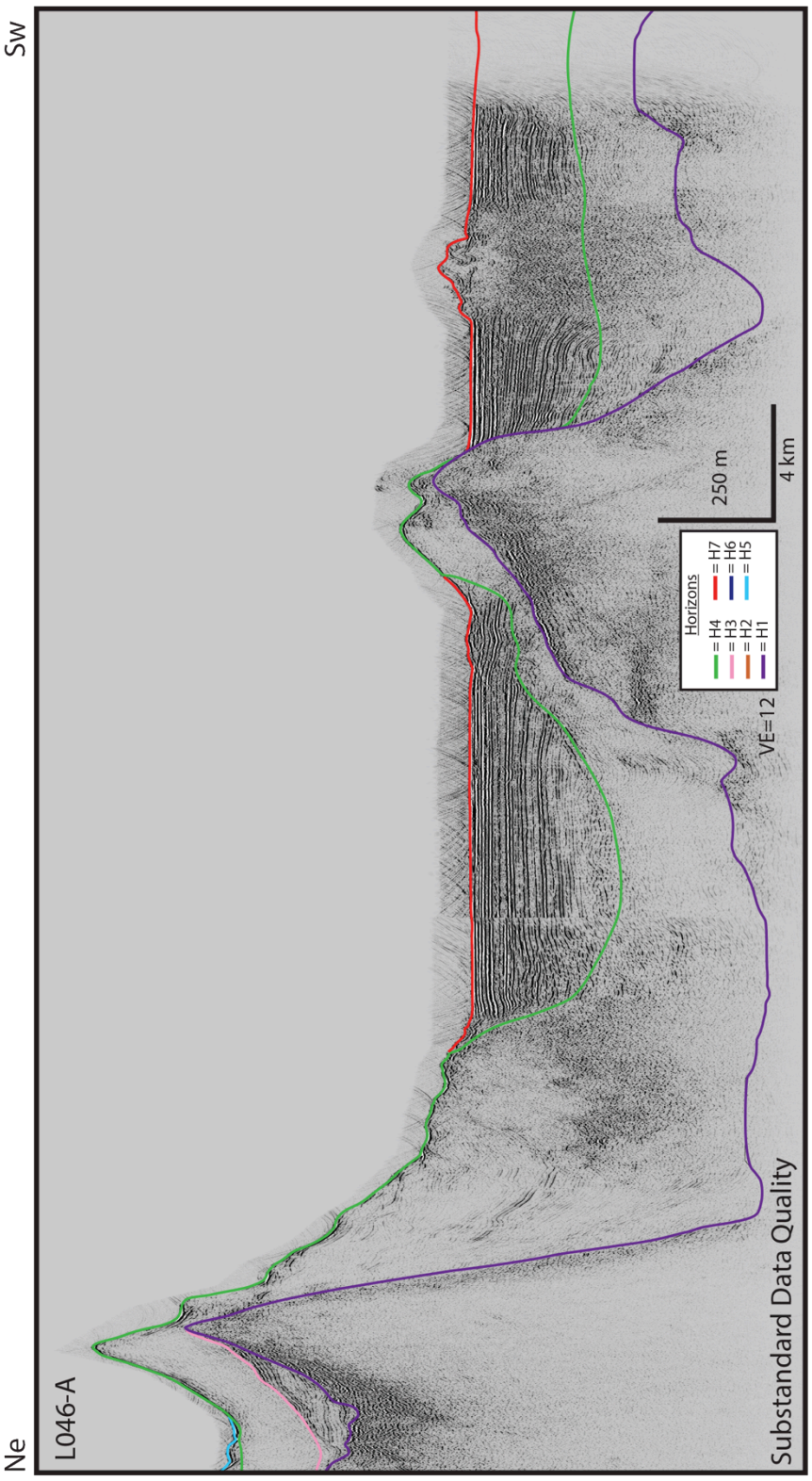
Sw
Ne
L046-A
Substandard Data Quality
VE=12
Horizons
H4
H3
H2
H1
H7
H6
H5
250 m
4 km

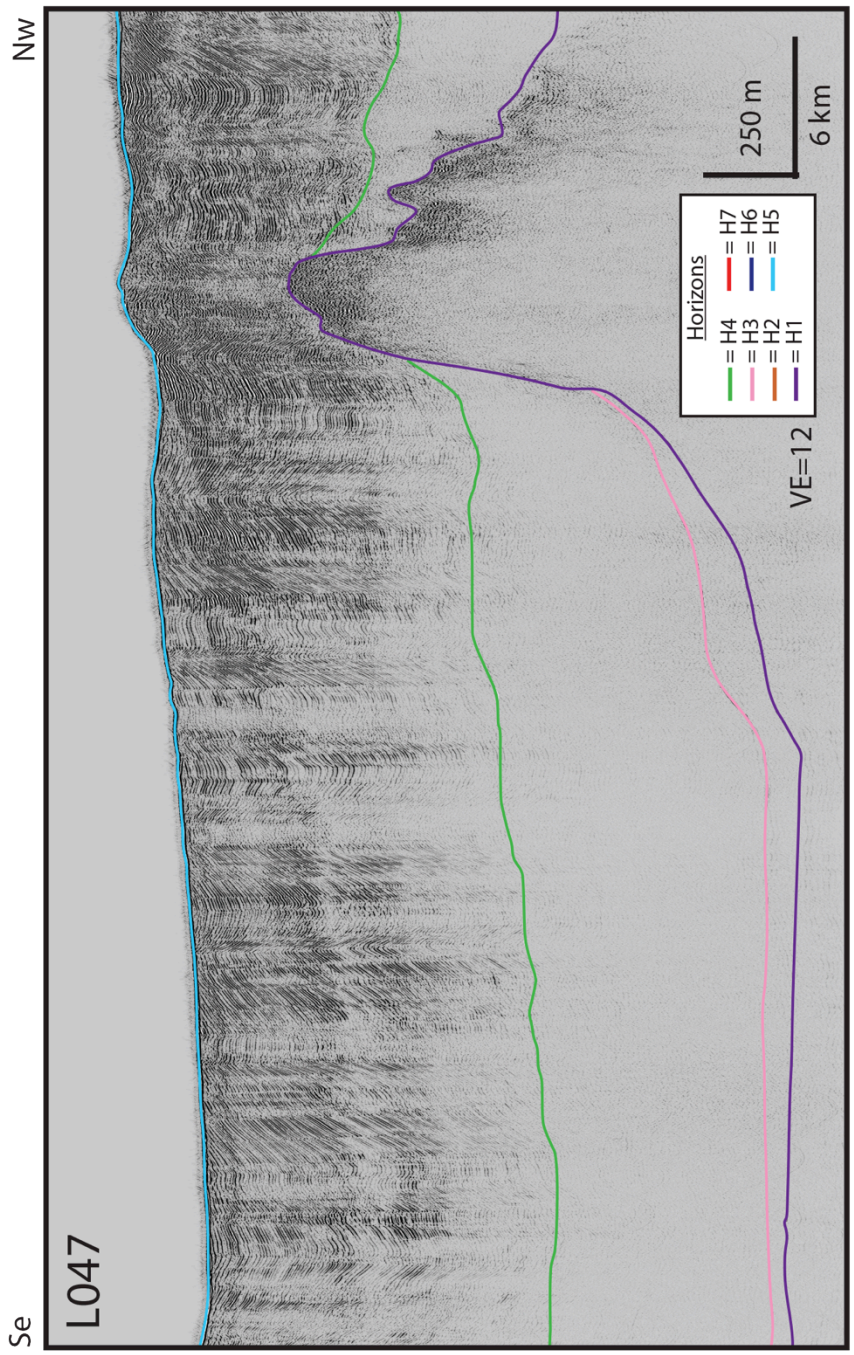
Nw
Se
L047
Horizons
= H4
= H3
= H2
= H1
= H7
= H6
= H5
250 m
6 km
VE=12

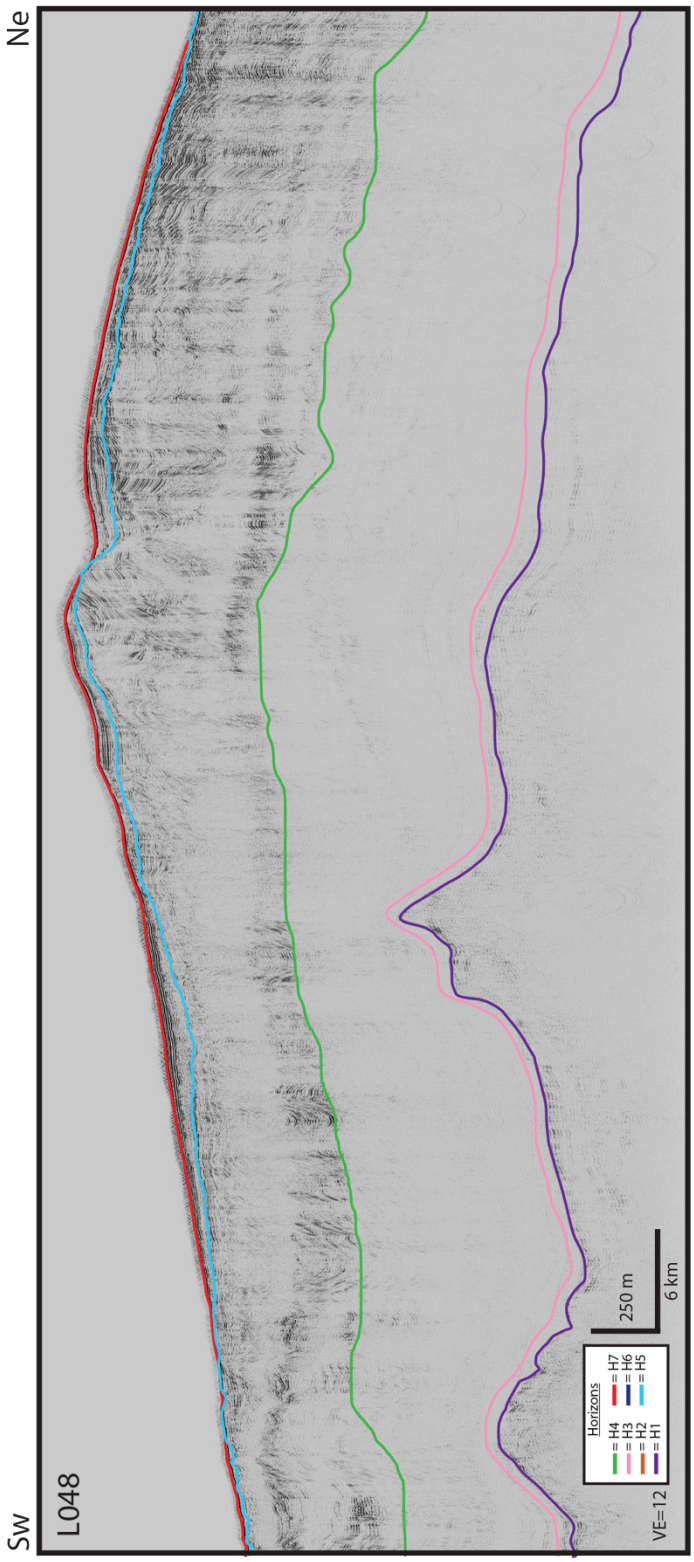
Ne
Sw
L048
Horizons
H4
H3
H2
H1
H7
H6
H5
250 m
6 km
VE=12

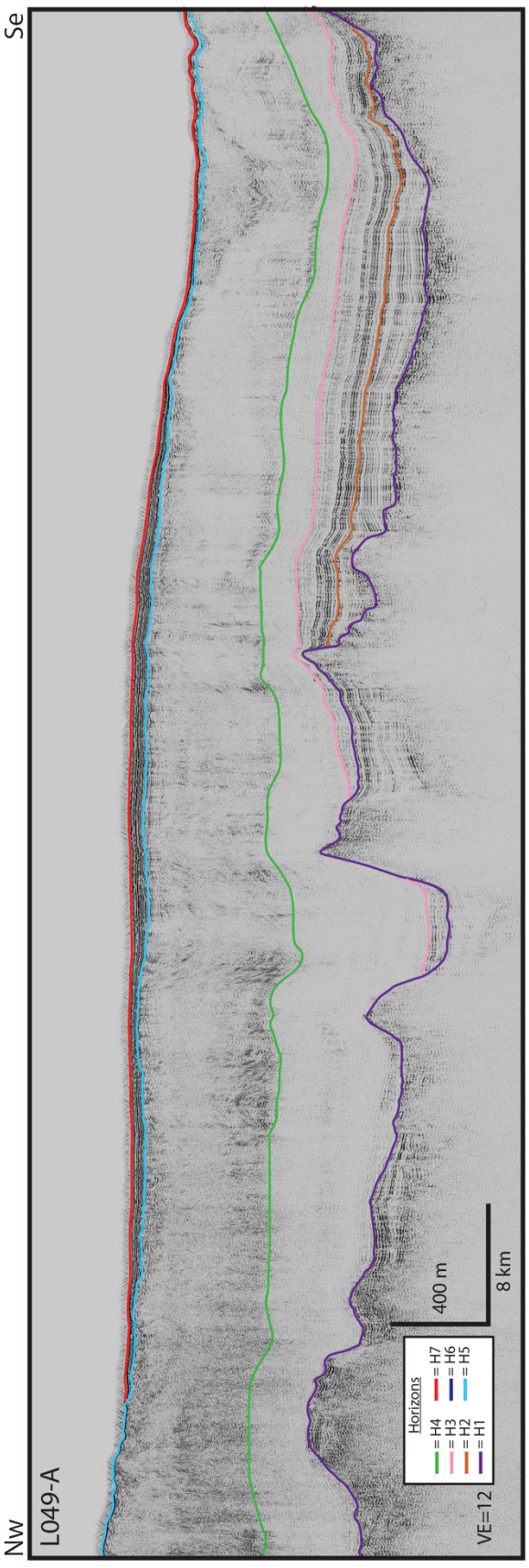
Se
Nw
L049-A
Horizons
= H7
= H6
= H5
= H4
= H3
= H2
= H1
400 m
8 km
VE=12

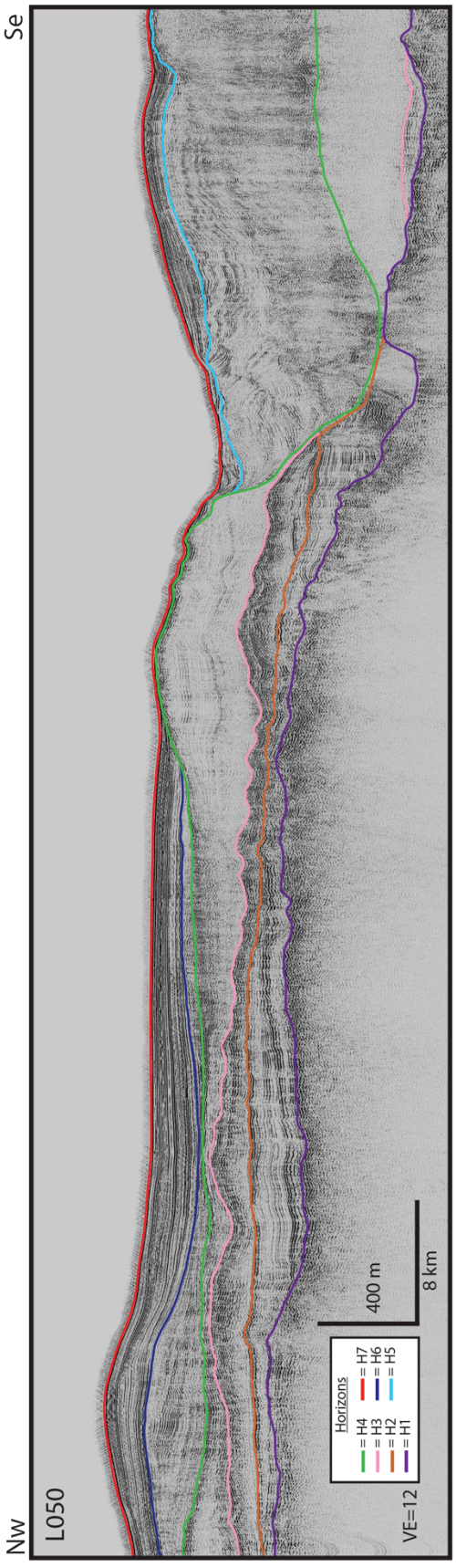
Se
Nw
L050
Horizons
H4 = H7
H3 = H6
H2 = H5
H1
400 m
8 km
VE=12

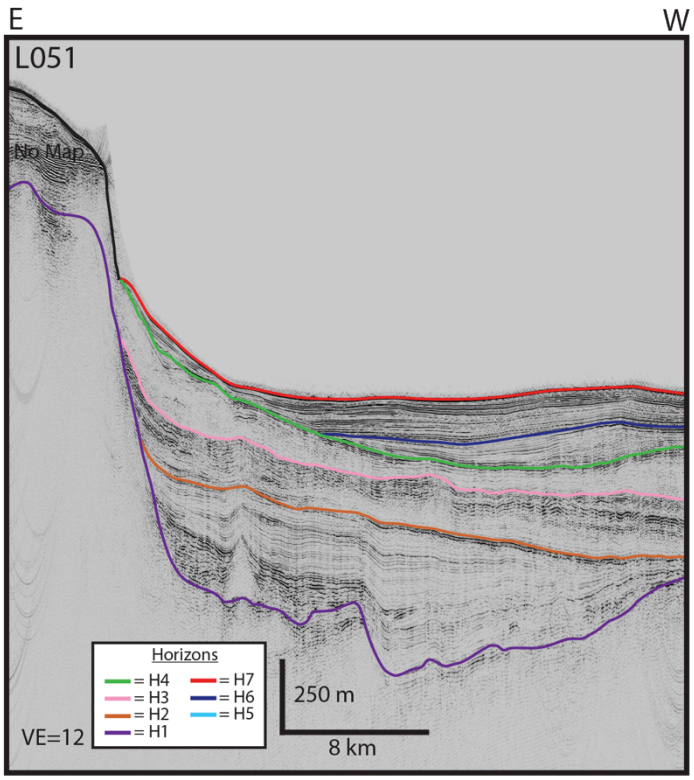
E
W
L051
No Map
Horizons
= H4
= H3
= H2
= H1
= H7
= H6
= H5
250 m
8 km
VE=12

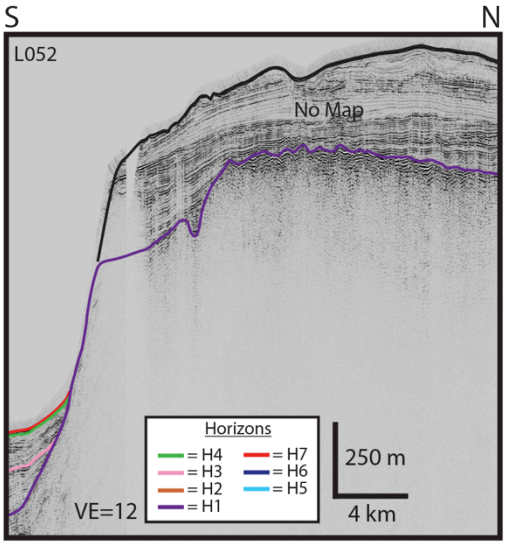
S
N
L052
No Map
Horizons
= H4
= H3
= H2
= H1
= H7
= H6
= H5
250 m
4 km
VE=12

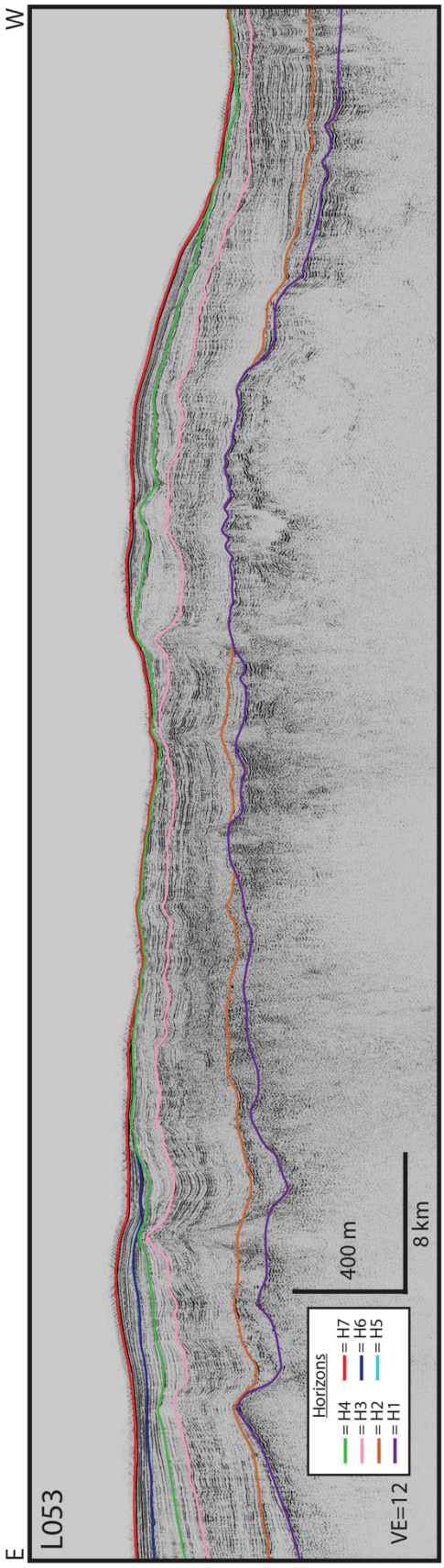
W
E
L053
Horizons
H4
H3
H2
H1
H7
H6
H5
400 m
8 km
VE=12

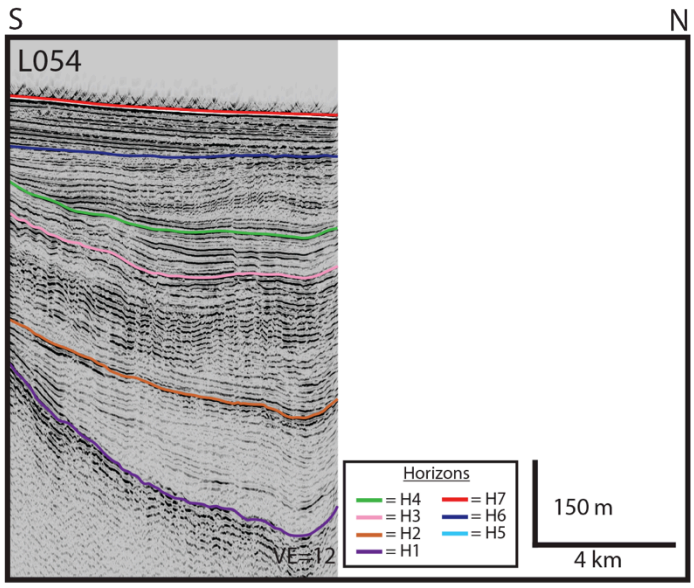
S
N
L054
Horizons
= H4
= H3
= H2
= H1
= H7
= H6
= H5
150 m
4 km
VE=12

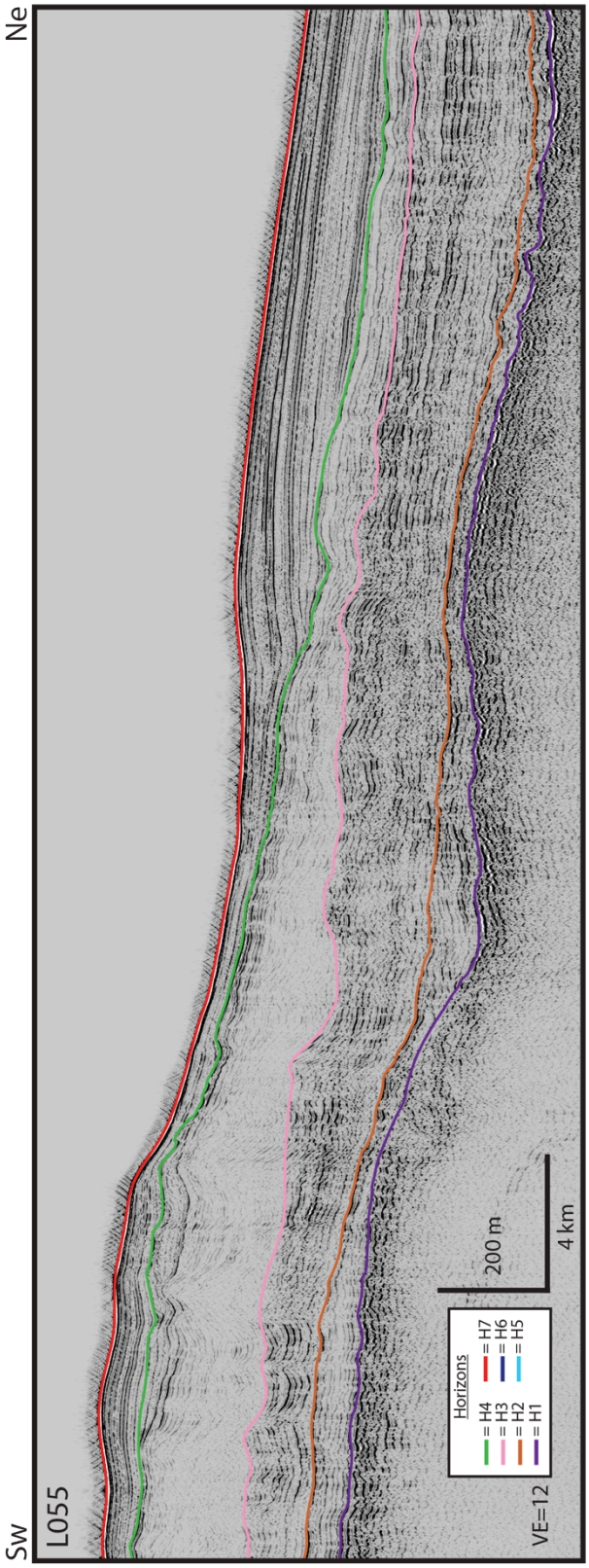
Ne
Sw
L055
Horizons
H4
H3
H2
H1
H7
H6
H5
200 m
4 km
VE=12

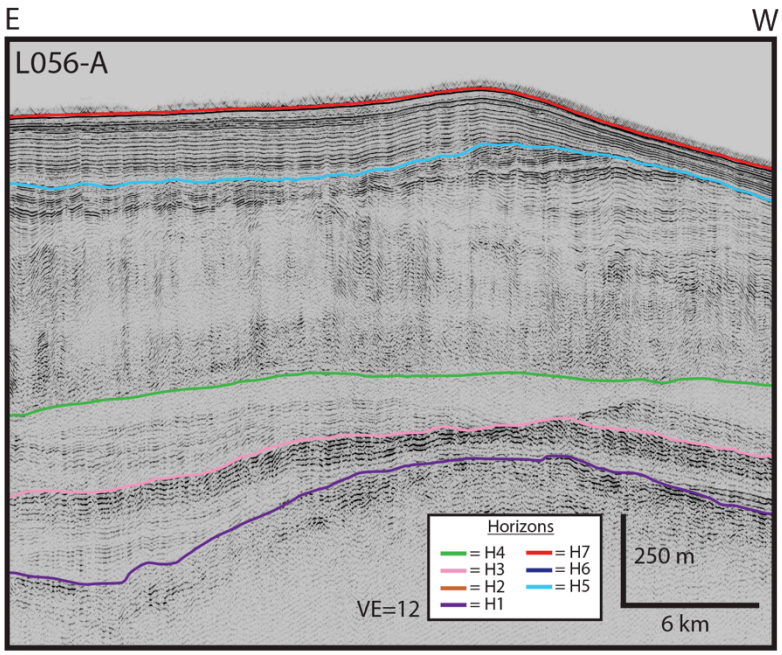
E
W
L056-A
Horizons
= H4
= H3
= H2
= H1
= H7
= H6
= H5
VE=12
250 m
6 km

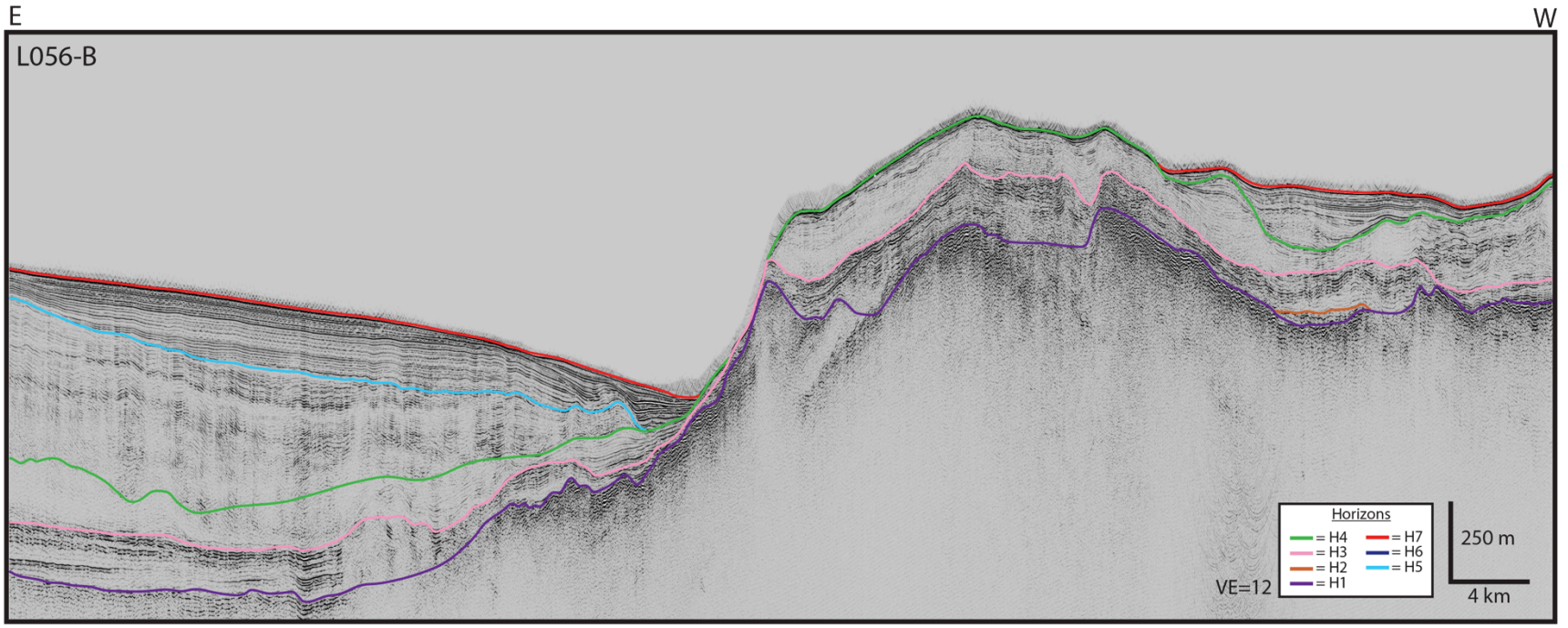
E
W
L056-B
Horizons
= H4
= H3
= H2
= H1
= H7
= H6
= H5
VE=12
250 m
4 km